
Black Hole Binaries

Jeffrey. E. McClintock

Harvard-Smithsonian Center for Astrophysics, 60 Garden St., Cambridge, MA 02138, USA

Ronald. A. Remillard

Center for Space Research, MIT, Cambridge, MA 02139, USA

4.1 Introduction

4.1.1 Scope of this review

We focus on 18 black holes with measured masses that are located in X-ray binary systems. These black holes are the most visible representatives of an estimated ~ 300 million stellar-mass black holes that are believed to exist in the Galaxy (van den Heuvel 1992; Brown & Bethe 1994; Timmes et al. 1996; Agol et al. 2002). Thus the mass of this particular form of dark matter, assuming $\sim 10M_{\odot}$ per black hole, is $\sim 5\%$ of the total baryonic mass (i.e., stars plus gas) of the Galaxy (Trimble 1999). Collectively this vast population of black holes outweighs the Galactic-center black hole, SgrA*, by a factor of ~ 1000 . These stellar-mass black holes are important to astronomy in numerous ways. For example, they are one endpoint of stellar evolution for massive stars, and the collapse of their progenitor stars enriches the universe with heavy elements (Woosley et al. 2002). Also, the measured mass distribution for even the small sample of 18 black holes featured here are already used to constrain models of BH formation and evolution and supernovae (Brown et al. 2000a; Nelemans & van den Heuvel 2001; Fryer & Kalogera 2001). Lastly, the observed BHBs apparently have been linked to the hypernovae believed to power gamma-ray bursts. This connection arises from the discovery by Israelian et al. (1999) that the companion of GRO J1655–40 is rich in α -particle nuclei (O, Mg, Si and S) and the arguments of Brown et al. (2000b) that the pollutants were ejected by the hypernova that formed the BH primary. An enrichment of α -particle nuclei has also been reported for SAX J1819.3–2525 (Orosz et al. 2001).

The main goal of this review is to discuss the X-ray timing and spectral properties of the 18 black holes plus some additional candidates with an eye to their importance to physics as potential sites for tests of general relativity (GR) in the strongest possible gravitational fields. Accordingly, the review focuses on several current areas of research that probe phenomena believed to occur very near the event horizon. These include high-frequency QPOs (40–450 Hz) observed from seven systems, relativistically broadened iron lines from the inner accretion disk, and thermal disk emission from near the innermost stable circular orbit allowed by GR. We also comment on evidence for the existence of the event horizon, which is based on a comparison of black-hole and neutron-star binaries and on models for advective accretion flows.

The black-hole binaries featured here are mass-exchange binaries that contain

2 *Black Hole Binaries*

an accreting black-hole primary and a degenerate secondary star. They comprise about 10% of all bright X-ray binaries. For background on X-ray binaries, see Chapter 1, and references therein. For comprehensive and excellent reviews on black-hole binaries, see Tanaka & Lewin (1995; hereafter TL95) and Tanaka and Shibazaki (1996; hereafter TS96). The thrust of this paper is to discuss the new results of the past decade. Throughout we make extensive use of the extraordinary data base amassed by NASA's Rossi X-ray Timing Explorer since January 1996 (Swank 1998), while building on the results detailed in the earlier review papers. Because of our page limit, several important topics are omitted such as X-ray reflection studies (Done & Nayakshin 2001), the estimated number of black-hole X-ray novae in the Galaxy, which is ~ 1000 (van den Heuvel 1992; TS96; Romani 1998), and the present and projected rates of discovery of black-hole binaries.

4.1.2 *The 18 black-hole binaries*

The first black-hole binary (BHB), Cygnus X-1, was established by Webster and Murdin (1972) and Bolton (1972); the second, LMC X-3, was found by Cowley et al. (1983). Both of these systems are persistently bright in X-rays; furthermore, they are classified as high-mass X-ray binaries (HMXBs) because their secondaries are massive O/B stars (White et al. 1995). The third BHB to be established, A0620-00, is markedly different (McClintock & Remillard 1986). A0620-00 was discovered as an X-ray nova in 1975 when it suddenly brightened to an intensity of 50 Crab* to become the brightest nonsolar X-ray source ever observed (Elvis et al. 1975). Then, over the course of a year, the source decayed back into quiescence to become a feeble ($10 \mu\text{Crab}$) source (McClintock et al. 1995). Similarly, the optical counterpart faded from outburst maximum by $\Delta V \approx 7.1$ mags to $V \approx 18.3$ in quiescence, thereby revealing the optical spectrum of a K-dwarf secondary.

During the past 20 years, black holes (BHs) have been established in 15 additional X-ray binaries. Remarkably, nearly all these systems are X-ray novae like A0620-00. Thus, in all there are now 18 confirmed BHBs. They are listed in Table 4.1 in order of right ascension. The coordinate name of each source is followed in the second column by its variable star name (or other name, such as Cyg X-1), which is useful for web-based literature searches. For X-ray novae, the third column gives the year of discovery and the number of outbursts that have been observed. As indicated in the table, among the confirmed BHBs, there are five recurrent X-ray novae and three persistent sources, Cyg X-1, LMC X-3 and LMC X-1. As indicated in the fourth column, these latter three sources are high-mass X-ray binaries and are the only truly persistent sources among the BHBs.

Two of the X-ray novae are peculiar: GRS 1915+105 has remained bright for more than a decade since its eruption in August 1992; GX339-4 (1659-487), which was discovered by Markert et al. in 1973, undergoes frequent outbursts followed by very faint states, but it has never been observed to reach the *quiescent* state (Hynes et al. 2003). Columns 5 and 6 give the peak X-ray flux and a distance estimate for each source. The orbital period and the spectral type of the secondary are given in the remaining two columns. The first one or two references listed for each binary

* $1 \text{ Crab} = 2.6 \times 10^{-9} \text{ erg s}^{-1} \text{ keV}^{-1} = 1.06 \text{ mJy @ } 5.2 \text{ keV}$ for a Crab-like spectrum with photon index $\Gamma = 2.1$.

Table 4.1. *Confirmed black-hole binaries: primary properties*

Source	Alternative name ^a	Year ^b	Type ^c	$F_{x,\max}$ (μJy^d)	D (kpc)	P_{orb} (hr)	Spec.	References
0422+32	V518 Per	1992/1	L,T	3000	2.6 ± 0.7	5.1	M2V	1,2
0538–641	LMC X–3	–	H,P	44	50 ± 2.3	40.9	B3V	3,4
0540–697	LMC X–1	–	H,P	25	50 ± 2.3	101.5	O7III	3,5,6
0620–003	V616 Mon	1975/2	L,T	50000	1.2 ± 0.1	7.8	K4V	7,8,9,10
1009–45	MM Vel	1993/1	L,T	800	5.0 ± 1.3	6.8	K7/M0V	11,12
1118+480	KV UMa	2000/1	L,T	40	1.8 ± 0.5	4.1	K5/M0V	13,14
1124–684 ^e	GU Mus	1991/1	L,T	3000	5 ± 1.3	10.4	K3/K5V	15,15a,16
1543–475	IL Lupi	1971/4	L,T	15000	7.5 ± 0.5	27.0	A2V	17,18
1550–564	V381 Nor	1998/5	L,T	7000	5.3 ± 2.3	37.0	G8/K8IV	19
1655–40	V1033 Sco	1994/2	L,T	1600	3.2 ± 0.2	62.9	F3/F5IV	20,21,22
1659–487 ^f	V821 Ara	–	L,T	900	4	42.1:	–	23,24
1705–250	V2107 Oph	1977/1	L,T	3600	8 ± 2	12.5	K3/7V	7,25,26
1819.3–2525	V4641 Sgr	1999/1	L,T	13000	7.4–12.3	67.6	B9III	27
1859+226	V406 Vul	1999/1	L,T	600	11	9.2:	–	28,29
1915+105	V1487 Aql	1992/1	L,T	2000	11–12	804.0	K/MIII	30,31,32,33
1956+350	Cyg X–1	–	H,P	1320	2.4 ± 0.5	134.4	O9.7Iab	34,35
2000+251	QZ Vul	1988/1	L,T	11000	2.7 ± 0.7	8.3	K3/K7V	35a,7,36,37
2023+338	V404 Cyg	1989/3	L,T	20000	2.2–3.7	155.3	K0III	38,39,40

^a Name recognized by the SIMBAD Database and the Astrophysics Data System (ADS).

^b Year of discovery/number of outbursts observed (Chen et al. 1997; this work).

^c ‘H’ – HMXB, ‘L’ – LMXB, ‘T’ – transient, ‘P’ – persistent; Liu et al. 2001

^d $1 \mu\text{Jy} = 10^{-29} \text{ergs cm}^{-2} \text{s}^{-1} \text{Hz}^{-1} = 2.4 \times 10^{-12} \text{ergs cm}^{-2} \text{s}^{-1} \text{keV}^{-1}$; Liu et al. 2001

^e Commonly known as Nova Muscae 1991.

^f Commonly known as GX339–4.

REFERENCES: ¹Esin et al. 1997; ²Filippenko et al. 1995a; ³Freedman et al. 2001; ⁴Cowley et al. 1983; ⁵Hutchings et al. 1987; ⁶Cowley et al. 1995; ⁷Barret et al. 1996b; ⁸Gelino et al. 2001b; ⁹Marsh et al. 1994; ¹⁰McClintock & Remillard 2000; ¹¹Barret et al. 2000; ¹²Filippenko et al. 1999; ¹³McClintock et al. 2001a; ¹⁴Wagner et al. 2001; ¹⁵Orosz et al. 1996; ^{15a}Gelino et al. 2001a; ¹⁶Shahbaz et al. 1997; ¹⁷Orosz et al. 2002b; ¹⁸Orosz et al. 1998; ¹⁹Orosz et al. 2002a; ²⁰Hjellming & Rupen 1995; ²¹Orosz & Bailyn 1997; ²²Shahbaz et al. 1999; ²³Cowley et al. 1987; ²⁴Hynes et al. 2003; ²⁵Remillard et al. 1996; ²⁶Filippenko et al. 1997; ²⁷Orosz et al. 2001; ²⁸Zurita et al. 2002; ²⁹Filippenko & Chornock 2001; ³⁰Mirabel & Rodriguez 1994; ³¹Fender et al. 1999b; ³²Greiner et al. 2001a; ³³Greiner et al. 2001b; ³⁴Herrero et al. 1995; ³⁵Gies & Bolton 1982; ^{35a}Harlaftis et al. 1996; ³⁶Filippenko et al. 1995; ³⁷Casares et al. 1995; ³⁸Shahbaz et al. 1994; ³⁹Casares & Charles 1994; ⁴⁰Casares et al. 1993.

provide fundamental information including the orbital period and the spectral type. The remaining references support the distance estimates.

The data in Table 4.1 reveal considerable diversity among the BHBs. For example, these 18 binary systems range in size from tiny XTE J1118+480 with an orbital period $P_{\text{orb}} = 0.17$ days and a separation between the BH and its companion of $a \approx 2.8 R_{\odot}$ to GRS 1915+105 with $P_{\text{orb}} = 33.5$ days and $a \approx 95 R_{\odot}$. Only six of these 18 systems were established as dynamical BHBs a decade ago (TL95). As indicated in Table 4.1, all of the 15 X-ray novae are low-mass X-ray binaries (LMXBs) with a companion-star mass $M_2 \lesssim 1 M_{\odot}$ (White et al. 1995). The BHBs 4U1543–47 and SAX J1819.3–2525 have relatively massive secondaries: $2.7 \pm 1.0 M_{\odot}$ and

4 *Black Hole Binaries*

$2.9 \pm 0.2 M_{\odot}$, respectively (Orosz et al. 2002b). Nevertheless, we classify them as LMXBs because their secondary masses are comparable to the mass of HZ Her ($2.3 \pm 0.3 M_{\odot}$; Reynolds et al. 1997), which is the secondary of the well-known LMXB Her X-1 (Liu et al. 2001). Furthermore, a $2\text{--}3 M_{\odot}$ secondary is much less massive than the O/B secondaries ($\gtrsim 10 M_{\odot}$) found in HMXB systems.

BHBs manifest themselves in five rather distinct spectral/temporal states defined in the 1–10 keV band (e.g. van der Klis 1994; TL95; TS96). The three most familiar are (1) the *high/soft* (HS) state, a high-intensity state dominated by thermal emission from an accretion disk; (2) the *low/hard* (LH) state, a low-intensity state dominated by power-law emission and rapid variability; and (3) the *quiescent* state an extraordinarily faint state also dominated by power-law emission. The remaining two states, (4) the *very high* (VH) state and (5) the *intermediate* (IM) state, are more complex; recently they have come to the fore, as they have now been observed in an appreciable number of sources. These five BH states and the transitions between them are the focus of §4.3, where they are discussed and illustrated in detail.

Additional data specific to the BH primaries are contained in Table 4.2. Of special importance is the mass function, $f(M) \equiv P_{\text{orb}} K_2^3 / 2\pi G = M_1 \sin^3 i / (1 + q)^2$. The observables on the left side of the equation are the orbital period, P_{orb} , and the half-amplitude of the velocity curve of the secondary, K_2 . On the right, the quantity of most interest is the BH mass, M_1 ; the two additional parameters are the orbital inclination angle, i , and the mass ratio, $q \equiv M_2/M_1$, where M_2 is the mass of the secondary. Thus a secure value of the mass function can be determined for a quiescent X-ray nova or an HMXB such as Cyg X-1 by simply measuring the radial velocity curve of the secondary star. The mass function, $f(M)$ and an estimate of the BH mass, M_1 , are given in the second and third columns of Table 4.2. An inspection of the equation for $f(M)$ shows that the value of the mass function is the absolute minimum mass of the compact primary. Thus, for 12 of the 18 BHBs, the very secure value of $f(M)$ alone is sufficient to show that the mass of the compact X-ray source is $> 3 M_{\odot}$ (Table 4.2), which is widely agreed to exceed the maximum stable mass of a neutron star (NS) in general relativity (Rhoades & Ruffini 1974; Kalogera & Baym 1996). For the remaining half-dozen systems, some additional data are required to make the case for a BH. The evidence for BHs in these 18 systems is generally very strong (see Ch. 5). Thus, assuming that GR is valid in the strong-field limit, we choose to refer to these compact primaries as BHs, rather than as BH candidates. We note, however, our reservations about three of the systems listed in the table: (1) The mass function of LMC X-1 is quite uncertain (Table 4.2); (2) the orbital period of XTE J1859+226 is not firmly established (Filippenko & Chornock 2001; Zurita et al. 2002); and (3) the dynamical data for GX 339-4 were determined in outburst by a novel technique and neither the orbital period nor the velocity amplitude are securely determined (Hynes et al. 2003).

High frequency QPOs (HFQPOs) in the range 40–450 Hz are observed for the four systems with data given in the fourth column. Low-frequency QPOs (LFQPOs) are also observed from these systems and ten others, as indicated in column 5. Most of the systems are at one time or another detected as radio sources and at least five have exhibited resolved radio jets (column 6; see Mirabel & Rodriguez 1999). An X-ray jet (two-sided) has been observed from XTE J1550-564 (Corbel et al. 2003).

Table 4.2. *Confirmed black-hole binaries: X-ray and optical data*

Source	$f(M)^a$ (M_\odot)	M_1^a (M_\odot)	$f(\text{HFQPO})$ (Hz)	$f(\text{LFQPO})$ (Hz)	Radio ^b	E_{max}^c (MeV)	References
0422+32	1.19±0.02	3.2–13.2	–	0.035–32	P	0.8, 1–2:	1,2,3,4,5
0538–641	2.3±0.3	5.9–9.2	–	0.46	–	0.05	6,7
0540–697	0.14±0.05	4.0–10.0:	–	0.075	–	0.02	8,7
0620–003	2.72±0.06	8.7–12.9	–	–	P,J?	0.03:	9,10,11
1009–45	3.17±0.12	6.3–8.0	–	0.04–0.3	– ^d	0.40, 1:	12,4,13
1118+480	6.1±0.3	6.5–7.2	–	0.07–0.15	P	0.15	14,15,16,17
1124–684	3.01±0.15	6.5–8.2	–	3.0–8.4	P	0.50	18,19,20,21
1543–475	0.25±0.01	7.4–11.4 ^e	–	7	– ^f	0.20	22,4
1550–564	6.86±0.71	8.4–10.8	92,184,276	0.1–10	P,J	0.20	23,24,25,26,27
1655–40	2.73±0.09	6.0–6.6	300,450	0.1–28	P,J	0.80	28,29,30,31,54
1659–487	> 2.0 ^g	–	–	0.09–7.4	P	0.45, 1:	32,33,4,13
1705–250	4.86±0.13	5.6–8.3	–	–	– ^d	0.1	34,35
1819.3–2525	3.13±0.13	6.8–7.4	–	–	P,J	0.02	36,37
1859+226	7.4±1.1	7.6–12:	150,187	0.5–10	P,J?	0.2	38,39,40,41
1915+105	9.5±3.0	10.0–18.0:	40,67,113,165	0.001–10	P,J	0.5, 1:	42,43,44,4,13
1956+350	0.244±0.005	6.9–13.2	–	0.035–12	P,J	1.5, 3–5:	45,46,47,48,49
2000+251	5.01±0.12	7.1–7.8	–	2.4–2.6	P	0.3	18,50,51
2023+338	6.08±0.06	10.1–13.4	–	–	P	0.4	52,53

^a Orosz et al. 2002b, except for 1659–487; colon denotes uncertain value.

^b Radio properties: ‘P’ - persistent over 10 or more days and/or inverted spectrum; ‘J’ - relativistic jet detected.

^c Maximum energy reported; colon denotes uncertain value.

^d No observations made.

^e Orosz, private communication.

^f Very faint (e.g., see IAUC 7925).

^g For preferred period, $P = 1.76$ days, $f(M) = 5.8 \pm 0.5 M_\odot$; Hynes et al. 2003.

REFERENCES: ¹van der Hooft et al. 1999; ²Vikhlinin et al. 1992; ³Shrader et al. 1994; ⁴Grove et al. 1998; ⁵van Dijk et al. 1995; ⁶Boyd et al. 2000; ⁷Nowak et al. 2001; ⁸Ebisawa et al. 1989; ⁹Owen et al. 1976; ¹⁰Kuulkers et al. 1999; ¹¹Coe et al. 1976; ¹²van der Hooft et al. 1996; ¹³Ling et al. 2000; ¹⁴Wood et al. 2000; ¹⁵Revnivtsev et al. 2000b; ¹⁶Fender et al. 2001; ¹⁷McClintock et al. 2001a; ¹⁸Rutledge et al. 1999; ¹⁹Belloni et al. 1997; ²⁰Ball et al. 1995; ²¹Sunyaev et al. 1992; ²²This work; ²³Remillard et al. 2002b; ²⁴Corbel et al. 2001; ²⁵Wu et al. 2002; ²⁶Corbel et al. 2003; ²⁷Sobczak et al. 2000b; ²⁸Remillard et al. 1999; ²⁹Strohmayer 2001a; ³⁰Hjellming & Rupen 1995; ³¹Hannikainen et al. 2000; ³²Revnivtsev et al. 2001; ³³Corbel et al. 2000; ³⁴Wilson & Rothschild 1983; ³⁵Cooke et al. 1984; ³⁶Hjellming et al. 2000; ³⁷Wijnands & van der Klis 2000; ³⁸Cui et al. 2000a; ³⁹Markwardt 2001; ⁴⁰Brocksopp et al. 2002; ⁴¹Dal Fiume et al. 1999; ⁴²Morgan et al. 1997; ⁴³Strohmayer 2001b; ⁴⁴Mirabel & Rodriguez 1994; ⁴⁵Vikhlinin et al. 1994; ⁴⁶Cui et al. 1997b; ⁴⁷Stirling et al. 2001; ⁴⁸Ling et al. 1987; ⁴⁹McConnell et al. 2000; ⁵⁰Hjellming et al. 1988; ⁵¹Sunyaev et al. 1988; ⁵²Han & Hjellming 1992; ⁵³Sunyaev et al. 1991b; ⁵⁴Tomsick et al. 1999.

As shown in column 7, power-law emission extending to ~ 1 MeV has been observed for five sources. The references listed in the last column support the X-ray QPO, radio, and E_{max} data given in columns 3–6.

The dynamical evidence for massive ($M > 3 M_\odot$) collapsed stellar remnants is indisputable. However, this evidence alone can never establish the existence of BHs. At present, the argument for BHs depends on the assumption that GR is the correct theory of strong gravity. To make an airtight case that a compact object

is a BH with an event horizon, we must make clean quantitative measurements of relativistic effects that occur in the near vicinity of that object. That is, we must measure phenomena that are predicted by GR to be unique to BHs. A possible route to this summit is to measure and interpret the effects of strong-field gravity that are believed to be imprinted on both high-frequency quasi-periodic oscillations (HFQPOs; see §4.4) and on X-ray emission lines (§4.2.4). Another approach, which is discussed in §4.3.4, is based on sensing the qualitative differences between an event horizon and the material surface of a NS.

4.1.3 *Black hole candidates*

Certain characteristic X-ray properties of the 18 established BHs are often used to identify a candidate BH when the radial velocities of the secondary cannot be measured (e.g., because the secondary is too faint or interstellar extinction is too high). These frequently observed characteristics of the established BHBs, which are discussed in detail by TL95, include an ultrasoft X-ray spectrum (1–10 keV), a power-law spectral tail that extends beyond 20 keV, characteristic state transitions (see §4.1.2; §4.3), and rapid temporal variability. However, none of these putative BH signatures has proved to be entirely reliable; all of them have been forged by systems known to contain a NS primary (TL95). This is not surprising since the general spectral/temporal phenomena named above originate in an accretion flow that is expected to be fairly similar whether the primary is a BH or a weakly magnetized NS. Another characteristic of all BHBs is a complete absence of either periodic pulsations or type I X-ray bursts, which are the very common signatures of NS systems.

Nevertheless, despite the limitations of these spectral/temporal identifiers, they have served as useful guides and have allowed the identification of a number of probable BH primaries, which we refer to as BH candidates or BHCs. In order to economize on acronyms, we also use BHC to refer to the binary system that hosts the BH candidate. A list of 22 BHCs is given in Table 4.3. These systems are less well-known than the BHBs listed in Table 4.1. Therefore, to aid in their identification we have included in most cases the prefix to the coordinate source name that identifies the discovery mission (e.g. EXO = *EXOSAT*). For the four sources with variable star names, the prefix is omitted. In columns 2, 3 and 4 we give the best available coordinates and their uncertainties (if they exceed 10''). These coordinates are also an excellent resource for interrogating ADS and SIMBAD.

In column 5 we list the characteristics that indicate the BHC classification, e.g., an observation of one or more of the canonical states of a BHB. A source classified as “ultrasoft” in the older literature (e.g. White & Marshall 1984) is assumed here to have been observed in the HS state. Resolved radio jets have been observed for three of the BHCs, and this is also noted in column 5. Characteristic temporal variability (§4.4) and broad Fe K α emission lines (§4.2.4) can also be important BH indicators, but these are not explicitly noted in Table 4.3. Selected references are cited in the last column. The coordinate data can be found in the first reference. The following few references support the BH characteristics given in column 5. For several sources, a few additional references provide limited information on optical/IR/radio counterparts, etc.

We have assigned a grade to each BHC that is based both on how thoroughly

Table 4.3. *Candidate black-hole binaries^a*

Source	RA(2000)	DEC(2000)	r_x^b	BH trait ^c	Grade ^d	References
1354–645 (BW Cir)	13 58 09.74	-64 44 05.2		LH,HS	A	1,2,3,4
1524–617 (KY TrA)	15 28 16.7	-61 52 58		LH,HS	A	5,6,7
4U 1630–47	16 34 01.61	-47 23 34.8		LH,HS	A	8,9,10,11
XTE J1650–500	16 50 01.0	-49 57 45		LH,HS,VH	A	12,13,14,15,16
SAX J1711.6–3808	17 11 37.1	-38 07 06		LH,HS	B	17,18
GRS 1716–249 ^e	17 19 36.93	-25 01 03.4		LH	B	19,20,21
XTE J1720–318	17 19 59.06	-31 44 59.7		LH,HS	C	22,23,24
KS 1730–312	17 33 37.6	-31 13 12	30''	LH,HS	C	25,26
GRS 1737–31	17 40 09	-31 02.4	30''	LH	B	27,28,29
GRS 1739–278	17 42 40.03	-27 44 52.7		LH,HS,VH	A	30,31,32,33,34
1E 1740.7–2942	17 43 54.88	-29 44 42.5		LH,HS,J	A	35,36,37,38,39
H 1743–322	17 46 15.61	-32 14 00.6		HS,VH	A	40,41,42,80,81,82
A 1742–289	17 45 37.3	-29 01 05		HS:	C	43,44,45,46
SLX 1746–331	17 49 50.6	-33 11 55	35''	HS:	C	47,48,49
XTE J1748–288	17 48 05.06	-28 28 25.8		LH,HS,VH,J	A	50,51,52,53,54
XTE J1755–324	17 55 28.6	-32 28 39	1'	LH,HS	B	55,56,57,58
1755–338 (V4134 Sgr)	17 58 40.0	-33 48 27		HS	B	59,42,60,61,62
GRS 1758–258	18 01 12.67	-25 44 26.7		LH,HS,J	A	63,38,64,65,66
EXO 1846–031	18 49 16.9	-03 03 53	11'' ^f	HS	C	67
XTEJ 1908+094	19 08 53.08	+09 23 04.9		LH,HS	B	68,69,70,71
1957+115 (V1408 Aql)	19 59 24.0	+11 42 30		HS	B	72,42,73,74,75
XTE J2012+381	20 12 37.70	+38 11 01.2		LH,HS	B	76,77,78,79

^a For additional references and information, see TL95 and Liu et al. 2001.

^b Positional uncertainty given if $r_x > 10''$.

^c 'LH' – low/hard state, 'HS' – high/soft state, 'VH' – very high state, 'J' – radio jet.

^d Qualitative grade indicating the likelihood that the candidate is in fact a BH.

^e GRS 1716–249 = GRO J1719–24 = X-ray Nova Oph 1993.

^f Alternative position also possible; see Parmar et al. 1993.

REFERENCES: ¹Kitamoto et al. 1990; ²Brocksopp et al. 2001; ³Revnivtsev et al. 2000a; ⁴McClintock et al. 2003b; ⁵Murdin et al. 1977; ⁶Kaluzienski et al. 1975; ⁷Barret et al. 1992; ⁸Hjellming et al. 1999; ⁹Tomsick & Kaaret 2000; ¹⁰Dieters et al. 2000; ¹¹Augusteijn et al. 2001; ¹²Groot et al. 2001; ¹³Kalemci et al. 2002; ¹⁴Homan et al. 2002; ¹⁵Miller et al. 2002b; ¹⁶Sanchez-Fernandez et al. 2002; ¹⁷in 't Zand et al. 2002a; ¹⁸Wijnands & Miller 2002; ¹⁹Mirabel et al. 1993; ²⁰van der Hooft et al. 1996b; ²¹Revnivtsev et al. 1998b; ²²Rupen et al. 2003; ²³Remillard et al. 2003a; ²⁴Markwardt & Swank 2003a; ²⁵Borozdin et al. 1995; ²⁶Vargas et al. 1996; ²⁷Ueda et al. 1997; ²⁸Cui et al. 1997a; ²⁹Trudolyubov et al. 1999; ³⁰Marti et al. 1997; ³¹Vargas et al. 1997; ³²Borozdin et al. 1998; ³³Wijnands et al. 2001; ³⁴Greiner et al. 1996; ³⁵Cui et al. 2001; ³⁶Churazov et al. 1993; ³⁷Smith et al. 1997; ³⁸Smith et al. 2002; ³⁹Marti et al. 2000; ⁴⁰Gursky et al. 1978; ⁴¹Cooke et al. 1984; ⁴²White & Marshall 1984; ⁴³Davies et al. 1976; ⁴⁴Wilson et al. 1977; ⁴⁵Branduardi et al. 1976; ⁴⁶Kennea & Skinner 1996; ⁴⁷Skinner et al. 1990; ⁴⁸White & van Paradijs 1996; ⁴⁹Motch et al. 1998; ⁵⁰Hjellming et al. 1998b; ⁵¹Revnivtsev et al. 2000c; ⁵²Kotani et al. 2000; ⁵³Miller et al. 2001; ⁵⁴Rupen et al. 1998; ⁵⁵Remillard et al. 1997; ⁵⁶Ogley et al. 1997; ⁵⁷Revnivtsev et al. 1998a; ⁵⁸Goldoni et al. 1999; ⁵⁹Bradt & McClintock 1983; ⁶⁰White et al. 1988; ⁶¹Pan et al. 1995; ⁶²Seon et al. 1995; ⁶³Rodriguez et al. 1992; ⁶⁴Sunyaev et al. 1991a; ⁶⁵Smith et al. 2001; ⁶⁶Rothstein et al. 2002; ⁶⁷Parmar et al. 1993; ⁶⁸Rupen et al. 2002; ⁶⁹in 't Zand et al. 2002b; ⁷⁰Woods et al. 2002; ⁷¹Chaty et al. 2002; ⁷²Margon et al. 1978; ⁷³Wijnands et al. 2002; ⁷⁴Yaqoob et al. 1993; ⁷⁵Nowak & Wilms 1999; ⁷⁶Hjellming et al. 1998a; ⁷⁷Campana et al. 2002; ⁷⁸Vasiliev et al. 2000; ⁷⁹Hynes et al. 1999; ⁸⁰Markwardt & Swank 2003b; ⁸¹Steehgs et al. 2003; ⁸²Homan et al. 2003.

the candidate has been observed and on the BH characteristics it has displayed. In fact, this grade is qualitative and subjective and meant only as a guide. Our sense of the grade is as follows: We would be surprised if even one of the nine A-grade BHCs contains a NS; on the other hand, we would not be surprised if one of the six C-grade BHCs contains a NS. In compiling Table 4.3, we have been selective. For example, we did not include systems such as SAX J1805.5–2031 (Lowes et al. 2002) and XTE J1856+053 (Barret et al. 1996a) primarily because we judged that the available information was too scanty. Thus the total number of binaries considered here (i.e. the systems listed in Tables 4.1–4.3 that contain either a BH or a BHC) is 40. For narrative discussions about many of the systems in Table 4.3, see TL95 and TS96. For additional data and as a supplement to the list of references given in Table 4.3, see Liu et al. (2001).

4.1.4 *X-ray Novae*

If we include the X-ray novae observed during the past decade, then about 300 binary X-ray sources are known (Liu et al. 2000; Liu et al. 2001). More than half of them are LMXBs, and roughly half of each type (i.e. LMXB and HMXB) are classified as transient sources. The HMXB transients are neutron-star/Be-star binaries, which are not relevant to this review, and we disregard them. The well-studied LMXB transients, on the other hand, correspond precisely to the X-ray novae that are listed in Tables 4.1–4.3. As the tables show, nearly all of the BHBs and BHCs are X-ray novae, which makes these systems central to this review. The behavior of A0620–00, described in §4.1.2 provides a clear-cut example of a classic X-ray nova. The principal hallmarks of an X-ray nova include both the discovery of the source during a violent outburst and a very large ratio of maximum to minimum X-ray intensity. Indeed, it is the extreme faintness of the quiescent accretion disk in these systems that allows one to view the companion star, leading to secure dynamical measurement of the BH mass (§4.1.2, §4.3.4; Ch. 5).

Recurrent eruptions have been observed for several of the X-ray novae listed in Table 4.1: e.g., A0620–00 in 1917 and 1975; H1743–322 in 1977 and 2003; GS 2023+338 in 1938, 1956 and 1987; 4U 1543–47 in 1971, 1983, 1992 and 2002; and 4U 1630–472 at ~ 1.8 -year intervals. However, most of the systems have been observed to erupt only once. Nevertheless, all X-ray novae are thought to be recurrent, with cycle times for some as long as several centuries or more. TS96 suggest an average cycle time of 10–50 years.

The outburst itself is due to a sudden surge in the mass accretion rate onto the BH. How do these infrequent, short surges arise following decades or even centuries of dormancy? The generally accepted mechanism is the disk instability model, which was developed initially for dwarf novae (Smak 1971; Osaki 1974; Cannizzo 1993) and extended to X-ray novae (e.g. Dubus et al. 2001). A key idea is that the rate of mass loss by the secondary through the inner Lagrangian point is roughly constant and the instability operates within the disk itself. In the *quiescent* state, the disk viscosity is extremely low and the time required for gas to make its way to the BH can be decades or more (compared to weeks in the outburst state). Therefore matter piles up in the outer disk. Eventually, at some radius a certain critical density is reached that triggers a local thermal instability. This instability is quickly propagated throughout

the disk via a heat wave, thereby causing active accretion to occur throughout the disk. This is the genesis of the outburst, during which the mass accretion rate onto the BH can exceed the transfer rate from the secondary by a factor of ~ 1000 or more. After several months, the surface density again falls, and the disk cools and returns to the *quiescent* state. The model has many complications, such as the effects of tidal torques on the accretion disk and heating of the disk by the impacting accretion stream (Lasota 2001).

4.1.5 Accretion onto black holes

The desire to understand observations of BHBs compels us to model the hydrodynamics and radiation processes of gas orbiting in the gravitational potential of a compact object (see Ch. 13 for a detailed review). The best-known such model is the thin accretion disk (Pringle & Rees 1972; Shakura & Sunyaev 1973; Novikov & Thorne 1973; Lynden-Bell & Pringle 1974). For nearly all of the systems included in Tables 4.1–4.3, the companion star fills its Roche equipotential lobe and a narrow stream of gas escapes the star through the inner Lagrangian (L_1) point. This gas has high specific angular momentum and cannot accrete directly on to the BH. It feeds into a thin disk of matter around the BH known as an accretion disk. Once entrained in the disk, the gas moves in Keplerian orbits with angular velocity $(GM/R^3)^{1/2}$. However, viscous dissipation slowly taps energy from the bulk orbital motion, and viscosity transports angular momentum outward. As a result, the gas gets hotter as it sinks deeper into the gravitational potential well of the BH. Near the BH the disk terminates because there are no stable particle orbits possible in the extreme gravitational field. The existence of an innermost stable circular orbit (ISCO) and other properties of BHs are discussed in many texts (e.g. Shapiro & Teukolsky 1983; Kato et al. 1998). In an astrophysical environment, a BH is completely specified by two numbers, its mass M , and its dimensionless spin parameter a_* , which has a value of between 0 for a Schwarzschild hole and 1 for a maximally-rotating Kerr hole. The defining property of a BH is its event horizon, the surface that bounds the interior region of spacetime that cannot communicate with the external universe. The radius of the event horizon of a Schwarzschild BH is $R_S \equiv 2R_g \equiv 2(GM/c^2) = 30 \text{ km}(M/10M_\odot)$, the innermost stable circular orbit is $R_{\text{ISCO}} = 6R_g$, and the corresponding maximum orbital frequency is $\nu_{\text{ISCO}} = 220 \text{ Hz}(M/10M_\odot)^{-1}$. For an extreme Kerr BH, the radii of both the event horizon and the minimum stable (prograde) orbit are identical, $R_K = R_{\text{ISCO}} = R_g$, and the maximum orbital frequency is $\nu_{\text{ISCO}} = 1615 \text{ Hz}(M/10M_\odot)^{-1}$. For the Kerr BH, it is well known that the rotational energy can be tapped electromagnetically (Blandford & Znajek 1977). The gas flows driven by this process are both anisotropic and self-collimating (Blandford 2002, and references therein), and they may be the source of the relativistic jets seen from several BHBs (Table 4.2).

Even for XTE J1118+480, the smallest system in Table 4.1, the outer radius of the accretion disk is expected to be roughly one solar radius $\sim 4 \times 10^4 R_g$, vastly larger than the BH event horizon. Thus a gas element of mass m that is destined to enter the BH starts far out with negligible binding energy. However, when it reaches the ISCO it will have radiated $0.057mc^2$ for a Schwarzschild BH or $0.42mc^2$ for an extreme Kerr BH. Moreover, 90% of this colossal binding energy is radiated within about $20R_g$ of

the center. At all disk radii, the binding energy liberated by viscous dissipation is radiated locally and promptly and results in a gas temperature that increases radially inward reaching a maximum of $T \sim 10^7$ K near the BH. This picture is the basis of the standard thin accretion disk model (Shakura & Sunyaev 1973). The thin disk spectrum has been formulated conveniently as a multi-temperature blackbody (Mitsuda et al. 1984; Makishima et al. 1986). The total disk luminosity in a steady state is $L_{\text{disk}} = G\dot{M}/2R_{\text{in}}$, where \dot{M} is the mass accretion rate and R_{in} is the radius of the inner edge of the disk. This model, often referred to as the Multicolor Disk (MCD) model, is widely used for the thermal component that is dominant in the HS state and is also present in the VH state. At high mass accretion rates, the thin disk extends all the way in to the ISCO (TL95; Sobczak et al. 1999) and the model provides a good account of the HS state (§4.3.5). Several authors have begun to consider additional relativistic corrections to the MCD model (e.g., Ebisawa et al. 1991; Zhang et al. 1997a; Gierlinski et al. 2001). However, quantitative analyses, e.g., a spectroscopic measurement of the inner disk radius when the source distance is known, will require more sophisticated models. Accretion disk models are being developed to incorporate MHD effects in the context of GR (e.g., McKinney & Gammie 2002), with additional considerations for radiation pressure and radiative transfer (Turner et al. 2002). Early results show that magnetic fields may couple matter in the “plunging region” to matter at radii greater than the ISCO, and thereby extract energy from very near the horizon (Agol & Krolik 2000). In the case of a rapidly-rotating Kerr hole, the spin/electromagnetic effects mentioned above may not only drive relativistic jets, but also may modify grossly the spectrum of the inner accretion disk (Wilms et al. 2001b; Miller et al. 2002b).

At lower mass accretion rates corresponding to several percent of the Eddington luminosity, a BHB usually enters the LH (i.e. *low/hard*) state and at very low accretion rates it reaches the *quiescent state*, which may be just an extreme example of the LH state. In both of these states, the spectrum of a BHB is dominated by a hard, thermal power-law component (photon index ~ 1.7 ; §4.3.6), which cannot be accounted for by a thermal accretion disk model; it is most plausibly explained as due to Comptonization of soft photons by a hot optically-thin plasma. Early models for the spectrum of the *quiescent state* postulated that the disk does not extend all the way down to the ISCO (Narayan 1996; Narayan et al. 1996). The disk is truncated at some larger radius and the interior volume is filled with a hot ($T_e \sim 100$ keV) advection-dominated accretion flow or ADAF (Narayan & Yi 1994, 1995; Narayan et al. 1996; Quataert & Narayan 1999). In an ADAF, most of the energy released via viscous dissipation remains in the accreting gas rather than being radiated away (as in a thin disk). The bulk of the energy is advected with the flow—hence the name ADAF. Only a small fraction of the energy is radiated by the optically thin gas before the gas reaches the center. The radiative efficiency of an ADAF, which depends on the uncertain fraction of the viscous energy that is channeled to the electrons, is expected to be ~ 0.1 – 1% , whereas the radiative efficiency discussed above for disk accretion is definitely $\geq 5.7\%$. There is little doubt that these radiatively inefficient flows have been observed in quiescent BHBs (§4.3.4) and from galactic nuclei (Baganoff et al. 2001; Loewenstein et al. 2001). However, the theoretical picture has become complex with variant models involving winds (ADIOS; Blandford & Begelman 1999)

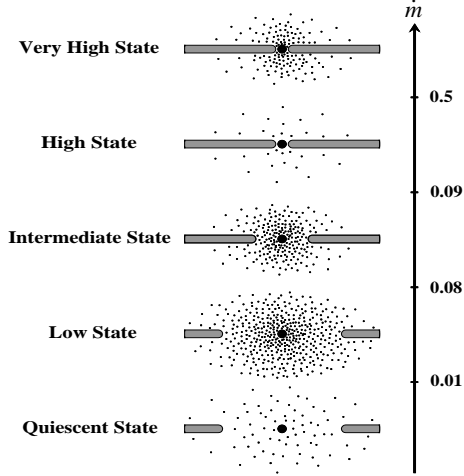


Fig. 4.1. Schematic sketch of the accretion flow in different spectral states as a function of the total Eddington-scaled mass accretion rate \dot{m} . The ADAF is represented by dots and the thin disk by the horizontal bars. The *very high* state is illustrated, but it is not included in the unification scheme (Esin et al. 1997).

and convection (CDAFs; Igumenshchev & Abramowicz 1999; Stone et al. 1999; Narayan et al. 2000; Quataert & Gruzinov 2000)

One attempt has been made to unify four of the five states of a BHB using both the MCD and ADAF models (Esin et al. 1997). Fig. 4.1 shows how the geometry of the accretion flow changes as the mass accretion rate \dot{m} varies (\dot{m} is the mass accretion rate expressed in Eddington units). The scenario indicates how a BH system progresses through five distinct states of increasing \dot{m} from the *quiescent* state to the VH state. In the three states at lower \dot{m} , the flow consists of two zones (disk and ADAF), as described above. For the two states of highest \dot{m} , the disk extends down to the ISCO. In all five states, the disk is bathed in a corona that is a seamless continuation of the ADAF. Apart from the VH state, the model treats consistently the dynamics of the accreting gas, the thermal balance of the ions and electrons in the ADAF and corona, and the radiation processes. The model has had significant successes in describing the spectral evolution of several BHBs (Esin et al. 1997; Esin et al. 1998). (For further discussion of the ADAF model, see §4.3.4.)

However, the four-state model of Esin et al. (1997) has important limitations. For example, it does not unify the most luminous state, the *very high* state, which is characterized by an unbroken power-law spectrum extending out to a few hundred keV or more (§4.3.7). Moreover, it does not account for the dynamic behavior of the corona, including strong flares and powerful low-frequency quasi-periodic oscillations (§4.4), nor does it account for the radio emission observed from most BHBs (Table 4.2). Furthermore, the “evaporation” process by which the cold gas in a thin disk feeds into a hot ADAF is at best qualitatively understood, and there is no quantitative model relating the disk truncation radius to the accretion rate \dot{m} (Narayan 2002, and references therein).

There are alternative models of the X-ray states, and many of them invoke a dynamic accretion disk corona that is fed by MHD instabilities in the disk. For example, in the model of Merloni & Fabian (2001a, 2001b) the hot corona that generates the power-law component is intimately connected with the thin accretion disk. Magnetic energy generated (presumably) by the sheared Keplerian disk creates magnetic flares that rise out of the disk because of the Parker instability. Within the framework of this model, Di Matteo et al. (1999) present a magnetic flare model for the two common states of GX339-4. In the HS state, the flares occur near the disk and heat it. The disk reradiates the observed soft thermal component, whereas the faint hard component is produced by Comptonization of the soft flux. In the LH state, the flares occur far above the disk and the density of soft seed photons is greatly reduced. Thus, the system is photon-starved, and the resultant Comptonized spectrum is hard. Merloni and Fabian (2002) also consider coronae as sources of powerful jets/outflows. They find that such outflows can render a source radiatively inefficient even if advection into the BH is unimportant.

It is generally agreed that the temperatures and optical depths of the corona are in the range 100–300 keV and 0.1–1 (e.g., Merloni & Fabian 2001b). There is little agreement, however, on the geometry and physical properties of the corona. Thus, a wide range of coronal models have been proposed (e.g., Haardt & Maraschi 1991; Dove et al. 1997a, 1997b; Meyer et al. 2000; Rozanska & Czerny 2000; Kawaguchi et al. 2000; Nowak et al. 2002; Liu et al. 2002). Liu et al. conclude that the chief snag is the magnetic fields that produce time variations and spatial inhomogeneities; this complexity is in addition to the complicated radiation/energy interaction between the disk and the corona. Because of the difficulty of the problem, some students of the corona choose to apply their models to large quantities of X-ray (and radio) data, an approach that has proved fruitful. For example, the studies of Cyg X-1 and Seyfert galaxies by Zdziarski et al. (2002, 2003) and GX339-4 by Wardzinski et al. (2002) have yielded several insightful results, such as correlations between the X-ray flux, X-ray spectral index, and the strength of the Compton reflected component from the disk.

In addition to the models discussed above (MCD, ADAF, and coronae), we mention briefly the jet model (e.g., Falcke & Biermann 1995), which is motivated by the observations of resolved radio and X-ray jets (Table 4.2), by observations of radio/X-ray correlations (e.g., Hannikainen et al. 2001; Corbel et al. 2000), and by successes in modeling the broadband spectra of some systems as synchrotron radiation. In the latter category, we point to the extraordinary multiwavelength spectrum obtained for XTE J1118+480 in the LH state that has been modeled successfully both as a thermal ADAF (Esin et al. 2001) and as a synchrotron jet source (Markoff et al. 2001, 2003). For a detailed discussion of the jet model, see Ch. 9.

4.1.6 Consequences of an event horizon

The properties of BHs and BH accretion flows are discussed in many texts (e.g. Shapiro & Teukolsky 1983; Kato et al. 1998; Abramowicz 1998). As mentioned above, the defining feature of a BH is its event horizon, the immaterial surface that bounds an interior region of spacetime that cannot communicate with the external universe. Since BHs lack a material surface, surface effects observed for NSs (e.g.

type I thermonuclear bursts) are absent for a BH. Similarly a BH cannot sustain a magnetic field anchored within it; hence periodic X-ray pulsations, which are observed for many NSs, cannot be generated by a BH. We note that none of the sources listed in Tables 4.1–4.3 has been observed to produce either type I bursts or periodic pulsations.

Both type I bursts and periodic pulsations are considered firm signatures of a NS (TL95). It is interesting to ask what fraction of cataloged, bright sources show either pulsations or type I bursts. We examined this question using the sources cataloged by van Paradijs (1995). We considered only the brighter sources ($F_x > 30 \mu\text{Jy}$) that have been optically identified. We excluded the confirmed and candidate BH systems listed in Tables 4.1–4.3. For the 21 HMXB systems that met our selection criteria, we found that 18 out of 21 (86%) pulse. For the 21 LMXB systems, we found that 12 burst and 2 pulse (67% burst or pulse). Thus a very high fraction of these sources manifest behavior that identifies them as NSs. It is also interesting to consider which systems have failed to produce detectable bursts or pulsations because they are either an unusual NS source or they contain a BH. The three non-pulsing HMXB sources are 1700–37, 1947+30 and Cyg X–3; the seven corresponding LMXB sources are LMC X–2, 1543–62, Sco X–1, GX349+2, GX9+9, 1822–00, and 0042+327.

4.1.7 *Revolutionary RXTE capability inaugurated 1996.0*

The *Rossi X-ray Timing Explorer (RXTE)* has been in continuous operation since its launch on 1995 December 30. Its prime objective is to investigate the fundamental properties of BHs, NSs and white dwarfs by making high time resolution observations near BH event horizons and stellar surfaces. It is the largest X-ray detector array ever flown, and it provides energy coverage from 2–200 keV. It features very high throughput (up to $\sim 150,000$ counts s^{-1}) and $\sim 1\mu\text{s}$ time resolution. *RXTE*'s year-round, wide-sky coverage and its fast response time has made it an extraordinary vehicle for the study of transient phenomena and for the support of multiwavelength science.

The observatory is comprised of two large area instruments (PCA and HEXTE) that act in concert, viewing the sky through a common 1° field of view. The third instrument is an All-Sky Monitor (ASM) that continuously surveys about 80% of the sky each orbit. For descriptions of the instruments and their capabilities, see Levine et al. (1996), Swank (1998), Rothschild et al. (1998), and Bradt et al. (2001). The Proportional Counter Array (PCA), which has a total net area of 6250 cm^2 , is the chief instrument aboard *RXTE*. The PCA consists of five sealed proportional-counter detectors. It is effective over the range 2–60 keV with 18% energy resolution at 6 keV. The High Energy Timing Experiment (HEXTE) covers the energy range 20–200 keV. It is comprised of eight NaI/CsI phoswich detectors with a combined net area of 1600 cm^2 . The HEXTE has provided important spectral information beyond the reach of the PCA. However, the modest count rates of the HEXTE (e.g., 284 counts s^{-1} for the Crab) limit its use for timing studies. Indeed, it is the PCA with a Crab count rate of 13,400 counts s^{-1} that has fulfilled the purpose of the mission and delivered the remarkable timing data for which *RXTE* is renowned.

But it is not the large area of the PCA alone that allowed *RXTE* to break through

to discover kHz QPOs in compact objects. Consider that *RXTE*'s predecessor, the Japanese X-ray astronomy satellite *Ginga* had detectors of similar design and a total net area two-thirds that of *RXTE* (Turner et al. 1989). *RXTE*'s decisive edge is its flexible and powerful data handling and telemetry capabilities. The Experiment Data System (EDS) can process count rates from the PCA up to $\gtrsim 35$ Crab and can time photon arrivals to $\sim 1\mu\text{s}$. In addition to a number of standard PCA modes, the PCA data stream can be binned and telemetered in 6 different modes simultaneously. A telemetry rate of 50 kbps is achieved fairly steadily, and rates up to 256 kbps can be achieved for periods of about a half-hour (Swank 1998).

The ASM is comprised of three wide-field proportional counter detectors that are mounted on a rotating boom. On a daily basis, it surveys up to about 80% of the sky and obtains about 5–10 observations per source. It locates bright sources to a typical accuracy of $\sim 5'$. In uncrowded regions it can monitor sources down to about 35 mCrab (2σ) in one 90-s exposure or about 10 mCrab in one day. On many occasions, the ASM has proved indispensable in alerting PCA/HEXTE observers to targets of opportunity, such as the appearance of a new transient or a state-change in a cataloged source. Furthermore, the ASM archive containing the continuous light curves of ~ 400 X-ray sources (in both Galactic and extragalactic classes) has been invaluable in studying the multiyear behavior of X-ray sources and in supplementing X-ray and multiwavelength (e.g., *Chandra* and *HST*) studies of individual sources. The data are also important to observers of AGN and gamma-ray bursts. Not only is the ASM data archive a public resource, but the intensity measurements and other basic results are made available immediately to the community by the XTE Science Operations Center.

4.2 X-ray light curves, spectra and luminosity data

4.2.1 ASM light curves of BH binaries and BH candidates

The ASM aboard *RXTE* has provided a continuous, seven-year record of the activity of more than 200 Galactic sources. The quality of the data and the extent of the coverage is totally unprecedented. To illustrate the great diversity of behavior among BHBs and BHCs, we show in Fig. 4.2–4.5 the 2–12 keV ASM light curves and the (5–12 keV)/(3–5 keV) hardness ratio (HR2) for 20 of the systems listed in Tables 4.1–4.3 that were active during the past seven years. These light curves should be compared to the heterogeneous collection of ~ 20 X-ray light curves collected by Chen et al. (1997). In making such comparisons, note that we use a linear intensity scale, whereas Chen et al. and most authors use a log scale. The light curves in Figs. 4.2–4.5 are ordered by RA, although we discuss them roughly in order of increasing complexity. An intensity of 1 Crab corresponds to $75.5 \text{ ASM c s}^{-1}$. A hardness ratio (HR2) of 0.5 (1.5) generally corresponds to the HS state (LH state). All good data are included, although the time interval for binning the counts has been tailored to the source intensity. The hardness ratio is not plotted in the absence of a detectable 5–12 keV flux. References are cited sparingly in the narrative descriptions of the light curves given below; see Tables 4.1–4.3 for further references. In the following, the term “classic” light curve refers to an outburst profile that exhibits a fast rise and an exponential decay, like those observed for several pre-

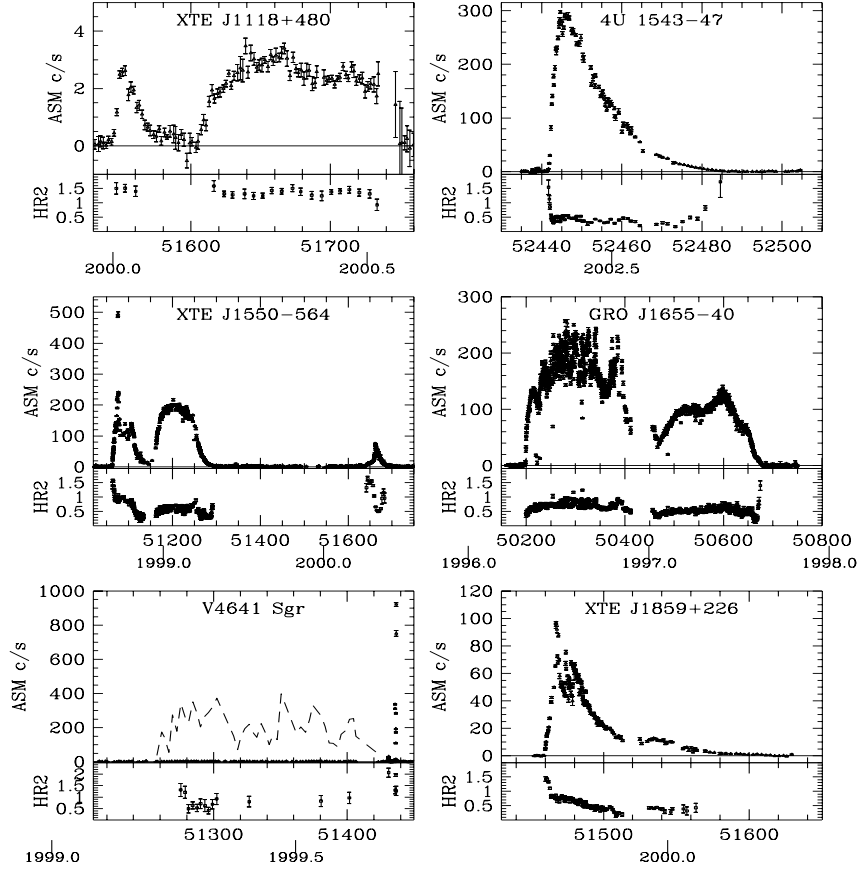


Fig. 4.2. Transient ASM light curves of six black-hole binaries.

RXTE BH X-ray novae including A0620-00, GS/GRS 1124-68, GS 2000+25 and GRO J0422+32 (TL95; Chen et al. 1997). These light curves typically show a secondary maximum (roughly a doubling of intensity) that occurs during the decline phase ~ 40 – 100 days after the onset of the outburst (TL95; Chen et al. 1997).

4.2.1.1 Black-hole binaries

Figure 4.2 shows the light curves of all six of the X-ray novae with short outburst cycles that were detected by the ASM (Table 4.1–4.2). *4U 1543-47*: An exceptionally clean example of a classic light curve with an e-folding decay time of

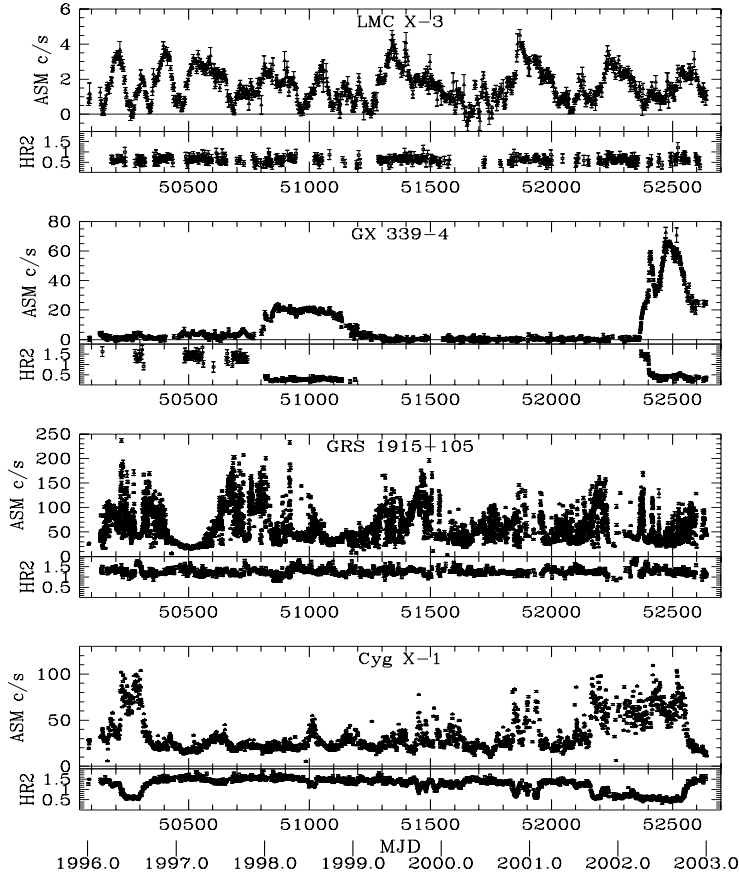


Fig. 4.3. Seven-year ASM light curves of four black-hole binaries.

≈ 14 days. It lacks a secondary maximum, presumably because the outburst is so brief. For details and references on three prior outbursts of this source, see Chen et al. (1997). *XTE J1859+226*: A second example of a classic light curve that does show a secondary maximum (at about 75 days after discovery). Note the intense variability near the primary maximum. *XTE J1118+480*: One of five X-ray novae that remained locked up in a hard state (corresponding to $\text{HR2} \approx 1.5$) throughout the outburst and failed to reach the HS state. Note the prominent precursor peak.

Also shown in Fig. 4.2 are the complex and similar light curves of two X-ray novae

with long orbital periods, GRO J1655–40 and XTE J1550–564. *GRO J1655–40*: This source has undergone two outbursts since its discovery in 1994 July. Shown here is the full light curve of the second, 16-month outburst. The double-peaked profile is quite unlike the classic profile of 4U 1543–47. During the first maximum in 1996, the source exhibited strong flaring and intense nonthermal emission (VH state). In 1997 the source spectrum was soft and thermal except for a hard episode at the very end of the outburst (Sobczak et al. 1999). Note the several absorption dips in the light curve of this high inclination system (Kuulkers et al. 1998). *XTE J1550–564*: The complex profile includes two dominant peaks during 1998–99, followed several hundred days later by a smaller peak in 2000. Not shown here are three very small outbursts (LH states) that have occurred subsequently. Some unusual characteristics include the slow 10-day rise following the source’s discovery on 1998 September 6, followed by the dominant (6.8 Crab) X-ray flare and the abrupt ~ 10 -day decay timescale following each outburst. The source was predominately in the VH or IM states during the first peak (1998), softening to the HS state during the second peak (1999). The spectral evolution through all of the X-ray states occurred much more rapidly during the small peak in 2000. *SAX J1819.3–2525 = V4641 Sgr*: As this extraordinary light curve shows, the source became active at a low level in the spring of 1999 (dashed line shows intensity $\times 50$). Five months later it underwent a brief, violent flare during which the 2–12 keV flux increased very rapidly (within 7 hours) from 1.6 to 12.2 Crab. Within two hours thereafter, the flux declined to less than 0.05 Crab (Wijnands & van der Klis 2000, and references therein).

Figure 4.3 shows the light curves of the two persistent BHBs (LMC X–3 and Cyg X–1) and two other BHBs that have been active throughout the *RXTE* era. *LMC X–3*: The light curve shows the large-amplitude cyclic modulation in the flux reported by Cowley et al. (1991); however, their ~ 198 -day cycle time is much shorter than is indicated by these data for the period 1999–2003. As the hardness ratio plot shows, the source remains in the HS state most of the time. However, at the local intensity minima, where there are gaps in the ASM HRs values due to statistical limitations, the PCA observations show transitions to the LH state (Wilms et al. 2001a). *GX 339–4*: As shown, the source underwent major eruptions into a soft spectral state ($HR \approx 0.5$) in 1998 and 2002. In the time between these two outbursts, the source was very faint (< 2 mCrab) compared to its customary hard-state intensity of ~ 30 mCrab, which it enjoyed prior to its 1998 outburst. Remarkably, this transient BHB has never been observed in a fully *quiescent* state (Hynes et al. 2003). *GRS 1915+105*: This source, which usually displays a hard spectrum, displays extraordinary flaring behavior on time scales from seconds to days. For a view of its remarkable temporal behavior on short time scales, see Morgan et al. (1997), Munro et al. (1999), Belloni et al. (2000), and Klein-Wolt et al. (2002). For a 1992 X-ray light curve showing the birth of this source, see Chen et al. (1997). *Cyg X–1*: Transitions between the LH and HS states were first observed in this archetypal BH source (§4.3.1). However, as this record shows, there are both gradual and rapid variations in the hardness ratio that blur the distinctions between the two states (see §4.3.8).

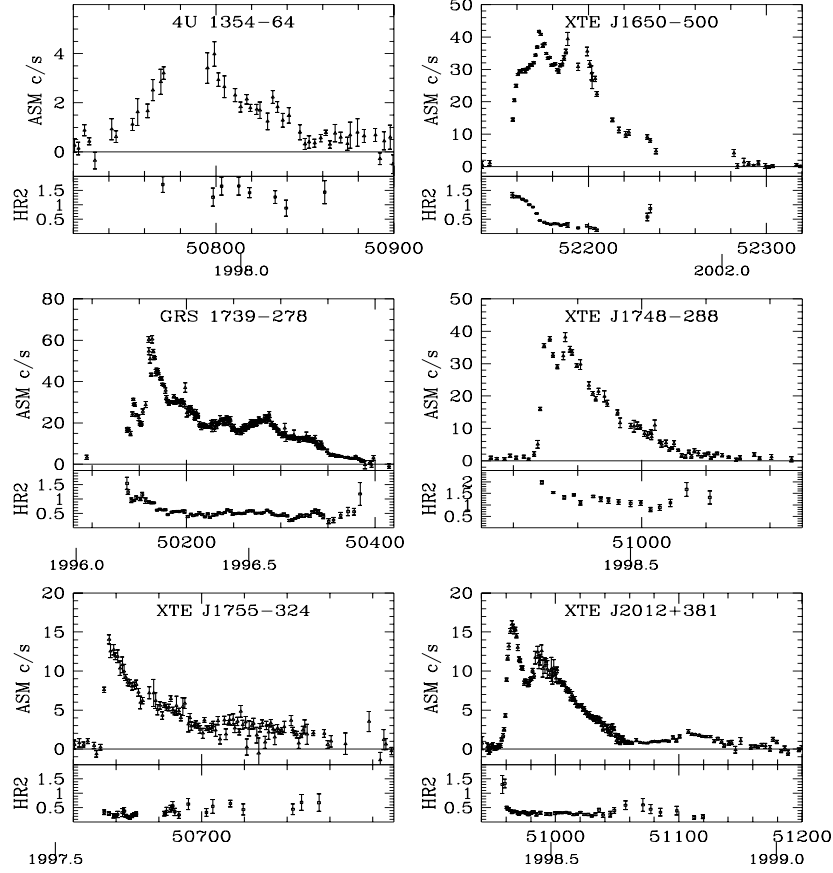


Fig. 4.4. Transient ASM light curves of six black-hole candidates.

4.2.1.2 Black-hole candidates

Figure 4.4 displays the light curves of six BHCs with short outburst cycles. *XTE J748-288*: This short duration outburst that begins and ends in a hard spectral state is similar to the classic light curve of 4U 1543-47 (Fig. 4.2). The $1/e$ decay time is ≈ 16 days. This source is heavily absorbed, and the values of the hardness ratio are consequently increased. *GRS 1739-278*: A somewhat longer duration outburst with a nearly classic profile that is punctuated by a precursor peak, $\sim 40\%$ variability near maximum, and undulations in intensity during the decay. Again, the source begins

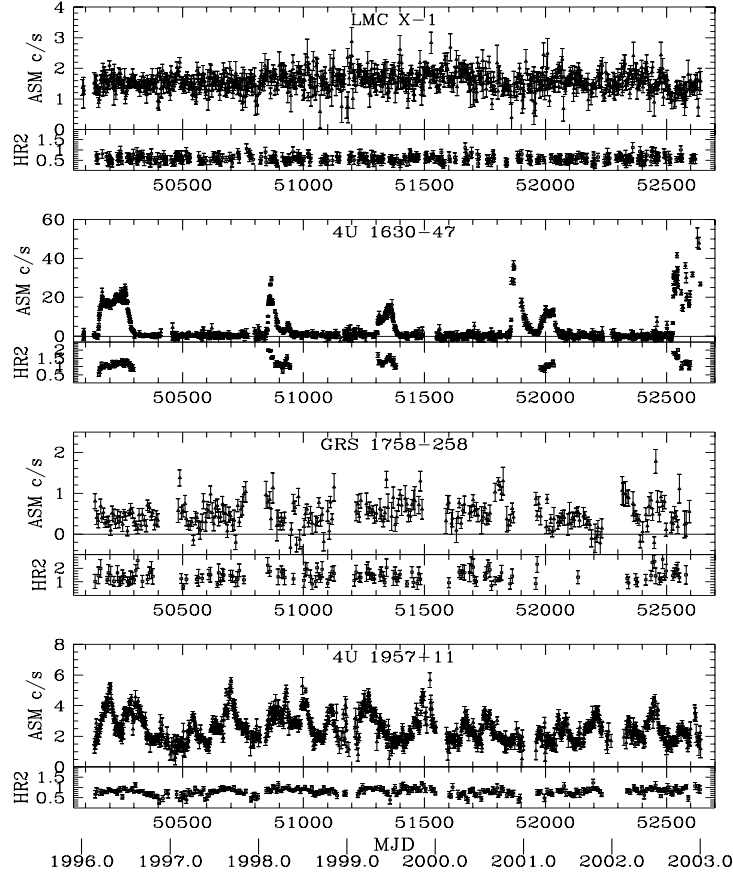


Fig. 4.5. Seven-year ASM light curves of three black-hole candidates and the black-hole binary LMC X-1.

and ends its outburst with a hard spectrum. *XTE J1755-324*: This brief outburst, following an abrupt rise, provides yet another example of a classic light curve. The outburst appears to be locked in the HS state. *XTE J2012+381*: This unusual light curve combines a classic rise to maximum followed directly by a precipitous drop in intensity. Also unusual are a large secondary maximum occurring just 30 days after discovery plus an additional late maximum at ~ 140 days. The outburst plainly starts in a hard state. *XTE J1650-500*: A complex light curve. At the onset of the outburst there is a very rapid rise followed by a slow rise. This unusual behavior is

accompanied by a remarkable, slow (~ 15 -day) transition from a hard spectral state to a soft one. *4U 1354-64*: A slow rise followed by a rather rapid decline. During this outburst, the source displayed an LH state spectrum (Brocksopp et al. 2001), whereas the source was somewhat brighter and did reach the HS state in its 1987 outburst (Kitamoto et al. 1990). This source may be identical to Cen X-2, which reached a peak intensity of 13 Crab in 1967 (Brocksopp et al. 2001).

In Fig. 4.5 we show the light curves of the BHB LMC X-1 and the light curves of three BHCs. *LMC X-1*: The source is continually in a soft spectral state and maintains a relatively steady intensity. *4U 1630-47*: The ~ 600 -day recurrence time of this BHC has been known for 25 years (Jones et al. 1976). Here we see five, nearly equally-spaced outbursts. Note the very different profiles and fluences of the outbursts. Note also that the 1996 outburst starts distinctively with a soft spectrum. *GRS 1758-258*: This hard Galactic center source has received much attention since its discovery by GRANAT/SIGMA in 1991. Its spectrum extends to at least 300 keV (Sunyaev et al. 1991a). During 2001 it underwent a transition to a soft state of very low intensity (Smith et al. 2001; Miller et al. 2002d); the low flux level during that event is evident in the ASM record shown here. *4U 1957+11*: The source has long been considered a BHC based on its “ultrasoft” spectrum (White & Marshall 1984), although Yaqoob et al. (1993) have argued that the primary is a NS. The source is seen to display a consistent flaring behavior and a soft spectrum over the 7-year interval.

It is often said that the spectra of BH X-ray novae *soften* during the initial rise to maximum (i.e. their spectra transition from a hard spectral state to a soft one during the rise). For several sources, the data in Figs. 4.2–4.5 support this view: 4U 1543-47, XTE J1550-564, XTE J1859+226, XTE J1650-500, GRS 1739-278, and XTE J2012+381. However, there are two clear counter-examples, sources whose spectra have been observed to *harden* during the initial rise: GRO J1655-40 (Fig. 4.2) and 4U 1630-47 (Fig. 4.5; first of 5 outbursts).

4.2.2 Synoptic studies of selected black-hole binaries

It is important to attempt to construct a unified spectral model that can be used to represent the energy spectra of all BHBs and to follow the several-month spectral evolution of a single source. The necessary elements of such a model can be deduced from a simple appraisal of the observational data: Cyg X-1 and other BHBs in the LH state show that the model must contain a thermal component, which can be well represented by a power law function (TL95). Similarly, the ultrasoft emission observed for A0620-00 and most BH X-ray novae in the HS state requires a thermal component. As noted above, this component is most widely modeled as a multi-temperature blackbody, which approximates the emission from an optically-thick (relativistic) accretion disk. This choice of a model, comprised of disk blackbody and power-law components, is somewhat arbitrary and the model has significant limitations. However, with a few refinements this model has proved to be widely applicable and the tool of choice in fitting the spectra of BHBs, as we now discuss.

Important studies of *Ginga* spectra using this model were made by Ebisawa et al. (1991, 1993, 1994). The authors added one important refinement to the model, namely, a broad absorption feature above 7 keV. This feature is associated with the

reflection of X-rays by an optically thick accretion disk (Ebisawa et al. 1994, and references therein). Using the amended model, a successful, quantitative comparison was made of the spectra of GS/GRS 1124–68, Cyg X–1, LMC X–3, GS 2000+25, LMC X–1, and GX339–4. In Fig. 4.6, we show the evolution during a full outburst cycle of the spectral parameters for one important source, GS/GRS 1124–68 (Nova Mus 1991; Ebisawa et al. 1994). The source was observed 51 times in 1991 over a span of 235 days using the *Ginga* Large Area Counter (LAC). The X-ray light curve of the source, with its fast rise and exponential decay, is shown in Fig. 4.6f. As noted in §4.2.1, this canonical form has been observed for many BH X-ray novae, including A0620–00 and GS2000+25 (TL95; Chen et al. 1997). The two parameters of the disk blackbody component, the radius of the inner edge of the disk, R^* , and the temperature there, T_{in} , are plotted in Figs. 4.6a–b. The photon spectral index, Γ , and the 2–20 keV flux in the power-law component are shown in Figs. 4.6c–d. Finally, the bolometric flux from the disk component appears in Fig. 4.6e. It is evident in several ways that an important transition occurs near MJD 48394: (1) Γ suddenly decreases from 2.2–2.6 to a value near 1.6; (2) the hard flux increases substantially (Fig. 4.6d, open circles) and the soft disk flux decreases; (3) both the apparent radius and temperature at the inner edge of the disk decrease substantially. This characteristic behavior, which has been observed for a number of BH X-ray novae, marks the transition from the HS (*high/soft*) state to the LH (*low/hard*) state. In conclusion, we note during the HS state the low temperature of the thermal component ($T_{\text{in}} \lesssim 1$ keV) and the constancy of the inner disk radius, which varies by only $\pm 25\%$. For further discussion and a logarithmic display of the fluxes, see Ebisawa et al. 1994.

We now compare these *Ginga* results for the classic BH X-ray nova GS/GRS 1124–68 to the results of a very similar spectral analysis of the irregular BH X-ray nova XTE J1550–564, which was observed extensively by *RXTE* during its 1997–1998 outburst (Sobczak et al. 2000b). A total of 209 pointed observations spanning the entire 255-day outburst were made using the PCA and HEXTE detectors. Sobczak et al. adopted very nearly the same spectral model and methodology as Ebisawa et al. (1994). The results for XTE J1550–564, which are shown in Fig. 4.7, are cast in precisely the same form as those displayed in Fig. 4.7 for GS/GRS 1124–68. The 2–20 keV light curve in Fig. 4.7f alone reveals the relative complexity of the results obtained for XTE J1550–564 (cf. Fig. 4.2). The outburst exhibits a “double-peaked” profile with an intensity lull centered near MJD 51140. This profile is different from the outbursts of classical X-ray novae such as GS/GRS 1124–68 and A0620–00 (TL95), but is similar to the outburst behavior of the BH X-ray nova GRO J1655–40. Other obvious gross differences from classical BH X-ray novae include the intense (6.8 Crab) flare that occurred on MJD 51076 and the slow (10 day) rise to maximum.

Here we remark on a few features of Fig. 4.7, ignoring the intense flare and the lull between the two maxima. For a more extensive discussion, see Sobczak et al. (2000b). During the initial rise, the spectrum is dominated by the power-law component (Figs. 4.7d–e), and the photon index gradually steepens from $\Gamma = 1.5$ to 2.5 (Fig. 4.7c). Strong 0.08–8 Hz QPOs are observed during this period (Cui et al. 1999). Following the initial rise, the plateau spectrum from MJD 51074 to 51115 remains dominated by the power-law component with $\Gamma \sim 2.4$ –2.9 (Fig. 4.7c). Throughout

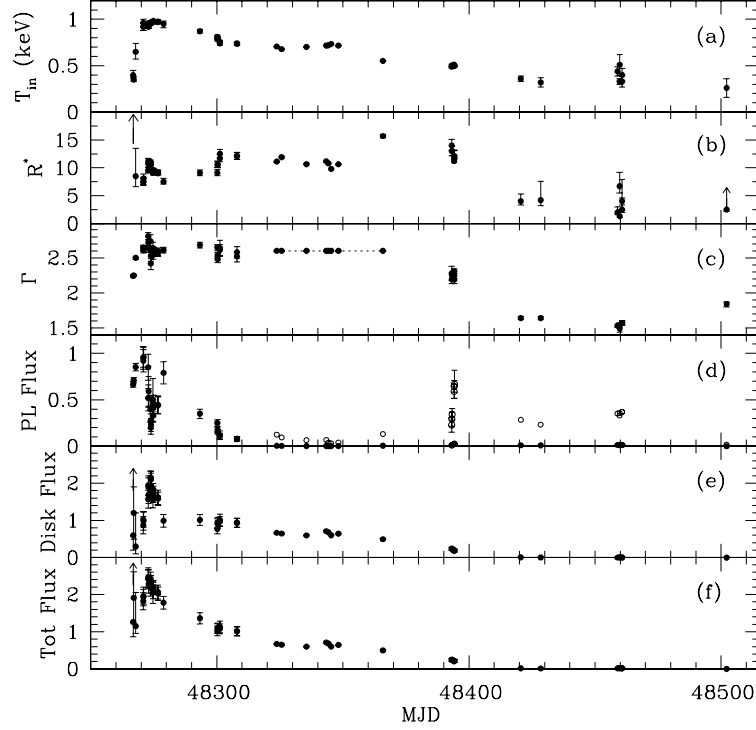


Fig. 4.6. Spectral parameters and fluxes for Nova Mus 1991 (GS/GRS 1124–68) obtained using the *Ginga* LAC (Ebisawa et al. 1994). The fluxes are in units of 10^{-7} erg cm $^{-2}$ s $^{-1}$. The open circles in (d) show a replot of the data x25 to highlight the behavior of the faint power-law component during the second half of the outburst cycle.

this time, whenever the power-law component contributes $\gtrsim 60\%$ of the total flux, strong 3–13 Hz QPOs are present. This behavior is consistent with the *very high* or *intermediate* states (§4.3.7 & §4.3.9). After MJD 51115, the source fades rapidly, the power-law component decays, the disk component begins to dominate the spectrum, and the source shows little temporal variability. This behavior marks the transition to the HS state. During the second half of the outburst (MJD 51150–51230), the disk contributes more than 85% of the flux and QPOs are very seldom observed. Moreover, Fig. 4.7c shows that Γ has doubled from $\Gamma \sim 2$ to 4. These features are typical of the HS state. Thus, in brief one can say that during the first half of the outburst QPOs are ubiquitous and the spectrum is dominated by the power-law component; these conditions correspond to the VH or IM states, and during the second half QPOs are scarce and the spectrum is dominated by emission from the accretion disk, which corresponds to the HS state.

In overview, in both GS/GRS 1124–68 and XTE J1550–564, we see time intervals where the thermal emission from the disk dominates the spectrum, while at other

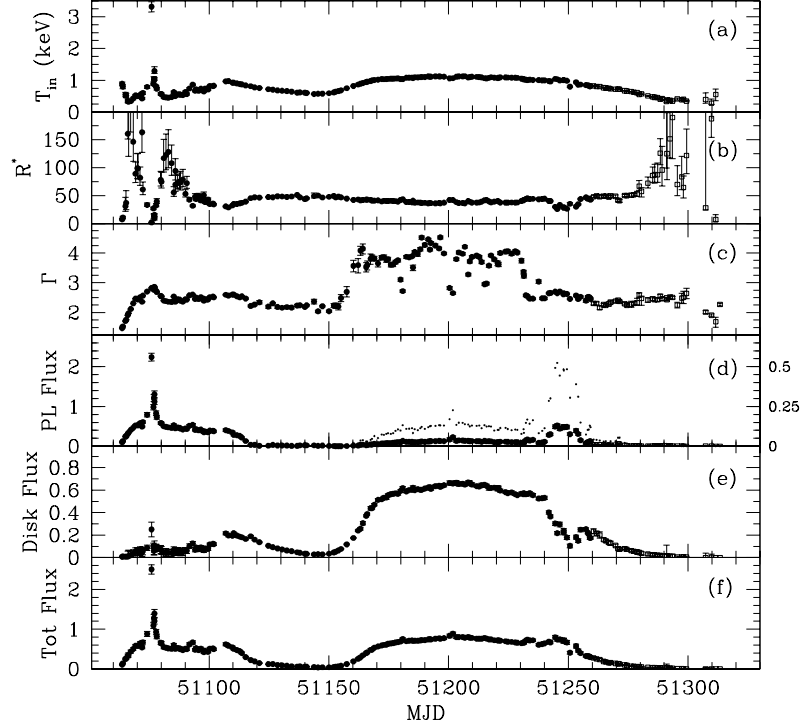


Fig. 4.7. Spectral parameters and fluxes ($10^{-7} \text{ erg cm}^{-2} \text{ s}^{-1}$) for XTE J1550–564 obtained using the *RXTE* PCA (Sobczak et al. 2000b). The error bars are typically smaller than the plotting symbols and are not visible. The small dots plotted without error bars in (d) correspond to the right axis; they highlight the behavior of the faint power-law component during the second half of the outburst cycle.

times the disk spectrum is substantially modified and a power-law component may dominate at either high or low luminosity. In other sources, such as Cyg X–1, the nonthermal LH state may be stable for many months or years, but its soft state spectrum does not resemble the thermal spectra seen from GS/GRS 1124–68 and XTE J1550–564. These results highlight the need to specify the physical properties of X-ray states while avoiding the confusing terminology that has developed during the past 30 years. We therefore return to this issue while seeking clearer definitions of X-ray states in §4.3.

We close this section by discussing the relationship between the radius of the inner disk, R_{in} , and the radius of the innermost stable circular orbit, R_{ISCO} (§4.1.5). Note in Fig. 4.7b the constancy of the inner disk radius, R_{in} , over a ~ 100 day interval during the HS state when the disk emission is dominant. For additional remarkable examples of this behavior in other BH X-ray novae, see Fig. 3.14 and Table 3.2 in TL95. Consider, for example, that the inner disk radius derived for GS 2000+25

varied by $<20\%$ as the X-ray flux decayed by almost two orders of magnitude. As TL95 point out, this constancy of R_{in} over a wide range of mass accretion rates is plausible behavior for an optically thick accretion disk if the parameter R_{in} is related to the radius of the innermost stable circular orbit, R_{ISCO} (§4.1.5). Indeed, R_{ISCO} appears to be the only quantity that is independent of mass accretion rate. For those BHBs with well-determined masses, distances and inclination angles, this hypothesis can be put to the test, although the results depend on two significant corrections to the disk blackbody model: general relativistic corrections to the inner disk radius (Zhang et al. 1997a) and “spectral hardening” corrections for the effects of electron scattering (Shimura & Takahara 1995). Sobczak et al. (1999) applied these corrections to extensive *RXTE* data for GRO J1655–40 and deduced an “effective” (i.e. corrected for spectral hardening) inner disk radius of $R_{\text{eff}} = 6.6R_g$ and a spin parameter of $a_* = 0.5$, with a limit of $a_* < 0.7$. The apparent precision of these results can be eyed with suspicion, since they are based on a nonrelativistic model that requires sizable *ad hoc* corrections, the accuracy of which has been challenged by Merloni et al. (2000). The practicality of this technique remains a subject of continued study. Nevertheless, these results do strongly support the idea that the observed constancy of the inner disk radius is intimately related to the value of R_{ISCO} .

4.2.3 *Relativistic iron emission lines*

Strong evidence for accretion disks in active galactic nuclei has come from X-ray observations of broad iron $K\alpha$ lines. In particular, in some Seyfert galaxies the very asymmetric profile of the Fe $K\alpha$ line (e.g., its extended red wing) suggests strongly that the emission arises in the innermost region of a relativistic accretion disk (for reviews see Fabian et al. 2000, Reynolds & Nowak 2003). The good energy resolution of *ASCA* provided the first clear evidence for such a line profile (Tanaka et al. 1995). In some cases, the line profile indicates the presence of an accretion disk extending down to the last stable circular orbit around the BH (Weaver et al. 2001). The broad Fe $K\alpha$ fluorescence line is thought to be generated through the irradiation of the cold (weakly-ionized) disk by a source of hard X-rays (likely an optically-thin, Comptonizing corona). Relativistic beaming and gravitational redshifts in the inner disk region can serve to create an asymmetric line profile.

In fact, the first broad Fe $K\alpha$ line observed for either a BHB or an AGN was reported in the spectrum of Cyg X–1 based on *EXOSAT* data (Barr et al. 1985). It was this result that inspired Fabian et al. (1989) to investigate the production of such a line in the near vicinity of a Schwarzschild BH, a result that was later generalized by Laor (1991) to include the Kerr metric. Other early studies of relativistically smeared Fe $K\alpha$ lines from BHBs were conducted by Done et al. (1991) and others. Their work was one part of a broader examination of the accretion geometry that is produced as hard X-rays from an overlying corona illuminate the optically-thick accretion disk. An Fe $K\alpha$ line and a reflected continuum is always generated in this case (George & Fabian 1991; Matt et al. 1991). For a recent study of the reflected spectrum of V404 Cyg, which is based on a reanalysis of *Ginga* data, see Zycki et al. (1999a, 1999b). A limitation of this study and most earlier work on BHBs was the use of proportional counter detectors (e.g., the *Ginga* LAC and the *RXTE* PCA,

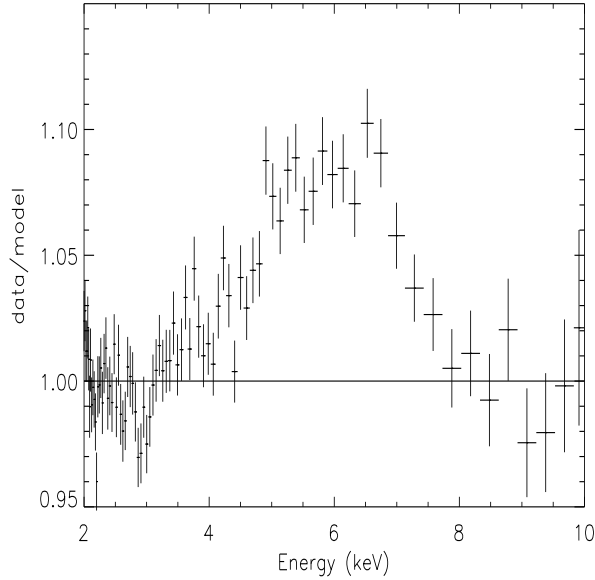


Fig. 4.8. Data/model ratio for XTE J16500-500. The model consists of multicolor disk blackbody and power-law components (Miller et al. 2002b). Note the non-Gaussian shape and low-energy extent of the line profile.

which have an energy resolution of only $\text{FWHM} \approx 1.2$ keV at Fe $K\alpha$). The iron $K\alpha$ studies done using *RXTE* and *Ginga* suffer both because the energy resolution is marginal and because the response matrices of the detectors are uncertain. These instruments can be used to estimate the widths of the lines, but claims that a line has been resolved into multiple components should be treated with reserve. Some iron $K\alpha$ sources that have been studied with *RXTE* include: GRO J1655-40 (Balucinska-Church & Church 2000); XTE J1748-288 (Miller et al. 2001); and GX 339-4 (Feng et al. 2001; Nowak et al. 2002).

More telling studies of the Fe $K\alpha$ line have been achieved using the MECS and HP-GSPC detectors aboard *BeppoSAX*, which have a resolution of ≈ 0.6 keV at Fe $K\alpha$. Broad line profiles (~ 4 –9 keV) have been observed for SAX J1711.6-3808 (in't Zand et al. 2002a) and XTE J1908+094 (in't Zand et al. 2002b); however these profiles are rather symmetric and may be more a product of Compton scattering than relativistic broadening. *BeppoSAX* studies have also revealed other systems with broad, asymmetric Fe $K\alpha$ line profiles that fit the bill for relativistic smearing: GRS 1915+105 (Martocchia et al. 2002) and V4641 Sgr (Miller et al. 2002a). Interestingly, for both systems the inner disk radius deduced from the line profile is consistent with the marginally stable circular orbit of a Schwarzschild BH. A Kerr metric is not required.

Recently, results of studies at higher resolution have appeared that make use of *XMM-Newton* and *Chandra*. Using the former observatory's EPIC-MOS1 detector,

Miller et al. (2002b) find for XTE J1650–500 a broad, skewed Fe $K\alpha$ emission line (Fig. 4.8) which suggests the presence of an extreme Kerr BH and indicates a steep radial falloff of disk emissivity with radius. An observation of Cyg X–1 with the HETGS grating and ACIS–S detector aboard *Chandra* revealed a broad line centered at ≈ 5.82 keV with a FWHM of ≈ 1.9 keV (Miller et al. 2002c). Also present was a smeared Fe edge at ≈ 7.3 keV. The authors conclude that the line is predominately shaped by Doppler/gravitational effects and to a lesser degree by Compton scattering due to reflection.

4.2.4 Super–Eddington luminosities

Recently there has been considerable interest in ultraluminous X–ray sources (ULXs) in external galaxies with 0.5–10 keV luminosities in the range $10^{39} - 10^{40}$ erg s $^{-1}$ (Makishima et al. 2000; Fabbiano et al. 2001; Humphrey et al. 2003; Ch. 12). The luminosities of ULXs greatly exceed the Eddington limit of a $1.4 M_{\odot}$ NS: $L_{\text{Edd}} = 1.3 \times 10^{38} (M_1/M_{\odot})$ erg s $^{-1}$. They also exceed by a factor of $\lesssim 1$ –10 the Eddington luminosity of a typical $10 M_{\odot}$ BH. This fact has led to the suggestion that the most luminous ULXs are a new class of accreting BHs with masses $\lesssim 100 M_{\odot}$ (Makishima et al. 2000; Fabbiano et al. 2001). Alternatively, it has been suggested that the ULXs are powered by conventional stellar–mass BHs that radiate anisotropically (King et al. 2001; Ch. 13). We examine this question by comparing as directly as possible the luminosities of the ULXs to the luminosities of the BHBs listed in Tables 4.1–4.2.

In terms of the maximum flux density, $F_{x,\text{max}}$ (Table 4.2), the 2–11 keV luminosity is: $L_x/L_{\text{Edd}} \approx 2.6 \times 10^{35} \times F_{x,\text{max}}(\mu\text{Jy})(D/10 \text{ kpc})^2$ (Bradt & McClintock 1983). For a Crab–like spectrum (§4.1.2), the flux in the 0.5–10 keV (ULX) band is a factor of 1.9 greater (although this is somewhat of an overestimate compared to the use of a thermal spectrum). Including this factor and using the distances and peak fluxes in Table 4.1, we find that the three most luminous BHBs are V4641 Sgr (6.4×10^{39} erg s $^{-1}$), 4U 1543–47 (4.2×10^{39} erg s $^{-1}$) and V404 Cyg (3.4×10^{39} erg s $^{-1}$). Thus, at peak luminosity, these three BHBs appear to be in the same league as the ULXs observed in external galaxies. Moreover, using the mass measurements from Table 4.1, it appears that all three BHBs were super–Eddington at maximum (0.5–10 keV): $L_x/L_{\text{Edd}} = 6.9, 3.4$ and 2.2 for V4641 Sgr, 4U 1543–47 and V404 Cyg, respectively.

This comparison of BHBs to ULXs carries two caveats: For the BHBs the distances are uncertain, and we have no direct measurements of the fluxes in the 0.5–2 keV band. Nevertheless, these results suggest that a few BHBs rival the most luminous ULXs. Further, they indicate that some or all of the ULXs may be BHBs (King et al. 2001). This suggestion seems even more plausible if one considers the small sample of Galactic BHBs (18 objects) compared to the far larger number of BHBs that have likely been detected, but not identified, in surveys of external galaxies.

We conclude by noting that super–Eddington luminosities have plainly been observed for a few NS systems. The most clear–cut case is A0535–668, the “LMC transient.” This pulsating NS binary with a firm distance of $D = 50$ kpc (Freedman et al. 2001) achieved a peak luminosity of $L_x \approx 1.2 \times 10^{39}$ erg s $^{-1}$, assuming isotropic emission (Bradt & McClintock 1983, and references therein.) This is 6.6

times (3.7 times) the Eddington luminosity of a canonical $1.4 M_{\odot}$ NS (or a hypothetical $2.5 M_{\odot}$ NS).

4.3 Emission states of black-hole binaries

As already discussed in §4.1.2, BHBs exhibit thermal and nonthermal components of X-ray emission, both of which can vary widely in intensity. It has long been recognized that BHBs undergo transitions between quasi-stable states in which one or the other of these emission components may dominate the X-ray luminosity. In the past, the study of BH emission states was based almost exclusively on X-ray spectral and timing studies. More recently, however, the results of these X-ray studies have been supplemented with critical contributions by radio, optical and gamma-ray observers to give us a more physical and fruitful framework for regarding the emission states of BHBs. In the following sections, we review the characteristic behavior that defines each of the principal X-ray states of BHBs. We then describe the current picture of each state in terms of physical structures and the nature of the accretion flow. Finally, we discuss the prospects of using these states to deduce the properties of BHBs.

4.3.1 Historical notes on X-ray states

In the spring of 1971, Tananbaum et al. (1971) observed a remarkable X-ray state change in Cyg X-1 during which the average soft flux (2–6 keV) decreased by a factor of 4 and the average hard flux increased by a factor of 2. Simultaneously, the radio counterpart of Cyg X-1 brightened. It was later found that luminous X-ray novae such as A0620-00 exhibited similar spectral transitions, suggesting that common emission mechanisms were at work in both persistent and transient BHCs (Coe et al. 1976). These early results suggested that such global spectral changes might signify important changes in accretion physics.

As the many light curves in §4.2 illustrate, the soft X-ray state is generally seen at higher luminosity, motivating frequent references to the “high/soft” (HS) state. In this state, the spectrum may also display a “hard tail” that contributes a small percentage of the total flux. As shown by the synoptic studies discussed in §4.2.3, the soft state is best explained as ~ 1 keV thermal emission from a multi-temperature accretion disk (see §4.1.5), as foreseen in the standard theory for accretion in BHBs (Shakura & Sunyaev 1973). However, it has been found that the soft state of Cyg X-1 is not consistent with a thermal interpretation (Zhang et al. 1997b), and this has caused considerable confusion as to the proper way to understand Cyg X-1 and/or describe the HS state. In seeking a physical basis for describing X-ray states, it turns out that Cyg X-1 is not a good choice as a prototype, and further remarks about the states in Cyg X-1 are given in a separate section below (§4.3.8).

In the hard state the 2–10 keV intensity is relatively low, prompting the use of the name “low/hard” (LH) state. The spectrum is decidedly nonthermal and conforms to a power-law with a typical photon index $\Gamma \sim 1.7$ (2–20 keV). In this state, the disk is either not detected at 2–10 keV (e.g., Belloni et al. 1999), or it appears much cooler and larger, compared to the parameters derived for the soft state (Wilms et al. 1999; McClintock et al. 2001b).

An additional X-ray state of BHBs was identified in the *EXOSAT* era by the

demonstration that X-ray QPOs appear when *both* disk and power-law components contribute substantial luminosity (e.g., $> 0.1L_{\text{Edd}}$; van der Klis 1995). In this state, which is referred to as the “very high” (VH) state, the power-law component is observed to be steep ($\Gamma \sim 2.5$). Initially, there were only two BHBs (GX339-4 and Nova Mus 1991) that displayed this behavior, but many additional examples have been seen in the *RXTE* era.

Initially it was thought that the two nonthermal states, i.e., the LH state and the VH state, could be distinguished from each other by differences in their photon spectral indices, luminosities, and power density spectra. However, with further study, as shown below, the means to distinguish the LH and VH states with X-ray observations appears to rely on the difference in the spectral index, while these states are not always distinguishable on the basis of luminosity or PDS characteristics. Furthermore, the need to distinguish the LH and VH states was emphasized in a $\sim 40\text{--}500$ keV study of seven BHBs with the OSSE instrument aboard the *Compton Gamma Ray Observatory* (Grove et al. 1998). The gamma-ray spectra of these sources separate naturally into two distinct groups which were found to correspond to the LH state and VH state, respectively: (1) For the first group it was shown that the X-ray LH state corresponds with a “breaking gamma ray state” in which the spectrum below ~ 100 keV is harder than that of the VH state, but then suffers an exponential cutoff near 100 keV. (2) The other group exhibits a power-law gamma-ray spectrum with photon index $2.5 < \Gamma < 3.0$ over the entire range of statistically significant measurements. This gamma-ray photon index is consistent with the X-ray photon index of the VH state. Furthermore, contemporaneous X-ray observations (e.g., with *ASCA*) confirmed that a luminous thermal component coexists with the power-law component, which is one characteristic of the VH state noted above.

4.3.2 *X-ray states as different physical accretion systems*

Several recent developments in the study of BHBs has taken us beyond a largely phenomenological description of X-ray states to one based on models of physical concepts (e.g., accretion disk, ADAF, jet, and corona). Although this work is still incomplete, the fundamental distinctions between the states are becoming clearer. For example, a key development in this regard is the recognition of a persistent radio jet structure associated with the LH X-ray state, which switches off when the source returns to the HS state (§4.3.6; Ch. 9). Another example is the very different coronal structure that is responsible for the clear-cut distinction afforded by gamma-ray observations between the LH state and the VH state mentioned above. Arguably, each X-ray state can be regarded as a different accretion system that can be used in unique ways to study accretion physics and the properties of accreting BHs.

In the sections below, we review each of the four canonical X-ray states of BHBs, including the long-lived *quiescent* state. We illustrate the uniform X-ray properties of each of the three outburst states by showing X-ray spectra and power spectra for several BHBs and BHCs observed by *RXTE*. We also discuss a possible fifth X-ray state, the “intermediate state,” as part of our discussion of the VH state. While presenting this overview, we suggest an alternative set of state names that are motivated by the emergent physical pictures mentioned above. Although the new state names depend critically on multiwavelength results (i.e., radio to gamma-

ray), we nevertheless attempt to motivate the use of these names solely using X-ray data. Our descriptions of the X-ray states differ from earlier ones because we consider the combined X-ray and multifrequency spectral characteristics of a source. Furthermore, based on extensive observations of many sources with *RXTE* (e.g. see §4.2.3), we abandon luminosity as a criterion for defining the states of BHBs (excluding quiescence).

4.3.3 Notes on X-ray spectral analyses

Many spectral models have been developed that describe one or more of the spectral states of BHBs. Their diversity is due, in part, to the very different spectral shapes observed in the various states, as will be illustrated below. Most of the models for the broad continuum components invoke thermal, inverse Compton, synchrotron, and/or bremsstrahlung emission. Some models closely constrain the relationship between spectral components (e.g., thermal emission providing seed photons for Comptonization) while other models choose parameters that allow the spectral components to vary independently. In presenting this review, we have adopted the following pragmatic and generic strategy. It has been widely demonstrated that the spectra of BHBs are well described by a model consisting of a multi-temperature accretion disk component and a power law component (which may require an exponential cutoff at high energy). This model provides a robust, first-order description of BHB spectra that covers all of the emission states, and we adopt it to help define the states and to compare the luminosities of the thermal and nonthermal components. We also include additional features in the model, such as Fe line emission and a disk reflection component, when the normalization parameter for such a feature is significant at the level of 5σ . In the following discussion on the various X-ray states, we comment on some physical interpretations and controversies, while paying special attention to the origin of the power-law component.

4.3.4 Quiescent state (QS)

As introduced in §4.1.5, most BHBs spend their time in a *quiescent* state that can be summarized as *an extraordinarily faint state* ($L_x < 10^{34} \text{ erg s}^{-1}$), *with a spectrum that is distinctly nonthermal and hard* (photon index, $\Gamma \sim 1.5 - 2.0$). The first short-period X-ray nova to be detected in quiescence was A0620-00 ($P_{\text{orb}} = 7.8 \text{ hr}$); its X-ray luminosity was several times $10^{30} \text{ erg s}^{-1}$, which is only $\sim 10^{-8}$ of its outburst luminosity (McClintock et al. 1995; Narayan et al. 1996). The long-period systems, however, are significantly more luminous in the *quiescent* state because their mass transfer rates are driven by the nuclear evolution of their secondaries rather than by gravitational radiation (Menou et al. 2000). For example, the X-ray luminosity of V404 Cyg ($P_{\text{orb}} = 155.3 \text{ hr}$) is typically $L_x \sim 10^{33} \text{ erg s}^{-1}$ (Kong et al. 2002), but can vary by an order of magnitude on a 1-day time scale (Wagner et al. 1994).

Only recently has it become possible to make sensitive measurements of the *quiescent* state using *Chandra* and *XMM-Newton*. The minimum *quiescent*-state luminosities (0.5–10 keV) of five BHs and stringent upper limits on two others have been reported by Garcia et al. (2001) and Narayan et al. (2002). Subsequently, sensitive observations of three additional BHBs have also been made in quiescence (Sutaria

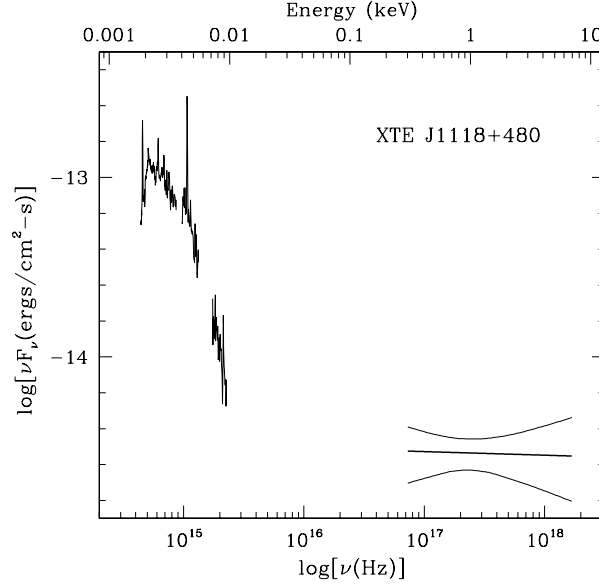


Fig. 4.9. Spectrum of XTE J1118+480 in the *quiescent* state based on simultaneous, multiwavelength observations. The optical spectrum of the mid-K dwarf secondary has been subtracted. Note the Planckian shape of the optical/UV continuum, which is punctuated by a dominant Mg II 2800Å line and a strong H α line on the far left. The best-fit X-ray model is indicated by the heavy, horizontal line; the 90% error box is defined by the flanking curved lines.

et al. 2002; Hameury et al. 2003; McClintock et al. 2003a). Considering only the five short-period systems ($P_{\text{orb}} \lesssim 1$ day; see Narayan et al. 2002) that have been detected, one finds that four of them (XTE J1118+480, GRO J0422+32, GRS 1009-45, and A0620-00) have Eddington-scaled luminosities that are within a whisker of $10^{-8.5}$. (GS 1124-683 is more luminous by about an order-of-magnitude.) As Garcia et al. (2001) and Narayan et al. (2002) show, the Eddington-scaled luminosities of several ostensibly similar X-ray novae that contain NS primaries are about 100 times higher. The authors argue that this result, in the context of the advection-dominated accretion flow model, provides strong evidence for the existence of event horizons in BH X-ray novae.

The spectra of quiescent BH X-ray novae determined using *Chandra* and *XMM-Newton* are well fitted by a single power-law plus interstellar absorption. The photon spectral indices measured for the two best-determined short-period systems are consistent with the value $\Gamma \approx 2$. Specifically, for A0620-00 and XTE J1118+480, respectively, one has $\Gamma = 2.07(+0.28, -0.19)$ (Kong et al. 2002) and $\Gamma = 2.02 \pm 0.16$ (McClintock et al. 2003a). The spectra appear to be somewhat harder for three long-period systems: The mean value of the photon index is $\Gamma \approx 1.4$, and the individual measurements range from 1.3 to 1.55 (Hameury et al. 2002; Kong et al.

2002). The long-period system V404 Cyg has the best determined spectral index: $\Gamma = 1.55 \pm 0.07$ (Kong et al. 2002).

A *quiescent*-state multiwavelength spectrum of the BH primary in XTE J1118+480 is shown in Figure 4.9 (McClintock et al. 2003a). This shortest-period BH X-ray nova ($P_{\text{orb}} = 4.1$ hr) is located at $b = 62^\circ$ and therefore the transmission of the ISM is very high (e.g., 70% at 0.3 keV). A very similar spectrum was observed earlier for A0620-00 (McClintock & Remillard 2000, which implies that the spectrum shown in Figure 4.9 represents the canonical spectrum of a stellar-mass BH radiating at $10^{-8.5} L_{\text{Edd}}$. The spectrum is comprised of two apparently disjoint components: a hard X-ray spectrum with a photon index $\Gamma = 2.02 \pm 0.16$, and an optical/UV continuum that resembles a 13,000 K disk blackbody spectrum punctuated by several strong emission lines.

The ADAF/disk model described in §4.1.5, accounts well for the following observations of BHBs that have been made in the QS, including those mentioned above: (1) The hard power-law spectra (Narayan et al. 1996; Narayan et al. 1997; Hameury et al. 1997; Quataert & Narayan 1999); (2) the faintness of BHs relative to NSs (Narayan et al. 1997; Garcia et al. 2001; Narayan et al. 2002; (3) the several-day delay in the optical/UV light curve when X-ray novae go into outburst (Hameury et al. 1997); and (4) the broadband spectrum shown in Figure 4.9 (McClintock et al. 2003a). Especially significant is the prediction, since confirmed by observations, that the accretion disk is truncated at a large inner radius in both the *quiescent* state and the LH state (Narayan 1996; Esin et al. 1997; McClintock et al. 2001b; McClintock et al. 2003a).

4.3.5 Thermal-dominant (TD) state or high/soft (HS) state

As discussed in §4.1.5, considerations of basic principles of physics predict that accreting BHs should radiate thermal emission from the inner accretion disk (Shakura & Sunyaev 1972). It was therefore readily accepted that the soft X-ray state of BHBs was due to such thermal emission. Confirmations of this picture are largely based on the successful ability to describe the soft X-ray component using the simple multi-temperature accretion disk model (MCD model; §1.1.6). The MCD model in combination with a power-law model is routinely used to deconvolve the thermal and power-law components in the spectra of BHBs. In Figures 4.10 and 4.11 we show the energy spectra and power spectra, respectively, of 10 BHBs in the “thermal-dominant” (TD) or “high/soft” (HS) X-ray state as observed by *RXTE*. The thermal component of the model, where it can be distinguished from the data, is shown as a solid line, and the power-law component is shown as a dashed line. Typically, below about 10 keV the thermal component is dominant. With two exceptions, the temperature of this component falls in the range 0.7–1.5 keV Table 4.4. The power-law component is steep ($\Gamma = 2.1 - 4.8$) and faint. In GRS 1915+105 the power-law falls off even more steeply with an e-folding cutoff energy of 3.5 keV; similar behavior has been reported for GRO J1655-40 (Sobczak et al. 1999).

In Fig. 4.10 we feature data for BHBs obtained during pointed observations with *RXTE*, while data for BHCs are shown in Fig. 4.11. For four sources (4U 1543-47, GX 339-4, XTE J1755-324, and XTE J2012+381), the energy spectra shown here

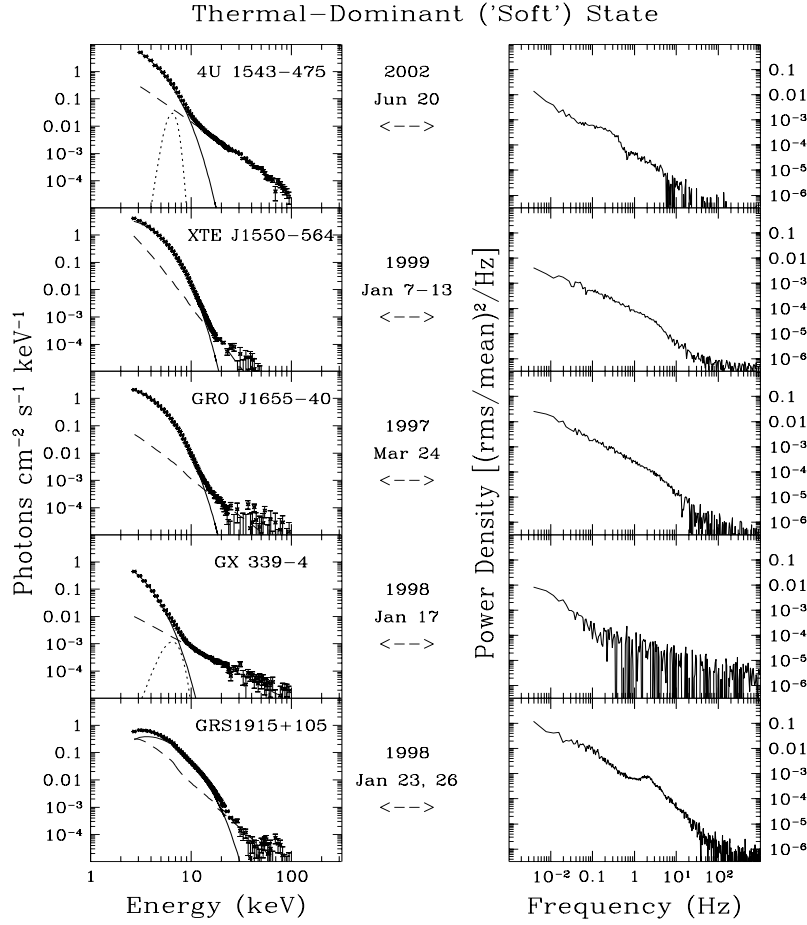


Fig. 4.10. Sample X-ray spectra of BHBs in the X-ray state for which the dominant component is thermal emission from the accretion disk. The energy spectra (left) are decomposed into a thermal component, which dominates below ~ 10 keV (solid line), and a faint power-law component (dashed line); GRS 1915+105 is modeled with a cutoff power-law (see text). For two of the BHBs, an Fe line component is included in the model (dotted line). The corresponding power spectra are shown in the panels on the right.

correspond to the maximum luminosity (for each source) that has been observed during *RXTE* pointings (i.e. considering any state).

In the power density spectra (PDS) in Figures 4.10 and 4.11, we see that the TD state is associated with either weak variability or continuum power that scales

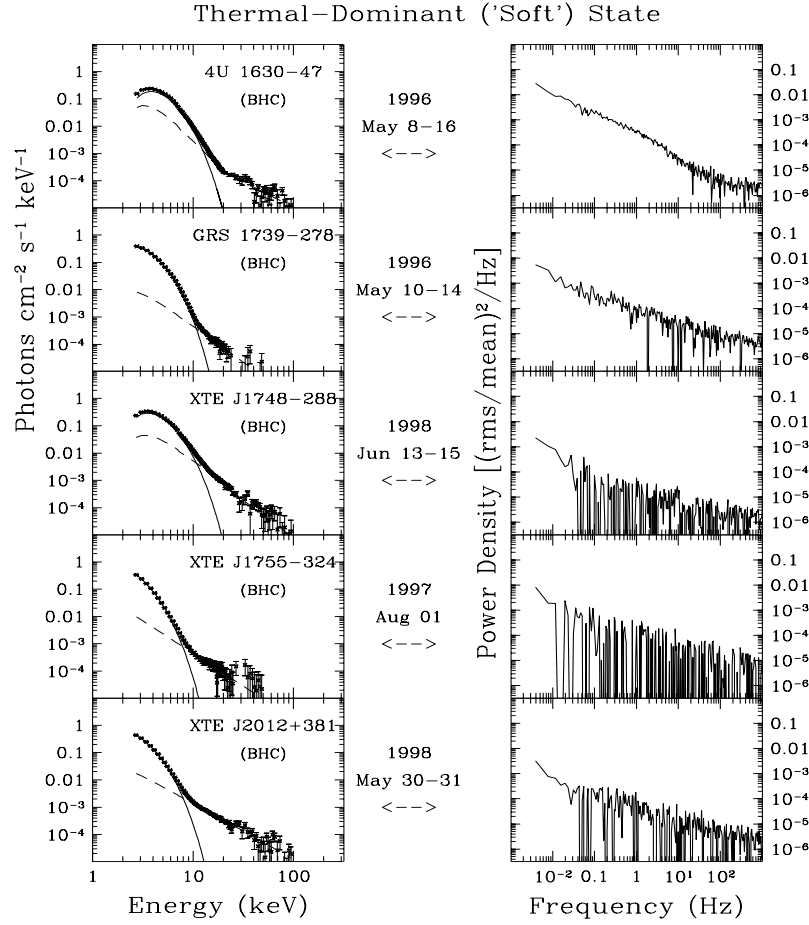


Fig. 4.11. *Left panels:* Sample X-ray spectra of BHCs in the TD X-ray state. In the panels on the left, the energy spectra are shown deconvolved into a thermal component due to the accretion disk (solid line) and a power-law component (dashed line). The corresponding power spectra are shown in the right half of the figure.

roughly as ν^{-1} , which is a power spectrum that is observed for many physical processes including turbulence (Mandelbrot 1999). The total integrated rms power in these PDS is significantly below that of the nonthermal X-ray states.

In the following section, we show that a transition to the LH state is followed by the appearance of a dominant, hard, power-law spectrum, while the accretion disk, if

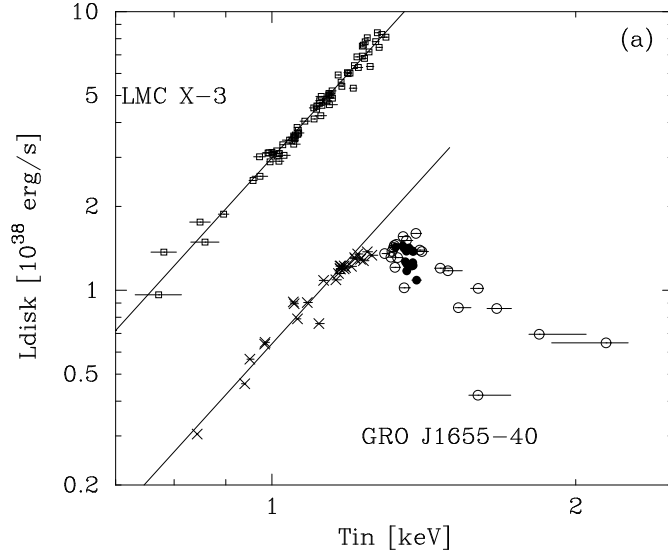


Fig. 4.12. The accretion disk luminosity *vs* temperature at the inner accretion disk (Kubota et al. 2001). For GRO J1655-40, the symbol type denotes the time periods: early outburst (filled circles), first phase (open circles), and second phase (crosses). The solid lines represent the $L_{\text{disk}} \propto T_{\text{in}}^4$ relation.

visible, shows a substantial decrease in temperature. On the other hand, a transition to the VH state (§4.3.7) is marked by a steeper power-law spectrum accompanied by either a normal (~ 1 keV) disk or one that appears hot and small. Usually, this latter transition is also accompanied by the presence of QPOs that appear when the disk contribution to the total, unabsorbed flux at 2–20 keV falls below the level of 0.75 (Sobczak et al. 2000a). *We thus define the TD state as a set of conditions for which the disk-flux fraction is above 75%, the PDS shows an absence of QPOs, and the power continuum is weak, falling below $10^{-3} (\text{rms/mean})^2 \text{ Hz}^{-1}$ at 1 Hz.*

As further support for a thermal interpretation of the soft X-ray component, many studies have found evidence for disk luminosity variations in which the inner disk radius (which scales as the square root of the thermal normalization constant) appears constant while the luminosity variations depend only on changes in temperature (§4.2.3). A recent demonstration of this effect is reported in a study of LMC X-3 (Kubota et al. 2001) and is illustrated in Fig. 4.12. The measured disk flux and apparent temperature successfully track the relation $L \propto T^4$ (solid line) expected for a constant inner disk radius. The figure also shows the deviations from this relation associated with the VH state of GRO J1655-40, a topic that is addressed in §4.3.7 below.

4.3.6 Low/hard (LH) X-ray state associated with a steady radio jet

The concept of X-ray states was originally motivated by the discovery that the spectra of both Cyg X-1 and several transient sources occasionally switch between a putative thermal condition and a decidedly nonthermal condition (§4.3.1).

The latter state, usually seen at luminosities below that of the TD state, is often modeled (e.g., 1–20 keV) as a power-law function with a photon index ~ 1.7 . In Cyg X–1 and a number of other sources, this state is accompanied by a broad enhancement at 20–100 keV which is interpreted as reflection of the power-law component from the surface of the inner accretion disk (Di Salvo et al. 2001). This component is discussed further at the end of this section.

In recent years there have been rapid advances in associating the X-ray LH state and the presence of a compact and quasi-steady radio jet (for a thorough review, see Ch. 9). This relationship, which constitutes one of the foundations of the “disk : jet” connection, is based on at least three arguments. First, VLBI radio images have shown a spatially-resolved radio jet during episodes of quasi-steady radio and hard X-ray emission from both GRS 1915+105 (Dhawan, Mirabel, & Rodriguez 2000) and Cyg X–1 (Stirling et al. 2001). In both instances the radio spectrum was flat or inverted. Second, more generally (i.e., when VLBI imaging is not available), X-ray sources that show prolonged periods (weeks to years) of hard X-ray emission and a relatively flat spectrum ($\Gamma \sim 1.7$) are highly likely to show correlated radio emission with a flat radio spectrum (Fender et al. 1999a; Fender 2001; Corbel et al. 2000; Klein-Wolt et al. 2002; Marti et al. 2002; Corbel et al. 2003). In one of these examples (GX 339-4; Corbel et al. 2000), the jet interpretation is further supported by the detection of 2% linear polarization with a nearly constant position angle. Finally, it is now routine to witness the quenching of the persistent radio emission whenever an X-ray source exits the LH state and returns to the TD state, thereby restoring its accretion disk (Fender et al. 1999b; Brocksopp et al. 1999; Corbel et al. 2000).

In Fig. 4.13, the five BHBs shown in the LH state are the same sources shown displaying TD spectra in Fig. 4.10. In the following cases, the data have been selected to coincide with specific radio observations: Flat-spectrum radio emission was reported for both XTE J1550–564 on 2000 June 1 during the decay of its second outburst (Corbel et al. 2001) and for GX 339-4 on 1999 March 3 (Corbel et al. 2000). In addition, both the radio and X-ray emission of GRS 1915+105 are fairly steady on 1997 October 22, which coincides with one of the days in which the core radio image shows the extended structure of a nuclear jet (Dhawan et al. 2000).

A second sample of BHBs and BHCs in the LH state is shown in Fig. 4.14. The LH state for XTE J1748–288 occurred during decay from the HS state (Revnivtsev et al. 2000c). On the other hand, the data shown for XTE J1118+480 and GS 1354-64 correspond with outburst maxima, since these X-ray novae never reached the HS state (Revnivtsev et al. 2000a; Frontera et al. 2001b). Associated radio emission for these two sources was reported with jet interpretations by Fender et al. (2001) and Brocksopp et al. (2001), respectively. Finally, GRS 1758–258 and Cyg X–1 spend most of their time in the LH state, and their energy spectra, which are shown in the bottom two panels of Fig. 4.14, are typical LH-state spectra. These *RXTE* observations happened to coincide with radio observations that confirm a flat radio spectrum: In the case of GRS 1758–258, core radio emission (as distinct from the extended radio lobes observed for this source) was reported on 1998 August 3 and 5 by Marti et al. (2002), and a clear detection of Cyg X–1 during 1997 December

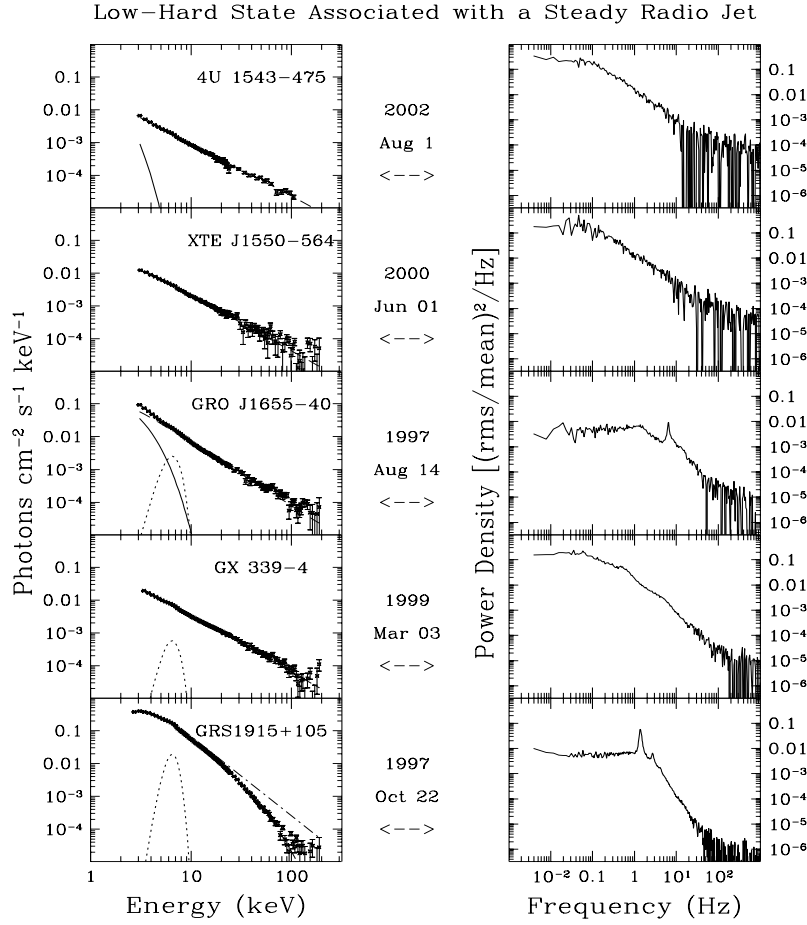


Fig. 4.13. Sample spectra of BHBs in the LH state. The energy spectra are characterized by a relatively flat power-law component that dominates the spectrum above 1 keV. A second characteristic of the LH state is the elevated continuum power in the PDS. This state is associated with the presence of a steady type of radio jet (see text). The selected X-ray sources are the same BHBs shown in Fig. 4.10. The individual spectral components include the power-law (dashed line) and, if detected, the accretion disk (dotted line) and a reflection component (long dashes).

12–17 is evident in the public archive of the Greenbank Interferometer available on the NRAO web site.

The physical condition of the accretion disk in the LH state is a subject of great

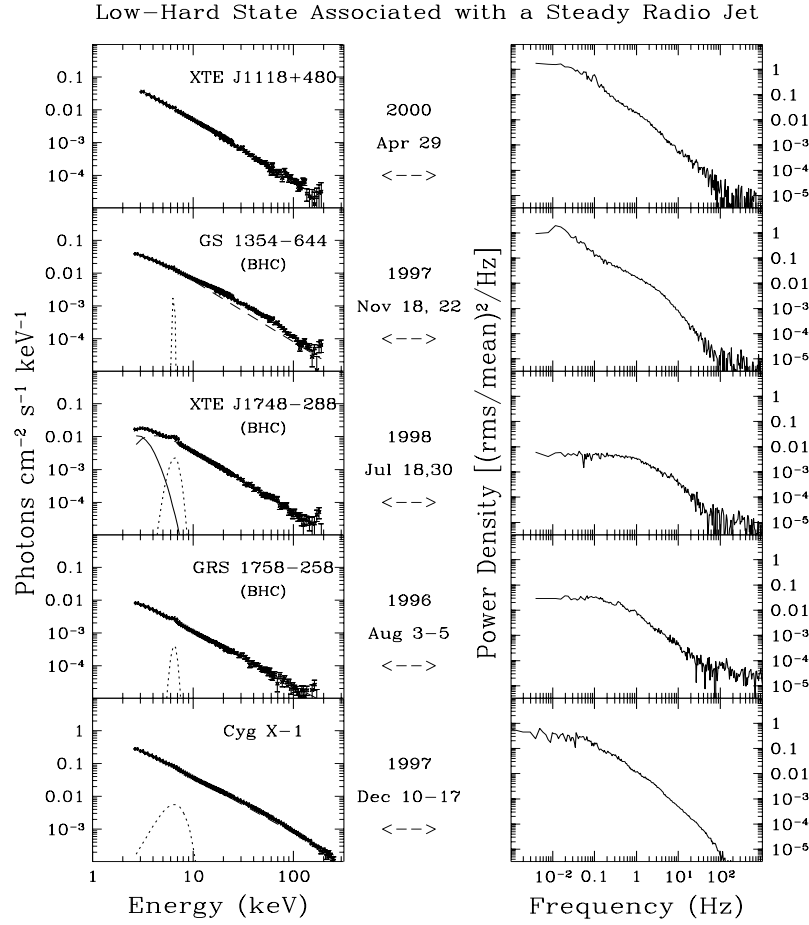


Fig. 4.14. A second sample of BHBs or BHCs seen in the LH state. The observations of XTE J1748-288 occurred during outburst decay, while XTE J1118+480 and GS 1354-64 are seen in the LH state at the peaks of their respective outbursts. GRS 1758-258 and Cyg X-1 spend most of their time in the LH state. There is radio coverage that confirms the presence of a flat radio spectrum for all the sources except XTE J1118+480. The line types denoting the spectral components follow the convention of Fig. 4.13

significance in the effort to build a detailed physical model for both the jet and the X-ray source. Observations with *ASCA*, which provided sensitivity in the range 0.5 to 9 keV, showed that the LH states of both GX 339-4 (Wilms et al. 1999)

and Cyg X-1 (Takahashi et al. 2001) exhibit power-law spectra with an additional soft X-ray excess that can be modeled as a large and cool (~ 0.1 – 0.2 keV) accretion disk. The spectral decompositions illustrated in Fig. 4.13 provide some evidence for a soft disk component in both GRO J1655-40 and GRS 1915+105, although *RXTE* is much less sensitive than *ASCA* to thermal spectra with temperatures well below 1 keV. By far, the best direct measurements of the temperature and inner radius of an accretion disk in the LH state have been made for XTE J1118+480, which suffers an extraordinarily small interstellar attenuation (e.g., only 30% at 0.3 keV). Based on simultaneous *HST*, *EUVE* and *Chandra* observations made in outburst, it was determined that the inner disk radius and temperature for the MCD model were $\gtrsim 100 R_g$ and ≈ 0.024 keV, respectively (McClintock et al. 2001b). Somewhat higher temperatures (≈ 0.035 – 0.052 keV) have been inferred from observations using BeppoSAX (Frontera et al. 2003).

While it seems clear that the blackbody radiation appears truncated at a large radius ($\sim 100 R_g$) in the LH state, the physical state of the hot material within this large radius is still a matter of debate. Is the disk completely truncated at this radius in the LH state, as envisioned in the ADAF model (e.g., Esin et al. 2001), or is a substantial amount of matter present in a relativistic flow that is entrained by the magnetic field of a jet (e.g., Markoff et al. 2001)? Or is the inner disk basically intact and either depleted of energy or veiled in some type of Compton corona? This latter possibility is strongly constrained by the absence of any thermal component of emission from the inner disk of XTE J1118+480 (Esin et al. 2001; Frontera et al. 2003).

Guidance in sorting out these options may eventually be gained from spectral analyses that focus on broad Fe emission features (see Reynolds and Nowak 2003) or the X-ray reflection component (Done & Nayakshin 2001). These spectral features depend on substantial density in the inner disk, while the Fe line additionally reveals the pattern of Keplerian flow modified by effects due to general relativity (see §4.2.4). Systematic studies of these features during different BHB states and transitions could help to determine the physical changes in the inner disk associated with the LH state. The reflection component is most apparent when the observer's line of sight has a low inclination with respect to the pole of the disk. One such system viewed at a low inclination angle is Cyg X-1, and a reflection analysis has been reported by Done & Zycki (1999). They find that the disk is physically truncated, but the transition radius (tens of R_g) is not as far from the event horizon as suggested by the value of R_{in} derived (i.e. taken literally) from the disk spectrum in the LH state.

The origin of the X-ray power-law is another aspect of the controversy concerning the appropriate physical model for the LH state. As noted above, we regard the power-law fit as a general signature of nonthermal radiation; however, the observed spectrum can be produced by several different radiation mechanisms. This is well illustrated in the case of XTE J1118+480, where the X-ray spectrum has been fitted by an ADAF model (Esin et al. 2001), a synchrotron model (Markoff et al. 2001) and a thermal-Comptonization model (Frontera et al. 2001b). At the present time, we expect valuable inputs from INTEGRAL observations that will further constrain the spectral shape of the LH state beyond 100 keV and any changes that may be correlated with luminosity.

Despite the large uncertainties that remain for physical models, it would appear that the association of the LH state with a steady radio jet is an important step forward. And it does remain possible to identify the LH state solely from X-ray spectral and temporal properties, as had been done in the past (TL95). Using Figs. 4.13 & 4.14 and Table 4.4, *we conclude that the LH state is well characterized by three conditions: the spectrum is dominated ($> 80\%$ at 2–20 keV) by a power-law spectrum, the spectral index is in the range $1.5 < \Gamma < 2.1$, and the power density at 1 Hz is well above $10^{-3} (\text{rms/mean})^2 \text{ Hz}^{-1}$.*

4.3.7 Steep power-law (SPL) state or very high (VH) state

There are times when BHBs become exceedingly bright ($L_x > 0.2L_{\text{Edd}}$), and the X-ray spectrum again displays substantial nonthermal radiation, which may constitute 40–90% of the total flux. In such cases the photon index is typically $\Gamma \geq 2.5$, which is steeper than the index ($\Gamma \sim 1.7$) seen in the LH state. The strength of this steep power-law component also coincides generally with the onset of X-ray quasi-periodic oscillations (QPOs) in the range 1–20 Hz. This type of behavior (i.e., high luminosity, a strong and steep power-law component, and X-ray QPOs) was initially seen in only two instances: during a bright outburst of GX 339-4 (Miyamoto et al. 1991) and near the time of maximum flux in X-ray Nova Muscae 1991 (= GS/GRS 1124-683; Miyamoto et al. 1993). The straightforward interpretation of these observations was that this “very high” (VH) state was a signature of the highest rate of mass accretion in a BHB system (van der Klis 1995).

As mentioned previously (§4.3.1), the high-energy spectra of several BHCs observed with OSSE on *CGRO* (40–500 keV) reinforced the distinction between the X-ray LH and VH states, showing that the LH-state spectra exhibit a steep cutoff near 100 keV (Grove et al. 1998). On the other hand, the X-ray VH-state spectra showed no evidence for a high-energy cutoff; i.e., in this state the photon index in the X-ray and gamma-ray bands is the same ($\Gamma \sim 2.5$ –3.0). The unbroken power-law spectra observed by OSSE for five sources suggested that these BHBs had also been observed in the VH state, although this was not confirmed by the simultaneous detection of X-ray QPOs.

The monitoring programs of *RXTE* have shown that the VH state is both more common and more complicated than originally envisioned. Some sources have shown the capacity to display both X-ray QPOs and a steep power-law component while maintaining luminosity levels at 2–20 keV (Remillard et al. 2002b; §4.5) that are well *below* the maxima seen even in their TD (HS) state. This topic is considered further in §4.3.9 below. In response to these developments, we hereafter refer to this state as the “steep power-law” state, or the SPL state, rather than the VH state. We adopt this new name because the steep power-law is a fundamental property of this state, whereas a very high luminosity is not an essential property. We view the presence of QPOs as a confirming property of the SPL state.

In Fig. 4.15 we show examples of the SPL state for the same five BHBs considered in Figs. 4.10 and 4.13. The photon index of the steep power-law component covers the range $2.4 < \Gamma < 3.0$ as shown in Table 4.4, and QPOs are present with central frequencies over the range 5–13 Hz. The spectra of XTE J1550-564 and GRO J1655-40 (Fig. 4.15) correspond to the highest luminosities that have been observed for these

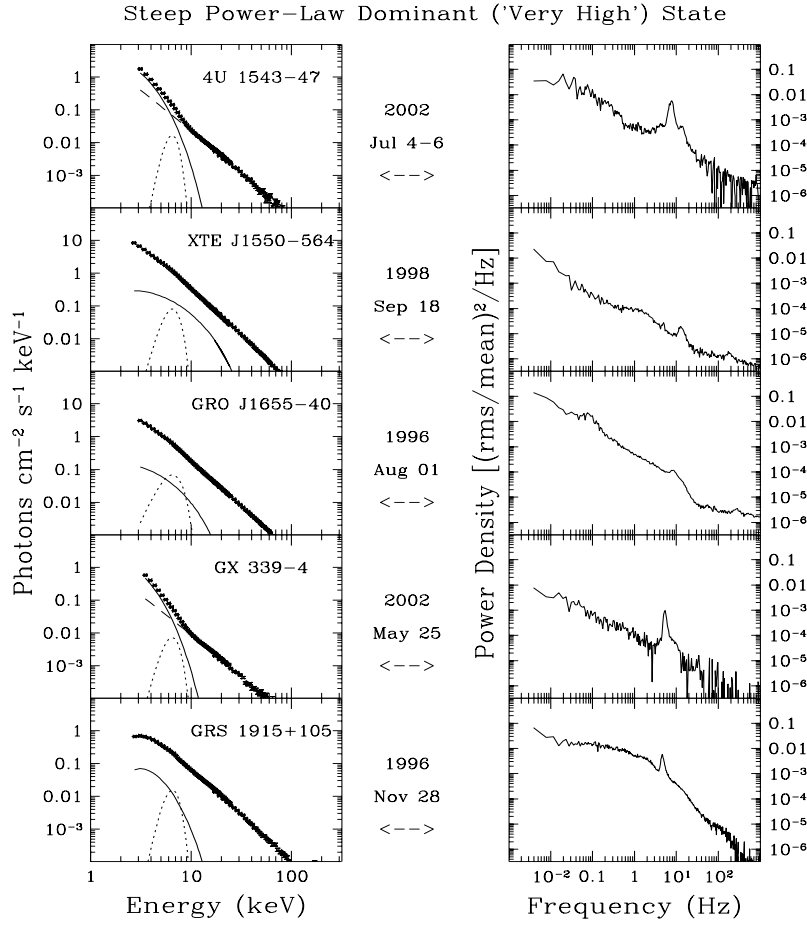


Fig. 4.15. X-ray spectra of BHBs in the SPL state, which is characterized by a strong and steep power-law component in the energy spectrum, along with the presence of X-ray QPOs. The dashed and dotted lines follow the convention of earlier figures.

sources during pointed observations with *RXTE* (Sobczak et al. 2000b; Sobczak et al. 1999); moreover, both observations revealed the presence of high-frequency QPOs, 186 Hz and 300 Hz, respectively (Remillard et al. 2002b). The relationship between the SPL state and high-frequency QPOs will be discussed in further in §4.4.3.

In Fig. 4.16 we show spectra of the SPL state for three BHCs and two additional BHBs. For three of the sources we have near-maximum) fluxes that have been

observed in *RXTE*s pointed selected observations that correspond to the maximum (or observations). For the two remaining sources we consider local maxima: the 1996 soft-state episode of Cyg X-1 and the second outburst of 4U 1630-47 (for references, see Tables 4.1-4.3). X-ray QPOs are seen in the top four panels (5-8 Hz in three cases and 31 Hz in the case of XTE J1748-288). The power spectrum of Cyg X-1 contains broad continuum features but no X-ray QPOs, although the energy spectrum indicates that the source is in the SPL state.

We can encompass all of these SPL examples with the following criteria (see also Sobczak et al. 2000a). *The SPL state is defined by (1) The presence of a power-law component in the X-ray spectrum with photon index, $\Gamma > 2.4$, and (2) Either X-ray QPOs are present (0.1-30 Hz) while the power-law contributes more than 20% of the total (unabsorbed) flux at 2-20 keV, or the power-law contributes more than 50% of the total flux without detections of QPOs.*

The radio properties of the SPL state are an important and complicated topic that calls for the heightened attention of observers. Here we highlight several salient results. The brightest days of GRO J1655-40 during its 1996-1997 outburst occurred in the SPL state (1996 August) when the source appeared radio-quiet (Tomsick et al. 1999). Similarly, Cyg X-1 becomes radio quiet whenever the spectrum switches from the LH state to an SPL-like state. On the other hand, the SPL state is also associated with the explosive formation of radio jets. For example, the giant X-ray flare in XTE J1550-564 (with SPL-state properties shown in Fig. 4.15) has been linked to a relativistic mass ejection that was observed as a superluminal separation of bipolar radio jets (Hannikainen et al. 2001). However, there is a distinct possibility that the X-ray flare in the SPL state may have occurred after the moment of ejection, at a time when the radio properties of the core (i.e., the inner disk) are unknown. This conjecture is supported by radio observations of the same source during the 2000 outburst when a radio flare was observed to decay below detectable levels while the source remained in the VH state (Corbel et al. 2001). We conclude that the best available evidence suggests that the SPL state is essentially radio quiet, and that the instability that causes impulsive jets further provides an accretion rebound that favors the SPL state.

The physical origin of the SPL spectrum, which has a strong, nonthermal component that extends upward in energy to ~ 1 MeV (Table 4.2), remains one of the outstanding problems in high-energy astrophysics. At stake is our understanding of accretion physics at those extraordinary times of peak luminosity. Equally important is our need to interpret the high-frequency X-ray QPOs associated with the SPL state. As discussed in §4.4.3, these fast QPOs may provide a constraint on the mass and spin of the accreting BH via an interpretation of the measured frequencies as effects of general relativity.

Most models for the SPL state invoke inverse Compton scattering as the operant radiation mechanism (see Zdziarski 2000). The SPL spectrum has been observed up to photon energies of ≈ 1 MeV in several sources: e.g., Cyg X-1, GRO J1655-40 and GRO J0422+32 (Table 4.2). The spectrum may extend to even higher energies, but present investigations are limited by photon statistics. The broad extent of this unbroken power-law spectrum has motivated proposals that the scattering occurs in a nonthermal corona, which may be a simple slab operating on seed photons

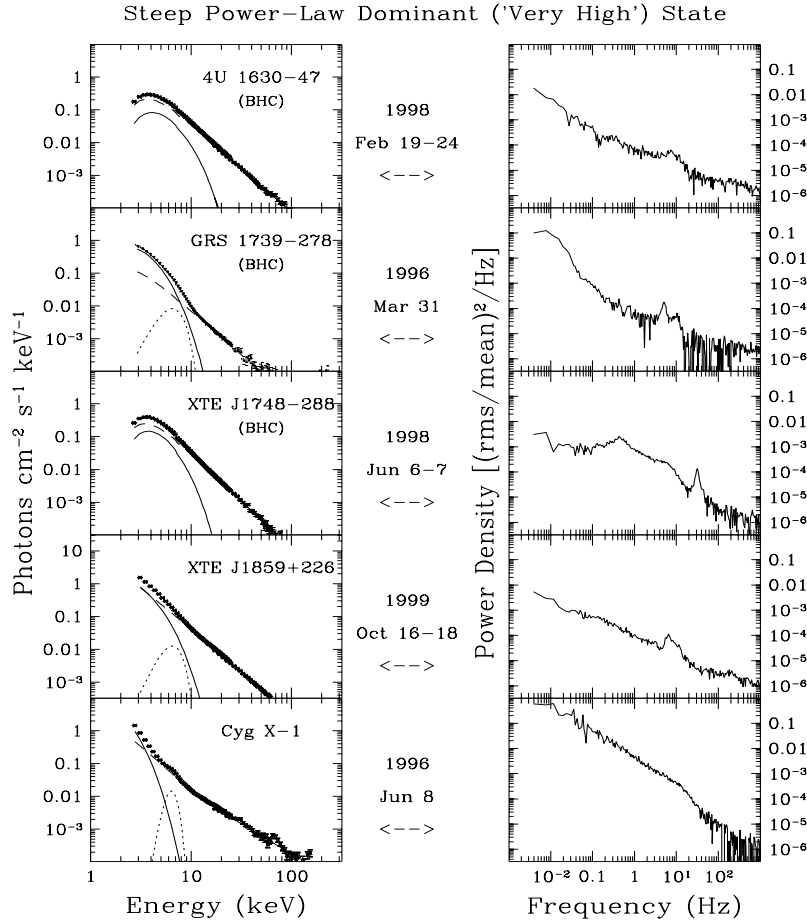


Fig. 4.16. Additional examples of sources in the SPL state. The observations were selected near the times of global or local maxima in the X-ray flux. Cyg X-1 is exceptional for its relatively low luminosity and for the absence of QPOs (see §4.3.8). The dashed and dotted lines follow the convention of earlier figures.

from the underlying disk (Gierlinski et al. 1999; Zdziarski et al. 2001). Further efforts to define the origin of the nonthermal, Comptonizing electrons has led to more complicated geometric models with feedback mechanisms, such as flare regions that erupt from magnetic instabilities in the accretion disk (Poutanen & Fabian 1999).

There are a number of alternative models for the SPL state. For example, bulk mo-

tion Comptonization has been proposed in the context of a converging sub-Keplerian flow within $50 R_g$ of the BH. The authors have suggested pair production as a means of extending the photon spectrum beyond the ~ 350 keV limit initially calculated for this model (see Turolla et al. 2002).

As noted above, Comptonization models are hard-pressed to explain the origin of the energetic electrons. As a further difficulty, a viable model must also account for the QPOs in the SPL state. This is important since very strong QPOs (1–10 Hz), such as those shown in Fig. 4.15 and Fig. 4.16, are a commonplace in this state. Further discussions about SPL models and X-ray QPOs are found in §4.4 below.

4.3.8 X-ray states of *Cygnus X-1* and *GRS 1915+105*

Here we briefly summarize the efforts to integrate the behavior of two uncommon BHBs within the framework of the TD, LH/radio jet, and SPL states.

We first return to the issue of Cyg X-1 and the nature of its transitions to a soft state of high intensity, which is unlike the canonical TD (HS) state. As noted earlier (§4.2.3; §4.2.1.1), contrary to expectations the 1996 soft-state spectrum of Cyg X-1 revealed a power-law spectrum, rather than a TD spectrum (Zhang et al. 1997a; Frontera et al. 2001a). Many observations during the soft state require either a broken power-law (above 10 keV) or a reflection component in order to achieve an acceptable fit (e.g. Cui et al. 1998; Fig. 4.16). Cyg X-1 has not been seen in the TD state, and the transition from the hard to soft X-ray spectra must be seen as a transition from the LH state to the SPL state (Gierlinski et al. 1999; Zdziarski et al. 2001). However, this SPL-like state is unusual in two respects: the absence of QPOs and the relatively low temperature of the accretion disk (table 4.4). Less surprising is the low luminosity of the SPL state (Zhang et al. 1997), since this is also seen in other sources (e.g., XTE J1550–564; Remillard et al. 2002a). Whether the SPL state in Cyg X-1 requires a higher mass accretion rate than the LH state is a matter of controversy (Zhang et al. 1997b; Frontera et al. 2001a).

In the unique case of GRS 1915+105, the wildly varying X-ray light curves indicate an imposing number of instability modes (Belloni et al. 2000). Nevertheless, within this complexity it is often possible to identify the canonical states of a BHB (Muno et al. 1999; Belloni et al. 2000). About half of the observations of GRS 1915+105 show fairly steady X-ray flux (rms $< 15\%$ in 1 s bins at 2–30 keV), and most of these intervals yield spectra and PDS that resemble either the TD or LH states (Muno et al. 1999; Fender 2001; Klein-Wolt et al. 2002). There are, however, some noteworthy differences encountered while interpreting GRS 1915+105 characteristics in terms of the canonical X-ray states. First, the condition of steady radio and X-ray emission extends to rather high luminosity, to $L_x > 10^{38}$ erg s $^{-1}$, which is a factor ~ 100 higher compared to the LH states observed in many other BHBs. Secondly, the X-ray photon index ($\Gamma \sim 2.2$) is steeper than usual, although it remains flatter than the index seen in the hard tail of the TD state ($\Gamma > 3$) or the index of the SPL state ($\Gamma > 2.5$; see Table 4.4). In short, the spectral indices in the LH, TD and SPL states for GRS 1915+105 appear shifted uniformly to somewhat higher values compared to other BHBs.

Overall, the spectral and temporal properties of Cyg X-1 and GRS 1915+105 are best integrated into the standard description of BH X-ray states if we relax the as-

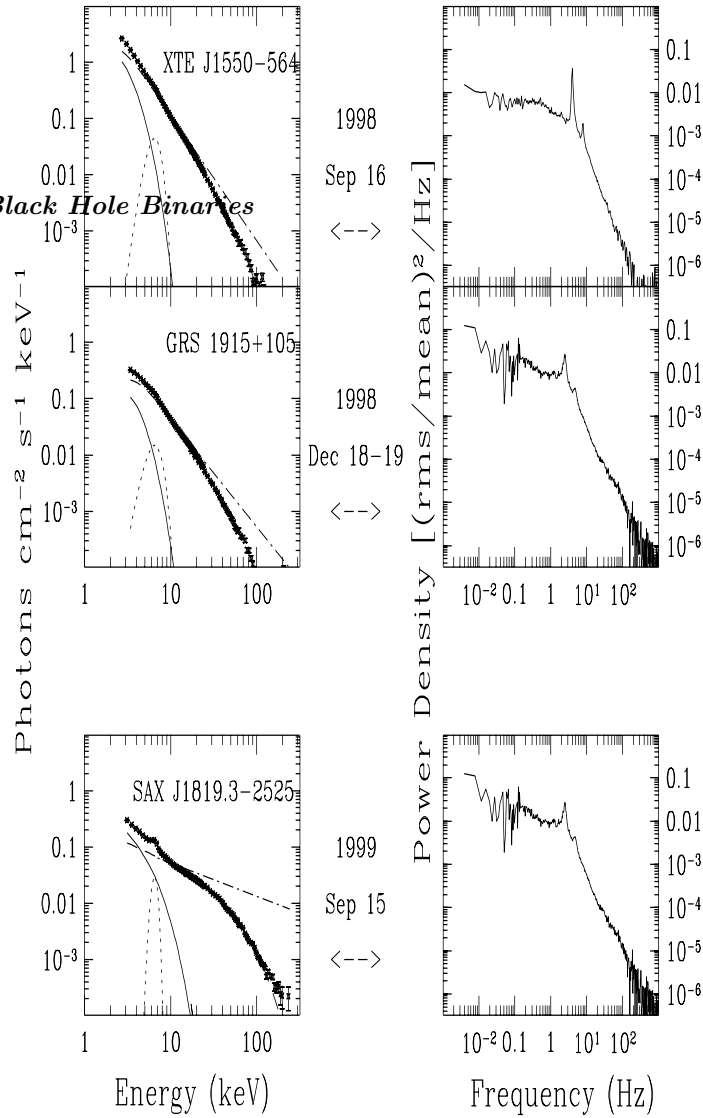


Fig. 4.17. Unusual spectra of three BHBs. The observations of XTE J1550–564 and GRS 1915+105 show spectral properties of the SPL state, but the PDS show a band-limited power continuum that is customarily seen as a characteristic of the LH state, rather than the SPL state. In the bottom panel, the flares and rapid fluctuations seen in SAX J1819.3–2525 (V4641 Sgr) do not coincide with any of the typical X-ray states of BHB systems.

sumptions regarding the relative or absolute luminosity ranges that are appropriate for the various states. As we will see in the following section, the spectral evolution of XTE J1550–564 motivates a similar conclusion, since the SPL luminosity in that source can lie well below the level of the TD state. Undoubtedly, there is an overall correlation between spectral states and luminosity intervals in accreting BHB systems. However, the canonical X-ray states are most usefully defined in terms of the properties of the X-ray spectrum and PDS, rather than in terms of luminosity.

Table 4.4. *Spectral Fit Parameters*

X-ray name	N_H (10^{22})	T_{DBB} (keV)	\pm (keV)	N_{DBB} \pm	Γ_{PL} \pm	N_{PL} \pm	Fe FWHM	N_{Fe} \pm	χ^2_ν	additional details
4U 1543-475	0.3	1.01	0.02	7419.	165.	2.57 0.02	5.42 0.21	0.61	.0479 .0031	3.62 feature at 4.4 keV
XTE J1550-564	2.0	1.12	0.03	3289.	74.	4.76 0.04	152. 17.	0.98 smedge at 9.2 keV
GRO J1655-40	0.9	1.16	0.03	1559.	21.	2.85 0.23	1.01 0.65	2.00 smedge at 8.0 keV
GX 339-4	0.2	0.71	0.03	2520.	62.	2.02 0.04	0.08 0.01	1.05	.0032 .0003	1.45
GRS1915+105	6.0	2.19	0.04	62.	5.	3.46 0.02	33.4 1.61	3.13 smedge at 6.7 keV
4U 1630-47	11.0	1.33	0.03	315.	7.	3.75 0.03	17.4 1.40	1.06 break at 20.8 keV to index 1.9
GRS 1739-278	3.0	0.95	0.04	972.	23.	2.65 0.15	.210 0.008	1.11	.0068 .0008	1.42
XTE J1748-288	10.4	1.79	0.02	42.4	2.1	2.60 0.02	14.6 0.4	1.18
XTE J1755-324	0.2	0.75	0.08	1486.	133.	2.40 0.15	0.11 0.04	1.78
XTE J2012+381	0.8	0.85	0.05	1176.	56.	2.06 0.04	0.16 0.015	1.32
4U 1543-475	0.3	0.38	0.07	645.	1338.	1.67 0.02	0.041 0.001	1.57
XTE J1550-564	2.0	1.70 0.10	0.108 0.021	1.13
GRO J1655-40	0.9	0.77	0.02	228.	37.	1.93 0.02	0.571 0.021	1.00	.0065 .0006	1.83
GX 339-4	0.2	1.75 0.02	0.168 0.028	0.90	.0013 .0003	0.98 plus reflection
GRS1915+105	6.0	2.11 0.02	0.231 0.043	0.91	.0458 .0003	2.39 plus reflection
XTE J1118+480	0.01	1.72 0.04	0.267 0.024	1.23
GS 1354-644	0.7	1.48 0.09	0.470 0.032	0.1	.0008 .0002	1.15 plus reflection
XTE J1748-288	10.4	0.48	0.05	5302.	479.	1.88 0.09	0.293 0.065	0.66	.0045 .0003	1.65
GRS 1758-258	1.0	1.67 0.07	0.053 0.010	0.36	.0004 .0001	1.84
Cyg X-1	0.5	1.68 0.07	0.446 0.025	1.44	.0206 .0018	3.40 plus reflection
4U 1543-47	0.3	0.93	0.07	3137.	138.	2.47 0.02	6.85 0.21	0.82	.0347 .0034	1.90
XTE J1550-564	2.0	3.31	0.20	7.76	0.70	2.82 0.05	200. 1.5	1.30	.2136 .0314	2.16 smedge at 8.5 keV
GRO J1655-40	0.9	2.22	0.20	9.89	1.6	2.65 0.05	75.3 1.1	1.32	.2321 .0157	4.45
GX 339-4	0.2	0.89	0.08	1917.	109.	2.42 0.02	2.34 0.08	0.97	.0178 .0017	1.39
GRS 1915+105	6.0	1.19	0.07	115.	31.	2.62 0.08	28.5 0.6	0.90	.0396 .0065	4.13
4U 1630-47	11.0	1.73	0.02	46.0	2.4	2.65 0.02	17.0 0.4	1.10
GRS 1739-278	3.0	1.01	0.06	1116.	38.	2.61 0.03	2.95 0.19	1.53	.0341 .0021	0.94
XTE J1748-288	10.4	1.36	0.02	210.	11.	2.92 0.02	26.2 1.2	0.96
XTE J1859+226	0.5	1.03	0.02	1164.	91.	2.55 0.08	14.5 0.31	1.33	.0426 .0060	1.36
Cyg X-1	0.5	0.49	0.03	55708.	2962.	2.68 0.03	7.65 0.37	0.73	.0270 .0016	1.78 breaks to index 1.83 above 12 keV
XTE J1550-564	2.0	0.74	0.02	6932.	562.	2.24 0.02	23.0 0.87	1.03	.121 .008	1.34 p.l. cutoff energy 51.7 keV
GRS 1915+105	6.0	0.88	0.03	775.	156.	1.91 0.02	4.51 0.18	1.28	.053 .004	1.45 p.l. cutoff energy 50.0 keV
SAX J1819.3-2525	0.3	1.63	0.06	38.	6.	0.59 0.03	0.25 0.02	0.47	.038 .003	1.46 p.l. cutoff energy 39.3 keV

4.3.9 *Intermediate (IM) states*

The LH-state energy spectra displayed in Figs. 4.13 and 4.14 show little or no spectral contribution from the accretion disk, while the PDS exhibit a “band-limited” power continuum (i.e., a flat power continuum that breaks to a steeper slope between 0.1 and 10 Hz). Such a band-limited power spectrum is sometimes seen in combination with a stronger contribution from the accretion disk. This condition of a BHB has been interpreted as an “intermediate” (IM) state that lies between the LH and TD states (e.g., Mendez & van der Klis 1997). We agree that the spectra of GRO J1655–40 shown in Fig. 4.13 does appear to represent a legitimate example of the IM state in the sense of a transition between the LH and TD states.

However, there are other cases that seem to display to a different type of intermediate or hybrid emission properties. For example, dozens of observations of XTE J1550–564 yielded energy spectra and QPOs that resemble the SPL state, but the PDS show band-limited continuum power that is reminiscent of the IM state described above (Homan et al. 2001). In Fig. 4.17 we show one example of this behavior for XTE J1550–564 and a very similar example for GRS 1915+105. It is problematic to interpret such observations of XTE J1550–564 as intermediate between the TD and LH states, since the energy spectra and QPOs resembles the SPL state (Sobczak et al. 2000). Similar concerns led to the suggestion that the SPL (or VH) state *itself* lies between the TD and LH states (Rutledge et al. 1999). However, this appears to be a radical suggestion, giving inadequate focus to the SPL state that is associated with the episodes of highest absolute luminosity, a distinct Gamma-ray spectrum, and occurrences of QPOs at both high and low frequency. Therefore, we do not consider this suggestion further.

It may seem more appropriate to describe the observations of XTE J1550–564 and GRS 1915+105 in Fig. 4.17 as “SPL states with band-limited power continua”. The significance of the band-limited power continuum is yet to be fully understood. This could suggest an IM state linking the LH and SPL states, a detail further supported by the fact that the disks in the two systems appear cooler and larger in these observations than they do in the respective TD states. However, such speculations may be ill-advised without considerations of sensitive radio measurements. We further note that the presence or absence of band-limited power observed in individual SPL-state observations of XTE J1550–564 is closely coupled to the amplitudes and phase lags of the associated QPOs (of types A, B, and C; Remillard et al. 2002a). Finally, while the energy spectra of XTE J1550–564 and GRS 1915+105 in Fig. 4.17 are distinctly steep, there is some ambiguity as to whether they are best modeled at a steep power-law or as a flatter power-law with an unusually low cutoff energy (~ 50 keV). In Table 4.4, we show the spectral parameters for the latter model, which is statistically preferred in the case of GRS 1915+105.

We conclude that it appears inappropriate to refer to both the observations of XTE J1550–564 and the very different observations of GRO J1655–40 (Fig. 4.13) as representing a single BHB state, namely, the IM state. On the other hand, state transitions and hybrid emission properties are to be expected and *X-ray spectra and PDS should be interpreted as IM states when necessary, while specifying which states can be combined to yield the the observed X-ray properties*. In summary, we describe the spectra of GRO J1655–40 (Fig. 4.13) as representing primarily an LH state or

perhaps an IM state between LH and TD. On the other hand, the spectra and PDS of XTE J1550–564 and GRS 1915+105 considered here appear to show an IM state that may be related to the SPL and LH states. Since transitions between these latter two states are not generally seen, this hybrid combination merits further scrutiny. In any case, we have shown that the IM state comes in different flavors, and that it is essential to describe an observation of an IM state by specifying the primary states that compose it.

4.3.10 *Anomalous behavior of SAX J1819.3–2525*

Finally, we consider whether BHBs have been observed in states that appear to fall entirely outside those considered thus far. The most obvious example is the case of the short-lived BHB SAX J1819.3–2525 (V4641 Sgr). The PCA observations of 1999 September 15.9 show the source in a unique flaring state (Wijnands & van der Klis 2000). The spectral hardness ratio remains remarkably constant throughout the brightest ~ 500 s of this observation, despite the rapid and strong intensity fluctuations. The spectrum and PDS for this central time interval are shown in Fig. 4.17. The spectral analysis shows a hot accretion disk and a broad Fe line, while the photon index is extraordinarily hard: $\Gamma = 0.60 \pm 0.03$ with a cutoff energy of 39 keV (Table 4.4).

This source is also distinguished as a new prototype for a “fast X-ray nova” (Wijnands & van der Klis 2000), since flares as bright as 12 Crab appeared and decayed on timescales shorter than 1 day (Fig. 4.4). The multifrequency spectrum, using the peak outbursts from SAX J1819.3–2525, have been interpreted in terms of super-Eddington accretion and the immersion of the binary in an extended envelope (Revnivtsev et al. 2002).

4.4 *Fast Temporal variations: QPOs and broad power peaks*

Power density spectra were discussed in the preceding section on X-ray states. As shown there, QPOs are prevalent in the SPL state, and they are sometimes seen in the LH state when thermal emission from the disk contributes some flux above 2 keV. In this section we briefly consider the QPOs of BHBs and BHCs in greater detail. For references on computing power density spectra (PDS), interpreting QPOs, and applying these techniques to the study of NS systems, see Chapter 2. We supplement this work by discussing X-ray timing results for BHBs. Following van der Klis, we define QPOs as features (usually modeled as a Lorentzian function) in the PDS that have coherence parameter $Q = \nu/\Delta\nu > 2$ (FWHM). Features with significantly lower Q values are regarded as “broad power peaks” and are discussed separately.

4.4.1 *Low frequency QPOs and accretion radiation mechanisms*

The X-ray PDS of many BH transients display low frequency QPOs (LFQPOs) roughly in the range 0.05 to 30 Hz. The significance of these oscillations can be summarized as follows.

(1) LFQPOs are almost always seen during the SPL state. They can be exceedingly strong (see Fig. 4.17), with rms amplitudes (expressed as a fraction of the mean count rate) as high as $r > 0.15$ for sources such as GRS 1915+105 (Morgan et al. 1997)

and XTE J1550–564 (Sobczak et al. 2000a). More generally, they are seen with $0.03 < r < 0.15$ whenever the steep power law contributes more than 20% of the flux at 2–20 keV (Sobczak et al. 2000a). LFQPOs have been observed at energies above 60 keV (Tomsick et al. 2001).

(2) In several sources, the LFQPO frequency has been shown to be correlated with the total flux from the accretion disk (but not with temperature or inner disk radius; Sobczak et al. 2000a; Munro et al. 1999; Trudolyubov et al. 1999). This conclusion, in combination with the the role of the steep power law mentioned above, suggests that LFQPOs may provide a vital clue on the coupling between the thermal and SPL components.

(3) LFQPOs can be quasi-stable features that persist for days or weeks. In GRS 1915+105, QPOs at 2.0–4.5 Hz persisted for 6 months during late 1996 and early 1997 (Munro et al. 2001).

(4) In a general sense, it can be argued that oscillations as distinct as these QPOs (often with $Q > 10$), represent global requirements for an organized emitting region. For example, in the context of models in which thermal radiation originates from MHD instabilities, one cannot accept the common picture of numerous and independent magnetic cells, which are distributed throughout the inner disk.

The effort to tie LFQPOs to the geometry and flow of accreting gas is complicated by the fact that LFQPO frequencies are much lower than the Keplerian frequencies for orbits in the inner accretion disk. For example, for a BH mass of $10 M_{\odot}$, an orbital frequency near 3 Hz coincides with a disk radius near $100 R_g$, while the expected radius for maximum X-ray emission lies in the range 1–10 R_g (depending on the value of the BH spin parameter). For the strongest QPOs in GRS 1915+105, efforts were made to track the individual oscillations to determine the origin of the frequency drifts and to measure the average “QPO-folded” oscillation profile (Morgan et al. 1997). The results show a random walk in QPO phase with only minor departures from a sinusoidal waveform. The ramifications of these results for QPO models remain uncertain.

There are now a large number of proposed LFQPO mechanisms in the literature, and we mention only a few examples here. The models are driven by the need to account for both the QPO frequency and also a mechanism to produce the allied power-law spectrum. The models include global disk oscillations (Titarchuk & Osherovich 2000), as well as radial oscillations of accretion structures, such as shock fronts (Chakrabarti & Manickam 2000) or a transition layer between the disk and a hotter Comptonizing region (Nobili et al. 2000). Another alternative, known as the “accretion-ejection instability,” invokes spiral waves in a magnetized disk (Tagger & Pellat 1999) with a transfer of energy out to the radius where material corotates with the spiral wave. This model thereby combines magnetic instabilities with Keplerian motion to explain the observed QPO amplitudes and stability. The sharpening and evaluation of these various QPO concepts requires the continued attention of theorists.

Further analyses of LFQPOs have revealed phase lags associated with these oscillations and their harmonics. The analysis technique uses Fourier cross spectra to measure both the phase lags and the coherence parameter (*versus* frequency) between different X-ray energy bands, e.g., 2–6 *vs.* 13–30 keV. Unexpectedly, both positive

and negative phase lags were found (Wijnands et al. 1999; Cui et al. 2000b; Reig et al. 2000; Munro et al. 2001), and suggestions were made to classify LFQPOs by phase lag properties. The expansion of LFQPO subtypes may not be widely viewed as a welcome complication. Nevertheless, it has been shown in the case of XTE J1550–564 that the properties of the phase lags clarify how LFQPO parameters correlate with both the accretion–disk and high–frequency QPO parameters (Remillard et al. 2002a).

4.4.2 Broad power peaks and comparisons of BH and NS systems

The study of broad features in the PDS has led recently to important developments. In many NS systems and in some of the thermal states of BHBs, the PDS can be decomposed into a set of four or five broad power peaks (Nowak 2000; Belloni et al. 2002), generally with $0.5 < Q < 1.0$. The evolution of these features has been linked to major behavioral changes in Cyg X–1. For example, the disappearance of the third broad power peak occurred just at the time Cyg X–1 left the LH state and its steady radio jet was quenched (Pottschmidt et al. 2003).

Broad PDS features are also involved in renewed efforts to contrast accreting BHB and NS systems via their variability characteristics. It has been proposed that the observed frequency limit for the power continuum provides a means to distinguish accreting BH and NS systems (Sunyaev & Revnivtsev 2000), since only the latter exhibit source variations above 500 Hz.

Finally, some studies have used both QPOs and broad power peaks to examine the relationship between low– and high–frequency features and to make comparisons between different NS subclasses and BHBs. There have been claims of a unified variability scheme that encompasses all X–ray binary types; the authors’ bottom–line conclusion is that all of the oscillations must therefore originate in the accretion disk (Psaltis et al. 1999; Belloni et al. 2002). However, many aspects of this work remain controversial, particularly the handling of BH HFQPOs and their association with the lower kHz QPO of NSs (Remillard et al. 2002a).

4.4.3 High–frequency QPOs and general relativity

The topic of high–frequency QPOs (HFQPOs) in BHBs (40–450 Hz) continues to evolve in the *RXTE* era. These transient QPOs have been detected in seven sources (4 BHBs and 3 BHCs). HFQPOs have rms amplitudes that are generally $\sim 1\text{--}3\%$ of the mean count rate in a given energy band. Remarkably, three sources exhibit pairs of QPOs that have commensurate frequencies in a 3:2 ratio (Remillard et al. 2002b; Remillard et al. 2003). In fact, GRS 1915+105 shows two pairs of HFQPOs; the complete set of four QPO pairs is shown in Fig. 4.18. In addition (see references in Tables 4.1 and 4.2), single–component HFQPOs have been observed in 4U1630–47 (184 Hz), XTE J1859+226 (190 Hz), XTE J1650–500 (250 Hz), and H 1743–322 (240 Hz); their profiles are similar to the 300 Hz QPO for GRO J1655–40 shown in the top left panel of Fig. 4.18. HFQPOs occur in the SPL state, except for the 67 Hz QPO (see Fig. 4.18) which appears in the TD state, especially when the TD state reaches luminosities $> 10^{38} \text{ erg s}^{-1}$.

The preponderance of evidence indicates that HFQPOs do not shift freely in frequency in response to luminosity changes, as do the kHz QPOs in NS systems (see

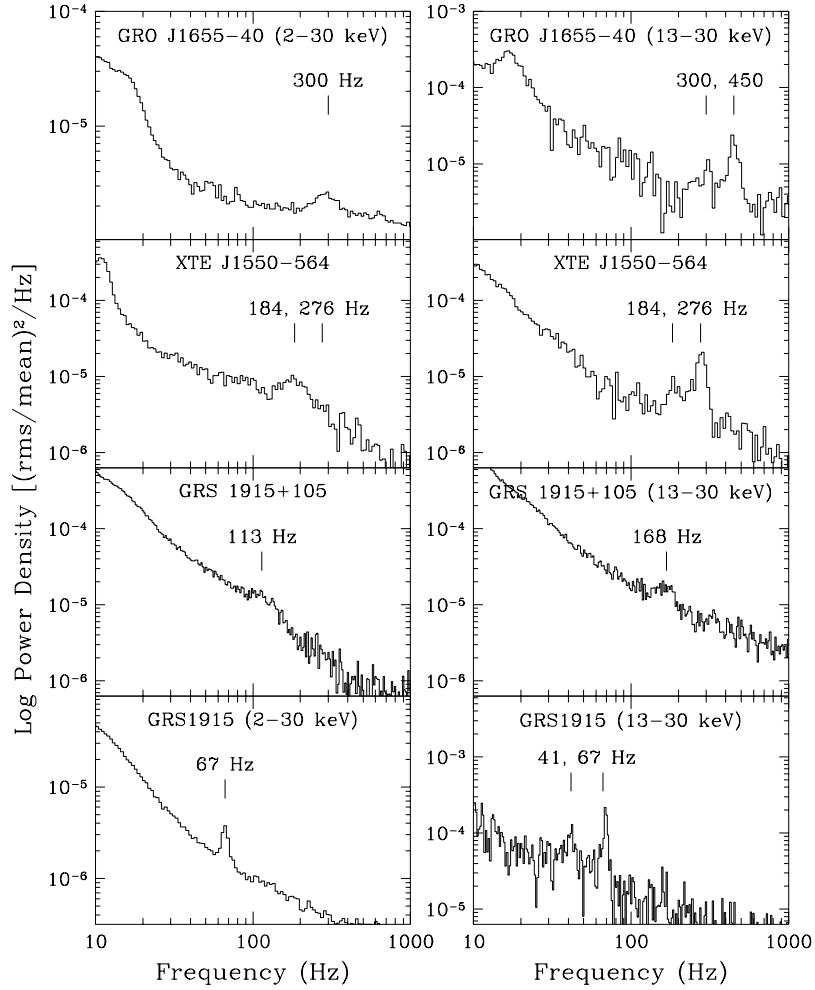


Fig. 4.18. Four pairs of HFQPOs observed in three black-hole binary systems. The energy band is 6–30 keV unless otherwise indicated. These usually subtle oscillations are only visible during a fraction of the observations for each source.

Ch. 2). Instead, they appear to exhibit an “X-ray voiceprint”. That is, the QPOs occur in harmonics of an unseen fundamental frequency which has a unique value for each BH. For the three cases that show 3:2 frequency pairs, the relationship between the HFQPO frequencies *vs.* BH mass (determined from binary analyses) scales as M_1^{-1} . This relationship is shown in Fig. 4.19, where we have plotted the frequency of the stronger feature (i.e. $2 \times \nu_0$), since the fundamental is generally not seen. These results offer strong encouragement for seeking interpretations of BH HFQPOs

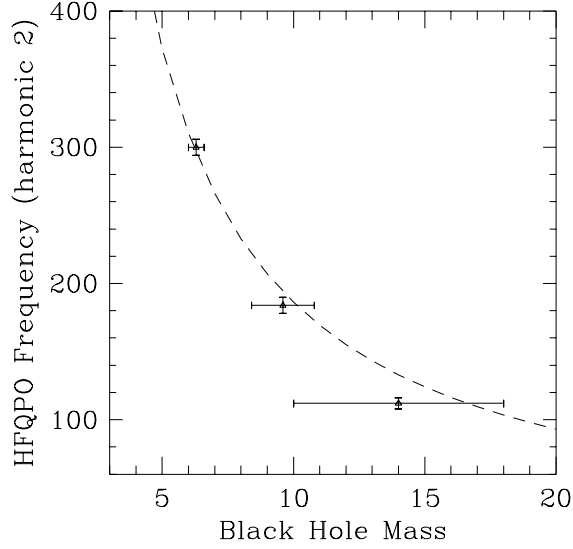


Fig. 4.19. Relationship between HFQPO frequency and black-hole mass for XTE J1550-564, GRO J1655-40, and GRS 1915+105. These three systems display a pair of HFQPOs with commensurate 3:2 frequency ratios. The frequencies are plotted for the strong and broad QPO known to represent $2 \times \nu_0$. The fundamental is generally not seen in the power spectra. The dashed line shows a M^{-1} relation that fits these data.

via GR theory, since each type of GR disk oscillation under strong gravity varies as M_1^{-1} , assuming the sampled BHs have similar values of the dimensionless spin parameter (a_*).

The commensurate HFQPO frequencies can be seen as strong support for the idea that HFQPOs may represent some type of resonance phenomenon involving oscillations describable by GR, as originally proposed by Abramowicz & Kluzniak (2001). Resonances in some form may be applicable to both BH and NS systems (Abramowicz, Karas, and Kluzniak 2003). We note that the 3:2 harmonic pattern cannot be attributed to a distorted sine wave with harmonic content because the individual detections (in a given energy band, on a given day) generally appear as a single peak in the PDS, and the QPO frequencies are recognized as $2\nu_0$ or $3\nu_0$ only when the ensemble of results is examined.

The resonance hypothesis (Abramowicz & Kluzniak 2001) has been discussed in terms of accretion blobs following perturbed orbits in the inner accretion disk. Unlike Newtonian gravity, GR predicts independent oscillation frequencies for each spatial coordinate for orbits around a rotating compact object, as seen from the rest frame of a distant observer. GR coordinate frequencies and their differences (i.e. beat frequencies) have been proposed to explain some of the X-ray QPOs from both NSs and BHs (Stella et al. 1999). At the radii in the accretion disk where X-rays orig-

inate, the GR coordinate frequencies are predicted to have varying, integral ratios. The commensurate frequencies in pairs of HFQPOs, noted above, can therefore be interpreted as a signature of resonance, e.g., between pairs of coordinate frequencies in the inner disk. Unlike the azimuthal and polar coordinate frequencies, the radial coordinate frequency reaches a maximum value and then falls to zero as the radius decreases toward the location of the innermost stable circular orbit (Kato 2001; Merloni et al. 2001). This ensures the possibility of commensurate coordinate frequencies somewhere in the inner disk. For example, there is a wide range in the dimensionless spin parameter, a_* , where one can find a particular radius that corresponds to a 2:1, 3:1, or 3:2 ratio in the orbital and radial coordinate frequencies. A resonance between the polar and radial coordinate frequencies is also possible. In the resonance concept, linear perturbations may grow at these radii, ultimately producing X-ray oscillations that represent some combination of the individual resonance frequencies, their sum, or their difference. However, there remain serious uncertainties as to whether such structures could overcome the severe damping forces and emit X-rays with sufficient amplitude and coherence to produce the observed HFQPOs (Markovic & Lamb 1998).

Models for “diskoseismic” oscillations adopt a more global view of the inner disk as a GR resonance cavity (Kato & Fukue 1980; Wagoner 1999). This paradigm has certain attractions for explaining HFQPOs, but integral harmonics are not predicted for the three types of diskoseismic modes derived for adiabatic perturbations in a thin accretion disk. Clearly, there is also a need to investigate the possibility of resonances within the paradigm of diskoseismology.

It has been argued by Strohmayer (2001a) that HFQPO frequencies are sufficiently high that they require substantial BH spin. For example, in the case of GRO 1655–40 the 450 Hz frequency exceeds the maximum orbital rotation frequency (ν_ϕ) at the innermost stable circular orbit around a Schwarzschild BH (i.e. $a_* = 0$; §4.1.5) of mass $M_1 = 6.3 \pm 0.5 M_\odot$ (Greene, Bailyn, & Orosz 2001). If the maximum Keplerian frequency is the highest frequency at which a QPO can be seen, then the the results for GRO J1655–40 require a Kerr BH with prograde spin, e.g. $a_* > 0.15$. However, the conclusion that spin is required may not be valid if the QPO represents the sum of two beating frequencies. On the other hand, even higher values of the spin parameter may be required ($a_* > 0.3$) if the QPO represents either a sum of coordinate frequencies (Remillard et al. 2002b) or resonant diskoseismic oscillations ($a_* > 0.9$; Wagoner et al. 2001).

Accurate and sensitive measurements of X-ray HFQPO frequencies may lead to a determination of the GR mechanism that is responsible for these oscillations, and ultimately to secure measurements of the spin parameter a_* for a number of BHs. These spin measurements would be very valuable in assessing the role of BH rotation in the production of jets (Blandford & Znajek 1977). This is especially true since the three systems with paired frequencies have a history of relativistic mass ejections during some (but not all) of their outbursts.

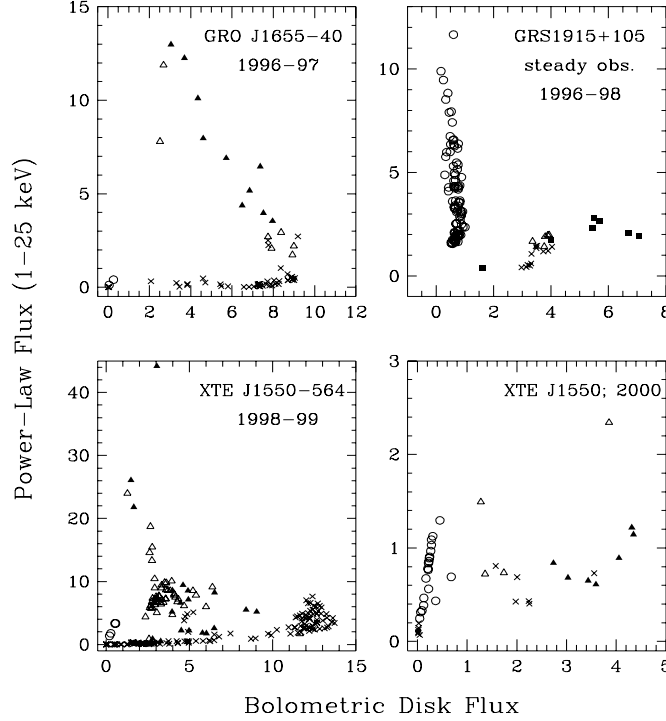


Fig. 4.20. Radiation energy division between the accretion disk and the power-law component. The symbol types denote the X-ray state as TD (x), LH (o), or SPL(Δ). Furthermore, in the SPL state, an open triangle is used when there is only an LFQPO, while a filled triangle denoted the additional presence of an HFQPO. Finally, the TD-like observations that show 67 Hz QPOs in GRS 1915+105 are shown with a filled square.

4.5 Energetics and Dependent Variables for Accretion Radiation

4.5.1 Division of Spectral Energy: Disk and Power-Law Components

A revealing view of the behavior of a BHB over the course of its entire outburst cycle can be obtained by plotting the flux in the power-law component vs. the flux from the accretion disk. Four such plots are shown in Fig. ??, where the various plotting symbols identify the emission states described in §4.4. The figure shows the flux diagrams for 3 BHBs, while considering two of the outbursts of XTE J1550-564 (Muno et al. 1999; Remillard et al. 2001; Remillard et al. 2002b). It has been shown that the emerging patterns in these flux diagrams are largely unaffected by the choice of integration limits, i.e. whether the energy measurements are computed in terms of bolometric flux or the integrated flux within the PCA instrument bandpass (e.g. 2–25 keV; Remillard et al. 2002a).

The TD points (“x” symbol; Fig. ??) for GRO J1655-40 and XTE J1550-564 (1998-99) are particularly well organized; they can be described as basically hori-

zontal tracks in which accretion energy is freely converted to thermal radiation from the accretion disk. These tracks correspond to the standard accretion disk model (Shakura & Sunyaev 1973), and they may also convey moderate Comptonization effects expected from MHD turbulence (e.g. Hawley & Krolik 2001), as these tracks all curve upward at high luminosity. We note that the TD points with the highest flux correspond to Eddington luminosities of 0.2 (GRO J1655-40), 0.6 (XTE J1550-564; 1998-99), and 0.4 (GRS 1915+105), using the values for mass and distance given in Tables 4.1 and 4.2.

Observations in the LH state (power-law contributes the majority of flux, while $1.4 < \Gamma < 2.2$) are plotted as circles in Fig. /reffig:flux3. These points form essentially vertical tracks with only minor flux contributions from the accretion disk. The LH points are known to coincide with fairly steady radio emission for GRS1915+105 (Muno et al. 2001) and XTE J1550-564 in 2000 (Corbel et al. 2001), as expected in the LH state.

Observations in the SPL state (QPOs and a power-law index, $\Gamma > 2.4$) are plotted as triangles in Fig. /reffig:flux3, and a solid symbol is used when there is an additional detection of an HFQPO above 100 Hz. The wide diversity in the relative contributions from the disk and power-law components within the SPL state are especially apparent for XTE J1550-564. These results, combined with the wide range in the luminosities of the TD and LH tracks shown in Fig. /reffig:flux3, cause us to abandon the use of luminosity requirements in defining the X-ray states of black hole binaries. Finally, detections of the 67 Hz QPO in GRS 1915+105 are shown as filled squares. They occur without the presence of any LFQPOs, and they appear to extend the TD branch out to $0.6 L_{Edd}$.

4.5.2 *Dependent Variables for Accretion Radiation*

Prior to the *RXTE* era, it was thought that the X-ray states primarily represented a simple progression in the accretion rate, and that the emission properties of BHB depended only on the accretion rate and the black hole mass (e.g. Tanaka & Lewin 1995). The behavioral complexity of sources such as XTE J1550-564 (Fig. /reffig:flux3) have challenged this viewpoint (Homan et al 2001; Remillard et al. 2002b), since it seems that any of the three active states of accretion may occur at a given luminosity.

So what other parameters must also be considered in the theory of black hole accretion? It is clear that black hole spin and the angle between the spin axis and disk axes must also be considered in a complete theory of black hole accretion, but these would not help to explain the types of rapid state transitions seen in many systems. As noted in several previous sections, MHD instabilities are widely suspected of playing a role in causing nonthermal radiation, and magnetic fields are additionally expected to play a leading role in the formation and collimation of jets. It then seems relevant to question whether a parameter of magnetism, such as the ratio of magnetic to gas pressure, must also be considered as a dependent variable of accreting systems. The continued development of 3-D MHD simulations are expected to be very fruitful in gaining a deeper understanding of the radiation of black hole binaries.

4.6 Concluding remarks

As reviewed in §4.4.3, high frequency QPOs, which range from 40 to 450 Hz, have been observed with *RXTE* for four BHBs and two BHCs. For those with known masses, the QPO frequency corresponds closely to the orbital frequency of the innermost stable orbit. Furthermore, three sources show evidence for harmonic (3:2) pairs of frequencies. The models for these QPOs (e.g. frame dragging and diskoseismic oscillations) invoke strong-field GR effects in the inner accretion disk, and they depend strongly on the spin of the BH. On the other hand, studies of broadened Fe K α emission lines (§4.2.4), which can also reveal the conditions in the very inner accretion disk, may prove as revealing as timing studies. The line photons that reach a distant observer are gravitationally redshifted and Doppler and transverse-Doppler shifted. Encoded in the line profile are the mass and spin of the BH. The most provocative result has been obtained for the BHC XTE J1650–500 (§4.2.4), where the line profile suggests the presence of an extreme Kerr BH.

Our hunch is that the compact objects we now pursue are the result of the complete gravitational collapse of matter. That is, that these objects possess an event horizon and are the BHs described by GR. Our challenge is to prove that this paradigm is correct by making clean quantitative measurements of relativistic effects in the strong gravitational fields near these objects. At present, no one can say which future mission can best help us meet this challenge: LISA, MAXIM, Constellation-X, or an X-ray Timing Observatory (XTO). Perhaps all of the approaches will be required. In any case, an XTO with effective area and telemetry ten times that of *RXTE* and with improved energy resolution, would be a powerful probe of physics near the event horizon. Consider that *RXTE* with just 1.6 times the effective area of *Ginga*, broke through to discover kHz QPOs in NSs, a discovery that led quickly to hard constraints on dense matter.

Acknowledgments

We thank Jon Miller, Mike Munro, David Smith, Jean Swank, John Tomsick, Emrah Kalemci, and Rudy Wijnands for their help in assembling the catalogue of candidate BHBs presented in Table 4.3. We are indebted to Andy Fabian, Jon Miller, Ramesh Narayan, Jerry Orosz and Andrej Zdziarski for a careful reading of portions of the manuscript and their valuable comments. We thank John Tomsick for the use of unpublished data on 4U1543–47, Ann Esin for supplying Fig. 4.1, Jon Miller for supplying Fig. 4.8, John Huchra for advice on the distance to the LMC, and Suresh Kumar for his assistance in typesetting the manuscript. This work was supported in part by the National Aeronautics and Space Administration under Grants NAG5–10813.

References

- Abramowicz, M.A. (1998) in *Theory of Black Hole Accretion Discs*, eds. M.A. Abramowicz, G. Bjornsson and J.E. Pringle (Cambridge U. Press, Cambridge), 50–60
- Abramowicz, M.A., Karas, V., and Kluzniak, W., et al. (2003), *PASJ*, in press (astro-ph/0302183)

- Abramowicz, M.A., and Kluzniak, W. (2001), *A&A*, **374**, L19–L20
- Agol, E., and Krolik, J.H. (2000), *ApJ*, **528**, 161–170
- Agol, E., Kamionkowski, M., Koopmans, L.V.E., and Blandford, R.D. (2002), *ApJ* **576**, L131–L135
- Augusteijn, T., Kuulkers, E. and van Kerkwijk, M.H. (2001), *ApJ* **375**, 447–454
- Baganoff, F.K., Bautz, M.W., Brandt, W.N., et al. (2001), *Nature* **413**, 45–48
- Ball, L., Kesteven, M.J., Campbell–Wilson, D., et al. (1995), *MNRAS* **273**, 722–730
- Balucinska–Church, M. and Church M.J. (2000), *MNRAS* **312**, L55–L59
- Barr, P., White, N.E. and Page, C.G. (1985), *MNRAS* **216**, 65P–70P
- Barret, D., Grindlay, J.E., Bloser, P.F., et al. (1996a), *IAU Circ.* 6519
- Barret, D., McClintock, J.E. and Grindlay, J.E. (1996b), *ApJ* **473**, 963–973
- Barret, D., Olive, J.F., Boirin, L. (2000), *ApJ* **533**, 329–351
- Barret, D., Roques, J.P., Mandrou, P., et al. (1992), *ApJ* **392**, L19–L22
- Belloni, T., Klein-Wolt, M., Mendez, M., et al. (2000), *A&A*, **355**, 271–290
- Belloni, T., Mendez, M., van der Klis, M., et al. (1999), *ApJ* **519**, L159–L163
- Belloni, T., Psaltis, D., and van der Klis, M. (2002), *ApJ*, **572**, 392–406
- Belloni, T., van der Klis, M., Lewin, W.H.G., et al. (1997), *A&A* **322**, 857–867
- Blandford, R.D. (2002), to appear in *Lighthouses of the Universe*, eds. M. Gilfanov, R. Sunyaev, et al. (Springer, Berlin), (astro-ph 0202265)
- Blandford, R.D. and Begelman, M.C. (1999), *MNRAS* **303**, L1–L5
- Blandford, R.D. and Znajek, R.L. (1977), *MNRAS* **179**, 433–456
- Bolton, C.T. (1972), *Nature* **240**, 124–126
- Borozdin, K.N., Aleksandrovich, N.L., Aref'ev, V.A., et al. (1995), *AstL* **21**, 212–216
- Borozdin, K.N., Revnivtsev, M.G., Trudolyubov, S.P., et al. (1998), *AstL* **24**, 435–444
- Boyd, P.T., Smale, A.P., Homan, J., et al. (2000), *ApJ* **542**, L127–L130
- Bradt, H., Levine, A.M., Remillard, R.A., & Smith, D.A. (2001), *MmSAI*, **73**, 256–271
- Bradt, H.V.D. and McClintock, J.E. (1983), *ARAA* **21**, 13–66
- Branduardi, G., Ives, J.C., Sanford, P.W., et al. (1976), *MNRAS* **175**, 47P–56P
- Brocksopp, C., Fender, R. P., Larionov, V., et al. (1999), *MNRAS*, **309**, 1063–1073
- Brocksopp, C., Fender, R.P., McCollough, M., et al. (2002), *MNRAS* **331**, 765–775
- Brocksopp, C., Jonker, P.G., Fender, R.P., et al. (2001), *MNRAS* **323**, 517–528
- Brown, G.E. and Bethe, H.A. (1994), *ApJ* **423**, 659–664
- Brown, G.E., Lee, C.-H., Wijers, R.A.M.J. and Bethe, H.A. (2000a), *Phys. Rep.* **333–334**, 471–504
- Brown, G.E., Lee, C.-H., Wijers, R.A.M., et al. (2000b), *NewA* **5**, 191–210
- Campana, S., Stella, L., Belloni, T., et al. (2002), *A&A* **384**, 163–170
- Cannizzo, J.K. (1993), *ApJ* **419**, 318–336
- Casares, Charles, P.A. and Marsh, T.R. (1995), *MNRAS* **277**, L45–L50
- Casares, J. and Charles, P.A. (1994), *MNRAS* **271**, L5–L9
- Casares, J., Charles, P.A., Naylor, T. and Pavlenko, E.P. (1993), *MNRAS*, **265**, 834–852
- Chakrabarti, S.K., and Manickam, S.G. (2000), *ApJ*, **531**, L41–L44
- Chaty, S., Mignani, R.P. and Israel, G.L. (2002), *MNRAS* **337**, L23–L26
- Chen, W., Shrader, C.R. and Livio, M. (1997), *ApJ* **491**, 312–338
- Churazov, E., Gilfanov, M., Sunyaev, R., et al. (1993), *ApJ* **407**, 752–757
- Coe, M.J., Engel, A.R. and Quenby, J.J. (1976), *Nature* **259**, 544–545
- Cooke, B.A., Levine, A.M., Lang, F.L., et al. (1984), *ApJ* **285**, 258–263
- Corbel, S., Fender, R.P., Tzioumis, A.K., et al. (2000), *A&A* **359**, 251–268
- Corbel, S., Kaaret, P., Jain, R.K., et al. (2001), *ApJ* **554**, 43–48
- Corbel, S., Nowak, M.A., Fender, R.P., et al. (2003), *A&A*, **400**, 1007–1012
- Cowley, A.P., Crampton, D. and Hutchings, J.B. (1987), *AJ* **92**, 195–199
- Cowley, A.P., Crampton, D., Hutchings, J.B., et al. (1983), *ApJ* **272**, 118–122
- Cowley, A.P., Schmidtke, P.C., Anderson, A.L. and McGrath, T.K. (1995), *PASP* **107**, 145–147
- Cowley, A.P., Schmidtke, P.C., Ebisawa, K. (1991), *ApJ* **381**, 526–533
- Cui, W., Ebisawa, K., Dotani, T., and Kubota, A (1998), *ApJ* **493**, L75–L78
- Cui, W., Heindl, W.A., Swank, J.H., et al. (1997a), *ApJ* **487**, L73–L76
- Cui, W., Schulz, N.S., Baganoff, F.K., et al. (2001), *ApJ* **548**, 394–400
- Cui, W., Shrader, C.R., Haswell, C.A. and Hynes, R.I. (2000a), *ApJ* **535**, L123–L127
- Cui, W., Zhang, S.N., and Chen, W. (2000b), *ApJ*, **531**, L45–L48

- Cui, W., Zhang, S.N., Chen, W., & Morgan, E.H. (1999), *ApJ*, **512**, L43–L46
- Cui, W., Zhang, S.N., Focke, W. and Swank, J.H. (1997b), *ApJ* **484**, 383–393
- Dal Fiume, D., Frontera, F., Orlandini, M. et al. (1999), *IAU Circ.* 7291
- Davies, R.D., Walsh, D. and Browne, I.W.A., et al. (1976), *Nature* **261**, 476–
- Dhawan, V., Mirabel, I. F., and Rodriguez, L. F. (2000), *ApJ* **543**, 373–385
- Dieters, S.W., Belloni, T., Kuulkers, E., et al. (2000), *ApJ* **538**, 307–314
- di Matteo, T., Celotti, A. and Fabian, A.C. (1999), *MNRAS* **304**, 809–820
- Di Salvo, T., Done, C., Zycki, et al. (2001), *ApJ* **547**, 1024–1033
- Done, C. and Nayakshin, S. (2001), *MNRAS* **328**, 616–622
- Done, C., Mulchaey, J.S., Mushotzky, R.F. and Arnaud, K.A. (1992), *ApJ* **395**, 275–288
- Done, C., and Zycki, P.T. (1999), *MNRAS*, **305**, 457–468
- Dove, J.B., Wilms, J. and Begelman, M.C. (1997a), *ApJ* **487** 747–758
- Dove, J.B., Wilms, J., Maisack, M. and Begelman, M.C. (1997b), *ApJ* **487**, 759–768
- Dubus, G., Hameury, J.-M and Lasota, J.-P. (2001), *A&A* **373**, 251–271
- Ebisawa, K., Makino, F., Mitsuda, K., et al. (1993), *ApJ* **403**, 684–689
- Ebisawa, K., Mitsuda, K. and Inoue, H. (1989), *PASJ* **41**, 519–530
- Ebisawa, K., Mitsuda, K. and Tomoyuki, H. (1991), *ApJ* **367**, 213–220
- Ebisawa, K., Ogawa, M., Aoki, T., et al. (1994), *PASJ* **46**, 375–394
- Elvis, M., Page, C.G., Pounds, K.A., et al. (1975), *Nature* **257**, 656–657
- Esin, A.A., McClintock, J.E. and Narayan, R. (1997), *ApJ* **489**, 865–889
- Esin, A.A., McClintock, J.E., Drake, J.J., et al. (2001), *ApJ* **555**, 483–488
- Esin, A.A., Narayan, R., Cui, W., et al. (1998), *ApJ* **505**, 854–868
- Fabbiano, G., Zezas, A. and Murray, S.S. (2001), *ApJ* **554**, 1035–1043
- Fabian, A.C., Iwasawa, K., Reynolds, C.S. and Young, A.J. (2000), *PASP* **112**, 1145–1161
- Fabian, A.C., Rees, M.J., Stella, L., and White, N.E. (1989), *MNRAS* **238**, 729–736
- Falcke, H. and Biermann, P.L. (1995), *A&A* **293**, 665–682
- Fender, R.P. (2001), *MNRAS*, **322**, 31–42
- Fender, R., Corbel, S., Tzioumis, T., et al. (1999a), *ApJ*, **519**, L165–L168
- Fender, R.P., Garrington, S.T., McKay, D.J., et al. (1999b), *MNRAS* **304**, 865–876
- Fender, R.P., Hjellming, R.M., Tilanus, R.P.J., et al. (2001), *MNRAS* **322**, L23–L27
- Feng, Y.X., Zhang, S.N., Sun, X., et al. (2001), *ApJ* **553**, 394–398
- Filippenko, A. V., Matheson, T. and Ho, L.C. (1995a), *ApJ* **455**, 614–622
- Filippenko, A.V. and Chornock, R. (2001), *IAU Circ.* 7644
- Filippenko, A.V., Leonard, D.C., Matheson, T., et al. (1999), *PASP* **111**, 969–979
- Filippenko, A.V., Matheson, T. and Barth, A.J. (1995b), *ApJ* **455**, L139–L142
- Filippenko, A.V., Matheson, T., Leonard, D.C., et al. (1997), *PASP* **109**, 461–467
- Freedman, W.L., Madore, B.F., Gibson, B.K., et al. (2001), *ApJ* **553**, 47–72
- Frontera, F., Amati, L., Zdziarski, A.A., et al. (2003), *astro-ph/0304261*
- Frontera, F., Palazzi, E., Zdziarski, A. A., et al. (2001a), *ApJ* **546**, 1027–1037
- Frontera, F., Zdziarski, A. A., Amati, L., et al. (2001b), *ApJ* **561**, 1006–1015
- Fryer, C. and Kalogera V. (2001), *ApJ* **554**, 548–560
- Garcia, M.R., McClintock, J.E., Narayan, R., et al. (2001), *ApJ* **553**, L47–L50
- Gelino, D.M., Harrison, T.E. and McNamara, B.J. (2001a), *AJ* **122**, 971–978
- Gelino, D.M., Harrison, T.E. and Orosz, J.A. (2001b) *AJ* **122**, 2668–2678
- George, I.M. and Fabian, A.C. (1991), *MNRAS* **249**, 352–367
- Gierlinski, M., Maciolek–Niedzwiecki, A. and Ebisawa, K. (2001), *MNRAS* **325**, 1253–1265
- Gierlinski, M., Zdziarski, A.A., Poutanen, J., Coppi, et al. (1999), *MNRAS* **309**, 496–512
- Gies, D.R. and Bolton, C.T. (1982), *ApJ* **260**, 240–248
- Goldoni, P., Vargas, M., Goldwurm, A., et al. (1999), *ApJ* **511**, 847–851
- Greene, J., Bailyn, C.D., and Orosz, J.A. (2001), *ApJ* **554**, 1290–1297
- Greiner, J., Cuby, J.G. and McCaughrean, M.J (2001a), *Nature* **414**, 522–525
- Greiner, J., Cuby, J.G., McCaughrean, M.J., et al. (2001b), *A&A* **373**, L37–L40
- Greiner, J., Dennerl, K. and Predehl, P. (1996), *A&A* **314**, L21–L24
- Groot, P., Udalski, A., Miller, J. (2001), *IAU Circ.* 7708
- Grove, J.E., Johnson, W.N., Kroeger, R.A., et al. (1998), *ApJ* **500**, 899–908
- Gursky, H., Bradt, H., Doxsey, R., et al. (1978), *ApJ* **223**, 973–978
- Haardt, F. and Maraschi, L. (1991), *ApJ* **380**, L51–L54

- Hameury, J.-M., Barret, D., Lasota, J.-P., et al. (2003), *A&A* **399**, 631–637
- Hameury, J.-M., Lasota, J.-P., McClintock, and J. E., Narayan, R. (1997), *ApJ* **489**, 234–243
- Han, X. and Hjellming, R.M. (1992), *ApJ* **400**, 304–314
- Hannikainen, D., Campbell–Wilson, D., Hunstead, R., et al. (2001), *ApSSS* **276**, 45–48
- Hannikainen, D.C., Hunstead, R.W., Campbell–Wilson, D., et al. (2000), *ApJ* **540**, 521–534
- Harlaftis, E.T., Horne, K. and Filippenko, A.V. (1996), *PASP* **108**, 762–771
- Hawley, J.F. and Krolik, J.H. (2001) *ApJ* **548** 348–367
- Herrero, A., Kudritzki, R.P., Gabler, R., et al. (1995), *A&A* **297**, 556–
- Hjellming, R.M. and Rupen, M.P. (1995), *Nature* **375**, 464–468
- Hjellming, R.M., Calovini, T.A. and Han, X.H. (1988), *ApJ* **335**, L75–L78
- Hjellming, R.M., Rupen, M.P. and Mioduszewski, A.J. (1998a), *IAU Circ.* 6924
- Hjellming, R.M., Rupen, M.P. and Mioduszewski, A.J. (1998b), *IAU Circ.* 6934
- Hjellming, R.M., Rupen, M.P., Hunstead, R.W., et al. (2000), *ApJ* **544**, 977–992
- Hjellming, R.M., Rupen, M.P., Mioduszewski, A.J., et al. (1999), *ApJ* **514**, 383
- Homan, J., Klein–Wolt, M., Rossi, S., et al. (2002), *ApJ* **586**, 1262–1267
- Homan, J., Miller J.M., Wijnands, R., et al. (2003); *ATEL* 162
- Homan, J., Wijnands, R., van der Klis, M., et al. (2001), *ApJS* **132**, 377–402
- Humphrey, P.J., Fabbiano, G., Elvis, M., et al. (2003), *MNRAS*, in press (astro-ph/0305345)
- Hutchings, J.B., Crampton, D., Cowley, A.P., et al. (1987), *AJ* **94**, 340–344
- Hynes, R.I., Roche, P., Charles, P.A. and Coe, M.J. (1999), *MNRAS* **305**, L49–L53
- Hynes, R.I., Steeghs, D., Casares, J., et al. (2003), *ApJ* **583**, L95–L98
- Igumenshchev, I.V. and Abramowicz, M.A. (1999), *MNRAS* **303**, 309–320
- in’t Zand, J.J.M., Markwardt, C.B., Bazzano, A., et al. (2002a), *A&A* **390**, 597–609
- in’t Zand, J.J.M., Miller, J.M., Oosterbroeck, T. and Parmar, A.N. (2002b), *A&A* **394**, 553–560
- Israelian, G., Rebolo, R., Basri, G. (1999), *Nature* **401**, 142–144
- Jones, C., Forman, W., Tananbaum, H. and Turner, M.J.L. (1976), *ApJ* **210**, L9–L11
- Kalemci, E., Tomsick, J.A., Rothschild, R.E., et al. (2002) *ApJ* **586**, 419–426
- Kalogera, V. and Baym, G. (1996), *ApJ* **470**, L61–L64
- Kaluzienski, L.J., Holt, S.S., Boldt, E.A., et al. (1975), *ApJ* **201**, L121–L124
- Kato, S. (2001), *PASJ*, **53**, 1–24
- Kato, S., and Fukue, J. (1980), *PASJ*, **32**, 377–388
- Kato, S., Fukue, J. and Mineshige, S. (1998). *Black–Hole Accretion Disks* (Kyoto U. Press, Japan)
- Kawaguchi, T., Shimura, T. and Mineshige, S. (2000), *NewAR* **44**, 443–445
- Kennea, J.A. and Skinner, G.K. (1996), *PASJ* **48**, L117–L117
- King, A.R., Davies, M.B., Ward, M.J., et al. (2001), *ApJ* **552**, L109–L112
- Kitamoto, S., Tsunemi, H., Pedersen, H., et al. (1990), *ApJ* **361**, 590–595
- Klein–Wolt, M., Fender, R.P., Pooley, G.G., et al. (2002), *MNRAS* **331**, 745–764
- Kong, A.K. H., McClintock, J.E., Garcia, M.R., et al. (2002), *ApJ* **570**, 277–286
- Kotani, T., Kawai, N., Nagase, F., et al. (2000), *ApJ* **543**, L133–L136
- Kubota, A., Makishima, K., & Ebisawa, K. (2001), *ApJ* **560**, L147–L150
- Kuulkers, E., Fender, R.P., Spencer, R.E., et al. (1999), *MNRAS* **306**, 919–925
- Kuulkers, E., Wijnands, R., Belloni, T., Mendez, M., et al. (1998), *ApJ* **494**, 753–758
- Laor, A. (1991), *ApJ* **376**, 90–94
- Lasota, J.-P. (2001), *NewAR* **45**, 449–508
- Levine, A.M., Bradt, H., Cui, W., et al. (1996), *ApJ* **469**, 33–36
- Ling, J.C., Mahoney, W.A., Wheaton, Wm.A. and Jacobson, A.S. (1987), *ApJ* **321**, L117–L122
- Ling, J.C., Wheaton, Wm.A., Wallyn, P., et al. (2000), *ApJS* **127**, 79–124
- Liu, B.F., Mineshige, S. and Shibata, K. (2002), *ApJ* **572**, L173–L176
- Liu, Q.Z., van Paradijs, J. and van den Heuvel, E.P.J. (2001), *A&A* **368**, 1021–1054
- Liu, Q.Z., van Paradijs, J. and van den Heuvel, E.P.J. (2001), *A&As* **147**, 25–49
- Loewenstein, M., Mushotzky, R.F., Angelini, L., et al. (2001), *ApJ* **555**, L21–L24
- Lowes, P., in ’t Zand, J.J.M., Heise, J., et al. (2002), *IAU Circ.* 7843
- Lynden–Bell, D. and Pringle, J.E. (1974), *MNRAS* **168**, 603–637
- Makashima, K., Kubota, A., Mizuno, T., et al. (2000), *ApJ* **535**, 632–643
- Makishima, K., Maejima, Y., Mitsuday, K., et al. (1986), *ApJ* **308**, 635–643
- Mandelbrot, B. B. (1999), *Multifractals and 1/f Noise: Wild Self-Affinity in Physics* (Springer-Verlag: Heidelberg)

- Margon, B., Thorstensen, J.R. and Bowyer, S. (1978), *ApJ* **221**, 907–911
- Markert, T.H., Canizares, C.R., Clark, G.W., et al. (1973), *ApJ* **184**, L67–L70
- Markoff, S., Falcke, H. and Fender, R. (2001a), *A&A* **372**, L25–L28
- Markoff, S., Nowak, M., Corbel, S., et al. (2003) *A&A* **397**, 645–658
- Markovic, D. and Lamb, F.K. (1998), *ApJ*, **507**, 316–326
- Markwardt, C. (2001), *ApSS* **276**, 209–212
- Markwardt, C.B. and Swank, J.H. (2003a), *IAU Circ.* 8056
- Markwardt, C.B. and Swank, J.H. (2003b), *ATEL* 133
- Marsh, T.R., Robinson, E.L. and Wood, J.H. (1994), *MNRAS* **266**, 137–154
- Marti, J., Mirabel, I.F., Chaty, S. and Rodriguez, L.F. (2000), *A&A* **363**, 184–187
- Marti, J., Mirabel, I.F., Duc, P.-A. and Rodriguez, L.F. (1997), *A&A* **323**, 158–162
- Marti, J., Mirabel, I.F., Rodriguez, L.F., and Smith, I. A. (2002), *A&A*, **386**, 571–575
- Martocchia, A., Matt, G., Karas, G., et al. (2002), *A&A* **387**, 215–221
- Matt, G., Perola, G.C. and Piro, L. (1991), *A&A* **247**, 25–34
- Mendez, M., and van der Klis, M. (1997), *ApJ* **479**, 926–932
- McClintock, J.E., Garcia, M.R., Caldwell, N., et al. (2001a), *ApJ* **551**, L147–L150
- McClintock, J.E., Haswell, C.A., Garcia, M.R., et al. (2001b), *ApJ* **555**, 477–482
- McClintock, J.E., Horne, K. and Remillard, R.A. (1995), *ApJ* **442**, 358–365
- McClintock, J.E., Narayan, R., Garcia, M.R., et al. (2003a), *ApJ*, in press (astro-ph/0304535)
- McClintock, J.E., Orosz, J.A., MacConnell, D.J., et al. (2003b), *ApJ*, submitted
- McClintock, J.E. and Remillard, R.A. (1986), *ApJ* **308**, 110–122
- McClintock, J.E. and Remillard, R.A. (2000), *ApJ* **531**, 956–962
- McConnell, M.L., Ryan, J.M., Collmar, W., et al. (2000), *ApJ* **543**, 928–937
- McKinney, J.C. and Gammie, C.F. (2002), *ApJ*, **573**, 728–737
- Menou, K., Esin, Ann A., Narayan, R., et al. (1999), *ApJ* **520**, 276–291
- Mendez, M. and van der Klis, M. (1997), *ApJ*, **479**, 926–932
- Merloni, A. and Fabian, A.C. (2001a), *MNRAS* **321**, 549–552
- Merloni, A. and Fabian, A.C. (2001b), *MNRAS* **328**, 958–968
- Merloni, A. and Fabian, A.C. (2002), *MNRAS* **332**, 165–175
- Merloni, A., Fabian, A. C., and Ross, R. R. (2000), *MNRAS* **313**, 193–197
- Merloni, A., Vietri, M., Stella, L., and Bini, D. (2001), *MNRAS*, **304**, 155–159
- Meyer, F., Liu, B.F. and Meyer-Hofmeister, E. (2000), *A&A* **361**, 175–188
- Miller, J.M., Fabian, A.C., in’t Zand, J.J.M., et al. (2002a), *ApJ* **577**, L15–L18
- Miller, J.M., Fabian, A.C., Wijnands, R., et al. (2002b), *ApJ* **570**, L69–L73
- Miller, J.M., Fabian, A.C., Wijnands, R., et al. (2002c), *ApJ* **578**, 348–356
- Miller, J.M., Fox, D.W., Di Matteo, T., et al. (2001), *ApJ* **546**, 1055–1067
- Miller, J.M., Wijnands, R., Rodriguez-Pascual, P.M., et al. (2002d), *ApJ* **566**, 358–364
- Mirabel, I.F. and Rodriguez, L.F. (1994), *Nature* **371**, 46–48
- Mirabel, I.F. and Rodriguez, L.F. (1999), *ARA&A* **37**, 409–443
- Mirabel, I.F., Rodriguez, L.F. and Cordier, B. (1993), *IAU Circ.* 5876
- Mitsuda, K., Inoue, H., Koyama, K., et al. (1984), *PASJ* **36**, 741–759
- Miyamoto, S., Iga, S., Kitamoto, S., and Kamado, Y. (1993), *ApJ* **403**, L39–L42
- Miyamoto, S., and Kitamoto, S. (1991), *ApJ* **374**, 741–743
- Morgan, E.H., Remillard, R.A. and Greiner, J. (1997), *ApJ* **482**, 993–1010
- Motch, C., Guillout, P., Haberl, F., et al. (1998), *A&AS* **132**, 341–359
- Muno, M.P., Morgan, E.H., and Remillard, R.A. (1999), *ApJ* **527**, 321–340
- Muno, M.P., Morgan, E.H., Remillard, R.A., et al. (2001), *ApJ*, **556**, 515–532
- Murdin, P., Griffiths, R.E., Pounds, K.A., et al. (1977), *MNRAS* **178**, 27P–32P
- Narayan, R. (1996), *ApJ* **462**, 136–141
- Narayan, R. (2002), to appear in *Lighthouses of the Universe*, eds. M. Gilfanov, R. Sunyaev, et al. (Springer, Berlin)
- Narayan, R., Garcia, M.R., and McClintock, J.E. (1997), *ApJ* **478**, L79–L82
- Narayan, R., Garcia, M. R., and McClintock, J. E. (2002), in *Proc. Ninth Marcel Grossmann Meeting on General Relativity*, eds. V.G. Gurzadyan, R.T. Jantzen, & R. Ruffini (World Scientific, Singapore), 405–425
- Narayan, R. and Insu, Y. (1994), *ApJ* **428**, L13–L16
- Narayan, R. and Insu, Y. (1995), *ApJ* **444**, 231–243

- Narayan, R., Igumenshchev, I.V. and Abramowicz, M.A. (2000), *ApJ* **539**, 798–808
- Narayan, R., McClintock, J.E. and Yi, I. (1996), *ApJ* **457**, 821–833
- Nelemans, G. and van den Heuvel, E.P.J. (2001), *A&A* **376**, 950–954
- Nobili, L., Turolla, R., Zampieri, L., and Belloni, T. (2000), *ApJ*, **538**, L137–L140
- Novikov, I.D. and Thorne, K.S. (1973), in *Black Holes*, eds. C. DeWitt and B. DeWitt, (Gordon & Breach, NY)
- Nowak, M.A. (2000), *MNRAS*, **318**, 361–367
- Nowak, M.A. and Wilms, J. (1999), *ApJ* **522**, 476–486
- Nowak, M.A., Wilms, J. and Dove, J.B. (2002), *MNRAS* **332**, 856–878
- Nowak, M.A., Wilms, J., Heindl, W.A., et al. (2001), *MNRAS* **320**, 316–326
- Ogley, R.N., Ash, T.D.C. and Fender, R.P. (1997), *IAU Circ.* 6726
- Orosz, J.A. and Bailyn, C.D. (1997), *ApJ* **477**, 876–896
- Orosz, J.A., Bailyn, C.D., McClintock, J.E. and Remillard, R.A. (1996), *ApJ* **468**, 380–390
- Orosz, J.A., Groot, P.J., van der Klis, M., et al. (2002a), *ApJ* **568**, 845–861
- Orosz, J.A., Jain, R.K., Bailyn, C.D., et al. (1998), *ApJ* **499**, 375–384
- Orosz, J.A., Kuulkers, E., van der Klis, M., et al. (2001), *ApJ* **555**, 489–503
- Orosz, J.A., Polisenky, E.J., Bailyn, C.D., et al. (2002b), *BAAS* **201**, 1511
- Osaki, Y. (1974), *PASJ* **26**, 429–436
- Owen, F.N., Balonek, T.J., Dickey, J., et al. (1976), *ApJ* **203**, L15–L16
- Pan, H.C., Skinner, G.K., Sunyaev, R.A. and Borozdin, K.N. (1995), *MNRAS* **274**, L15–L18
- Parmar, A.N., Angelini, L., Roche, P. and White, N.E. (1993), *A&A* **279**, 179–187
- Pottschmidt, K., Wilms, J., Nowak, M.A., et al. (2003), submitted to *A&A* (astro-ph/0202258)
- Poutanen, J. and Fabian, A. C. (1999), *A&A*, **306**, L31–L36
- Pringle, J.E. and Rees, M.J. (1972), *A&A* **21**, 1–9
- Psaltis, D., Belloni, T., and van der Klis, M. (1999), *ApJ*, **520**, 262–270
- Quataert, E. and Gruzinov, A. (2000), *ApJ* **539**, 809–814
- Quataert, E. and Narayan, R. (1999), *ApJ* **520**, 298–315
- Reig, P., Belloni, T., van der Klis, M., et al. (2000), *ApJ*, **541**, 883–888
- Remillard, R., Levine, A., Swank, J. and Strohmayer, T. (1997), *IAU Circ.* 6710
- Remillard, R.A., Levine, A.M., Morgan, E.H., et al. (2003a), *IAU Circ.* 8050
- Remillard, R.A., Morgan, E.H., McClintock, J.E., et al. (1999), *ApJ* **522**, 397–412
- Remillard, R.A., Morgan, E.H., and Muno, M. (2001), in *Proc. Ninth Marcel Grossmann Meeting on General Relativity*, eds. V.G. Gurzadyan, R.T. Jantzen, & R. Ruffini (World Scientific, Singapore), 2220–2223
- Remillard, R.A., Muno, M.P., McClintock, J.E., and Orosz, J.A. (2002a), *ApJ*, **580**, 1030–1042
- Remillard, R.A., Muno, M.P., McClintock, J.E., and Orosz, J.A. (2003b), *BAAS*, **35**, 648
- Remillard, R.A., Orosz, J.A., McClintock, J.E. and Bailyn, C.D. (1996), *ApJ* **459**, 226–235
- Remillard, R.A., Sobczak, G.J., Muno, M.P. and McClintock, J.E. (2002b), *ApJ* **564**, 962–973
- Revnivtsev, M.G., Borozdin, K.N., Priedhorsky, W.C. and Vikhlinin, A. (2000a), *ApJ* **530**, 955–965
- Revnivtsev, M., Gilfanov, M. and Churazov, E. (1998a), *A&A* **339**, 483–488
- Revnivtsev, M., Gilfanov, M. and Churazov, E. (2001), *A&A* **380**, 520–525
- Revnivtsev, M., Gilfanov, M., Churazov, E., et al. (1998b), *A&A* **331**, 557–563
- Revnivtsev, M., Gilfanov, M., Churazov, E., Sunyaev, R. (2002), *A&A* **391**, 1013–1022
- Revnivtsev, M., Sunyaev, R. and Borozdin, K. (2000b), *A&A* **361** L37–L39
- Revnivtsev, M.G., Trudolyubov, S.P. and Borozdin, K.N. (2000c), *MNRAS* **312**, 151–158
- Reynolds, C.S., & Nowak, M.A. (2003), *Phys.Rept.* **377**, 389–466
- Reynolds, A.P., Quaintrell, H., Still, M.D., et al. (1997), *MNRAS* **288**, 43–52
- Rhoades, C.E. and Ruffini, R. (1974), *Phys. Rev. Lett.* **32**, 324–
- Rodriguez, L.F., Mirabel, I.F. and Marti, J. (1992), *ApJ* **401**, L15–L18
- Romani, R.W. (1998), *A&A* **333**, 583–590
- Rothschild, R.E., Blanco, P.R., Gruber, D.E., et al. (1998), *ApJ* **496**, 538–549
- Rothstein, D.M., Eikenberry, S.S., Chatterjee, S., et al. (2002), *ApJ* **580**, L61–L63
- Rozanska, A. and Czerny, B. (2000), *A&A* **360**, 1170–1186
- Rupen, M.P., Brocksopp, C., Mioduszewski, A.J., et al. (2003), *IAU Circ.* 8054
- Rupen, M.P., Dhawan, V. and Mioduszewski, A.J. (2002), *IAU Circ.* 7874
- Rupen, M.P., Hjellming, R.M. and Mioduszewski, A.J. (1998), *IAU Circ.* 6938

- Rutledge, R.E., Lewin, W.H.G., van der Klis, M., et al. (1999), *ApJS* **124**, 265–283
- Sanchez-Fernandez, C., Zurita, C., Casares, J., et al. (2002), *IAU Circ.* 7989
- Seon, K., Min, K., Kenji, Y., et al. (1995), *ApJ* **454**, 463–471
- Shahbaz, T., Naylor, T. and Charles, P.A. (1997), *MNRAS* **285**, 607–612
- Shahbaz, T., Ringwald, F.A., Bunn, J.C., et al. (1994), *MNRAS*, **271**, L10–L14
- Shahbaz, T., van der Hooft, Casares, J., et al. (1999), *MNRAS* **306**, 89–94
- Shakura, N.I. and Sunyaev, R.A. (1973), *A&A* **24**, 337–366
- Shapiro, S.L. and Teukolsky, S.A. (1983), *Black Holes, White Dwarfs and Neutron Stars: The Physics of Compact Objects* (Wiley, New York)
- Shimura, T., and Takahara, F. (1995), *ApJ*, **445**, 780–788
- Shrader, C.R., Wagner, R.M., Hjellming, R.M., et al. (1994), *ApJ* **434**, 698–706
- Skinner, G.K., Foster, A.J., Willmore, A.P. and Eyles, C.J. (1990), *MNRAS* **243**, 72–77
- Smak, J. (1971), *Acta Astron.* **21**, 15–
- Smith, D.M., Heindl, W.A. and Swank, J. (2002), *ApJ* **578**, L129–L132
- Smith, D.M., Heindl, W.A., Markwardt, C.B. and Swank, J.H. (2001), *ApJ* **554**, L41–L44
- Smith, D.M., Heindl, W.A., Swank, J., et al. (1997), *ApJ* **489**, L51–L54
- Sobczak, G.J., McClintock, J.E., Remillard, R.A., et al. (1999), *ApJ* **520**, 776–787
- Sobczak, G.J., McClintock, J.E., Remillard, R.A., et al. (2000a), *ApJ*, **531**, 537–545
- Sobczak, G.J., McClintock, J.E., Remillard, R.A., et al. (2000b), *ApJ* **544**, 993–1015
- Steeghs, D., Miller, J.M., Kaplan, D., & Rupen, M. (2003), *ATEL* 146
- Stella, L., Vietri, M., and Morsink, S.M. (1999), *ApJ*, **524**, L63–L66
- Stirling, A.M., Spencer, R.E., de la Force, C.J., et al. (2001), *MNRAS* **327**, 1273–1278
- Stone, J.M., Pringle, J.E. and Begelman, M.C. (1999), *MNRAS* **310**, 1002–1016
- Strohmayer, T.E. (2001a), *ApJ* **552**, L49–L53
- Strohmayer, T.E. (2001b), *ApJ* **554**, L169–L172
- Sunyaev, R., Churazov, E., Gilfanov, M., et al. (1992), *ApJ* **389**, L75–L78
- Sunyaev, R., Gilfanov, M., Churazov, E., et al. (1991a), *SvAL* **17**, 50–54
- Sunyaev, R.A., Kaniovskii, A.S., Efremov, V.V., et al. (1991b), *SvAL* **17**, 123–130
- Sunyaev, R.A., Lapshov, I.Yu., Grebenev, S.A., et al. (1988), *SvAL* **14**, 327–333
- Sunyaev, R., & Revnivtsev, M. (2000), *A&A*, **358**, 617–623
- Sutaria, F. K., Kolb, U., Charles, P., et al. (2002), *A&A* **391**, 993–997
- Swank, J. (1998), in *Proceedings of the Symposium “The Active X-ray Sky: Results from BeppoSAX and Rossi-XTE”*, eds. L. Scarsi, H. Bradt, P. Giommi and F. Fiore, *Nuclear Physics B Proceedings Supplements* (astro-ph/9802188)
- Tagger, M. and Pellat, R. (1999), *A&A*, **349**, 1003–1016
- Takahashi, K., Inoue, H., and Dotani, T. (2001), *PASJ*, **53**, 1171–1177
- Tanaka, Y. and Lewin, W.H.G. (1995), in *X-ray Binaries*, eds. W.H.G. Lewin, J. van Paradijs, and E.P.J. van den Heuvel, (Cambridge U. Press, Cambridge) 126–174, TL95
- Tanaka, Y. and Shibazaki, N. (1996), *ARAA* **34**, 607–644, TS96
- Tanaka, Y., Nandra, K., Fabian, A.C. (1995), *Nature* **375**, 659–661
- Tananbaum, H., Gursky, H., Kellogg, E., et al. (1972), *ApJ* **177**, L5–L10
- Titarchuk, L. and Osherovich, V. (2000), *ApJ*, **542**, L111–L114
- Tomsick, J.A. and Kaaret, P. (2000), *ApJ* **537**, 448–460
- Tomsick J.A., and Kaaret, P. (2001), *ApJ*, **548**, 401–409
- Tomsick, J.A., Kaaret, P., Kroeger, R.A., and Remillard, R.A. (1999), *ApJ* **512**, 892–900
- Trimble, V. (2000), in *Allen’s Astrophysical Quantities*, ed. A. Cox, (Springer-Verlag, NY)
- Trudolyubov, S., Churazov, E., Gilfanov, M., et al. (1999b), *A&A* **342**, 496–501
- Turner, M.J.L., Thomas, H.D., Patchett, B.E., et al. (1989), *PASJ* **41**, 345–372
- Turner, N.J., Stone, J.M., and Sano, T. (2002), *ApJ*, **566**, 148–163
- Turolla, R., Zane, S., and Titarchuk, L. (2002), *ApJ* **576**, 349–356
- Ueda, Y., Dotani, T., Uno, S, et al. (1997), *IAU Circ.* 6627
- van den Heuvel, E.P.J. (1992), in *ESA, Environment Observation and Climate Modelling Through International Space Projects* (SEE N93–23878 08–88)
- van der Hooft, F., Kouveliotou, C., van Paradijs, J., et al. (1996a), *A&A* **120**, 141–144
- van der Hooft, F., Kouveliotou, C., van Paradijs, J., et al. (1996b), *ApJ* **458**, L75–L78
- van der Hooft, F., Kouveliotou, C., van Paradijs, J., et al. (1999), *ApJ* **513**, 477–490
- van der Klis M. (1994), *ApJS* **92**, 511–519

- van der Klis M. (1995) in X-ray Binaries, eds. W.H.G. Lewin, J. van Paradijs and E.P.J. van den Heuvel, (Cambridge U. Press, Cambridge), 252–307
- van Paradijs, J. (1995) in X-ray Binaries, eds. W.H.G. Lewin, J. van Paradijs and E.P.J. van den Heuvel, (Cambridge U. Press, Cambridge), 536–577
- van Paradijs, J. (1998) in The Many Faces of Neutron Stars, eds. R. Bucccheri et al., (Kluwer, Dordrecht)
- van Paradijs, J. and McClintock, J.E. (1995) in X-ray Binaries, eds. W.H.G. Lewin, J. van Paradijs and E.P.J. van den Heuvel, (Cambridge U. Press, Cambridge), 58–125
- Vargas, M., Goldwurm, A., Laurent, P., et al. (1997), *ApJ* **476**, L23–L26
- Vargas, M., Goldwurm, A., Paul, J., et al. (1996), *A&A* **313**, 828–832
- Vasiliev, L., Trudolyubov, S. and Revnivtsev, M. (2000), *A&A* **362**, L53–L56
- Vikhlinin, A., Churazov, E., Gilfanov, M., et al. (1994), *ApJ* **424**, 395–400
- Vikhlinin, A., Finoguenov, A., Sitdikov, A., et al. (1992), *IAU Circ.* 5608
- Wagner, R.M., Foltz, C.B., Shahbaz, T., et al. (2001), *ApJ* **556**, 42–46
- Wagner, R.M., Starrfield, S.G., Hjellming, R.M., et al. (1994), *ApJ* **429**, L25–L28
- Wagoner, R.V. (1999), *Physics Reports*, **311**, 259–269
- Wagoner, R.V., Silbergleit, A.S., and Ortega-Rodriguez, M. (2001), *ApJ*, **559**, L25–L28
- Wardzinski, G., Zdziarski, A., Gierlinski, M., et al. (2002), *MNRAS* **337**, 829–839
- Weaver, K.A., Gelbord, J. and Yaqoob, T. (2001), *ApJ* **550**, 261–279
- Webster, B.L and Murdin, P. (1972), *Nature* **235**, 37–38
- White, N.E. and Marshall, F.E. (1984), *ApJ* **281**, 354–359
- White, N.E. and van Paradijs, J. (1996), *ApJ* **473**, L25–L29
- White, N.E., Nagase, F. and Parmar, A.N. (1995) in X-ray Binaries, eds. W.H.G. Lewin, J. van Paradijs and E.P.J. van den Heuvel, (Cambridge U. Press, Cambridge) 1–57
- White, N.E., Stella, L. and Parmar, A.N. (1988), *ApJ* **324**, 363–378
- Wijnands, R. and Miller, J.M. (2002), *ApJ* **564**, 974–980
- Wijnands, R. and van der Klis, M. (2000), *ApJ* **528**, L93–L96
- Wijnands, R., Homan, J., and van der Klis, M. (1999), *ApJ* **526**, L33–L36
- Wijnands, R., Mendez, M., Miller, J.M. and Homan, J. (2001), *MNRAS* **328**, 451–460
- Wijnands, R., Miller, J.M. and van der Klis, M. (2002), *MNRAS* **331**, 60–70
- Wilms, J., Nowak, M.A., Dove, J.B., et al. (1999), *ApJ*, **522**, 460–475
- Wilms, J., Nowak, M.A., Pottschmidt, K., et al. (2001a), *MNRAS* **320**, 327–340
- Wilms, J., Reynolds, C.S., Begelman, M.C., et al. (2001b), *MNRAS* **328**, L27–L31
- Wilson, A.M., Carpenter, G.F., Eyles, C.J., et al. (1977), *ApJ* **215**, L111–L115
- Wilson, C.K. and Rothschild, R.E. (1983), *ApJ* **274**, 717–722
- Wood, K.S., Ray, P.S., Bandyopadhyay, R.M., et al. (2000), *ApJ* **544**, L45–L48
- Woods, P.M., Kouveliotou, C., Finger, M.H., et al. (2002), *IAU Circ.* 7856
- Woosley, S.E., Heger, A. and Weaver, T.A. (2002), *RvMP* **74**, 1015–1071
- Wu, K., Soria, R., Campbell–Wilson, D., et al. (2002), *ApJ* **565**, 1161–1168
- Yaqoob, T., Ebisawa, K. and Mitsuda, K. (1993), *MNRAS* **264**, 411–420
- Zdziarski, A.A. (2000), in Highly Energetic Physical Processes and Mechanisms for Emission from Astrophysical Plasmas, *Procs. IAU Symposium #195*, eds. C.H. Martens, S. Tsuruta, and M.A. Weber, ASP, 153–170, (astro-ph/0001078)
- Zdziarski, A.A., Grove, J.E., Poutanen, J., et al. (2001), *ApJ* **554**, L45–L48
- Zdziarski, A., Piotr, L., Gilfanov, M. and Revnivtsev, M. (2003), *MNRAS*, in press, (astro-ph/0209363)
- Zdziarski, A., Poutanen, J., Paciesas, W.S. and Wen, L. (2002), *ApJ* **578**, 357–373
- Zhang, S.N., Cui, W. and Chen, W. (1997a), *ApJ* **482**, L155–L158
- Zhang, S.N., Cui, W., Harmon, B.A., et al. (1997b), *ApJ* **477**, L95–L98
- Zurita, C., Sanchez–Fernandez, C., Casares, J., et al. (2002), *MNRAS* **334**, 999–1008
- Zycki, P.T., Done, C., and Smith, D.A. (1999a), *MNRAS* **305**, 231–240
- Zycki, P.T., Done, C., and Smith, D.A. (1999b), *MNRAS* **309**, 561–575